B. Petrographic and Structural Characterization

Johannes Duyster
Andrea Grawinkel
Agnes Kontny

B Petrographic and Structural Characterization

Johannes Duyster, Andrea Grawinkel & Agnes Kontny

KTB Feldlabor, D 92670 Windischeschenbach, Germany

B.1 Geological Setting

The KTB Hauptbohrung (KTB HB, main hole) is located in the Bavarian Oberpfalz at the western border of the Bohemian Massif, the most extensive surface exposure of crystalline rocks in central Europe.

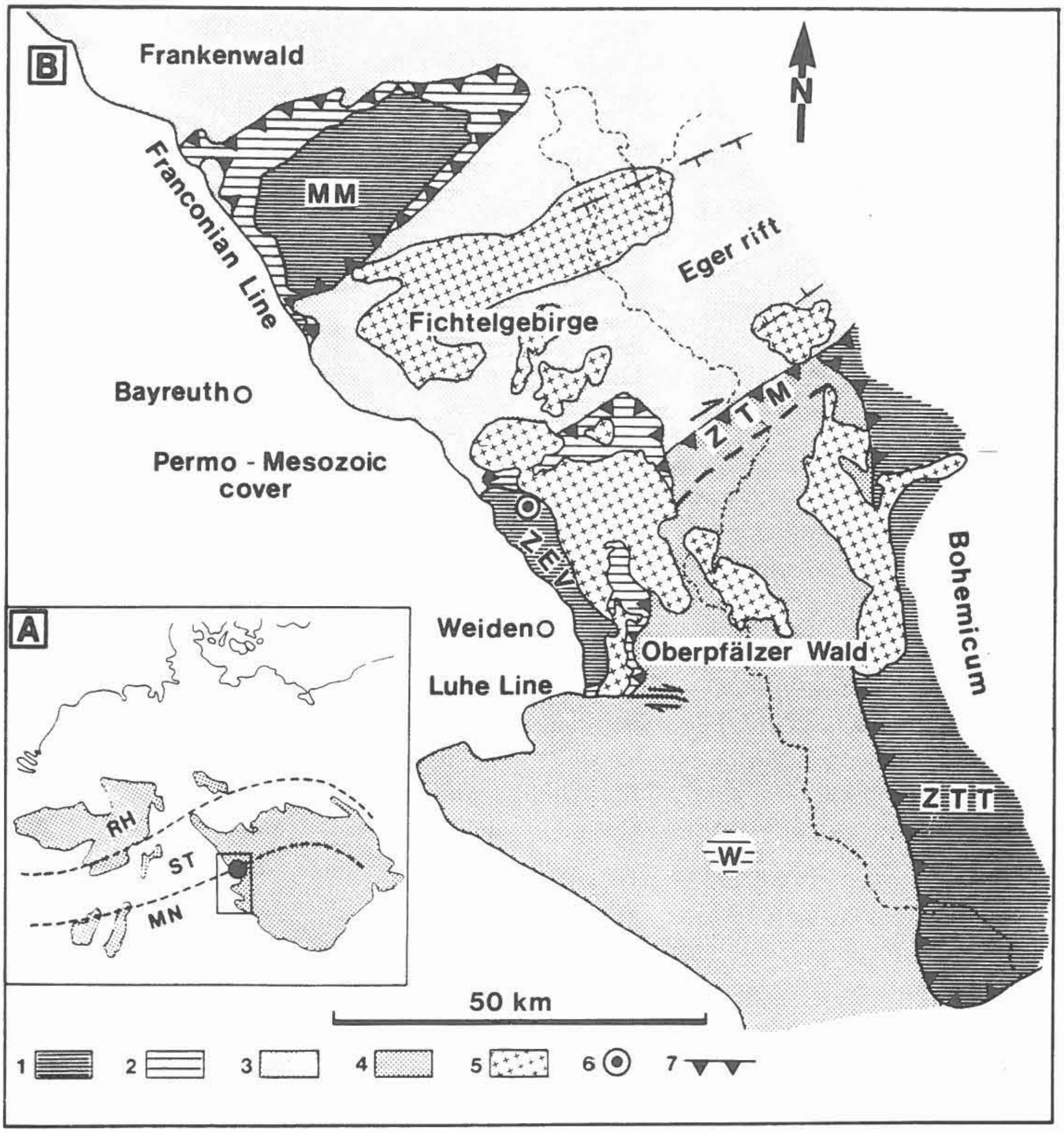

Fig. B.1.1 Geological sketch map of the western margin of the Bohemian Massif in NE Bavaria. A: Variscan basement outcrops in Middle Europe with zones according to Kossmat (1927). RH: Rhenohercynian Zone; ST: Saxothuringian Zone; MN: Moldanubian Region. B: Geological map: MM: Münchberg Massif, W: Winklarn, ZEV: Zone of Erbendorf-Vohenstrauß, ZTM: Zone of Tirschenreuth-Mähring, ZTT: Zone of Tepla Taus; 1,2 : Münchberg Massif, Zone of Erbendorf-Vohenstrauß: 3: Saxothuringian; 4: Moldanubian of the Oberpfälzer Wald; 5: late- to post-tectonic granites; 6: KTB drilling site; 7: overthrust; (after Weber 1990).

During the Variscan orogeny, a number of different tectonometamorphic units were juxtaposed in the Oberpfalz area (e.g. Blümel 1986, Franke 1989, Vollbrecht et al. 1989; Fig. B.1.1). The low- to medium-grade metamorphosed Saxothuringian unit to the north consists of Cambrian to Carboniferous sequences. It is separated from the high-grade metamorphic Moldanubian unit by a dextral eastnortheast trending strike-slip fault (Stettner 1979, Vollbrecht et al. 1989, Zulauf 1993). The Moldanubian unit in the Oberpfalz area is characterized by monotonous series of meta-graywackes, quartzites and metapelites with intercalations of calcsilicates. Both, Moldanubian and Saxothuringian have suffered pervasive low pressure, high temperature metamorphism during the middle Carboniferous (Blümel 1986, Hansen et al. 1989).

A third crystalline unit, the Zone of Erbendorf-Vohenstrauß (ZEV), was not affected by this low pressure metamorphism. The ZEV mainly consists of paragneisses, metabasalts and metagabbros with minor occurrences of marbles, calcsilicates, orthogneisses, lamprophyres and diorites. Metabasalt extrusion ages and metagabbro intrusion ages are of lower Ordovician (480 - 485 Ma, e.g. v. Quadt 1994, Grauert 1994, Hölzl & Köhler 1994) similar extrusion ages have been determined for the metatuffites (e.g. 488 ± 3 Ma, Söllner & Miller 1994).

The earliest metamorphic overprint recorded in both, the metabasites and the gneisses, has been dated as about 480 Ma by U/Pb ages of zircons and monazite (Grauert et al. 1994). The relics of high pressure mineral assemblages preserved in some of the metabasites point to pressures around 14 kbar at 750°C (O' Brien et al. 1992) and are attributed to this Ordovician event.

All ZEV rocks suffered a pervasive Barrovian type metamorphism in the early Devonian (ca. 380 Ma; Blümel 1986, Teufel 1988, Hansen et al. 1989, Kreuzer et al. 1989, 1993; Reinhardt 1992). The ZEV, the Münchberg Complex and the Mariánské Lázne Complex show a similar evolution and, are considered tpo be parts of the same „Münchberg-Tepla Terrane“ (Matte et al., 1990) (Fig. B.1.1).

In the late Carboniferous granites intruded into the Saxothuringian, the Moldanubian and the ZEV. Intrusive contacts of the Falkenberg Granite (311 Ma, Rb-Sr whole rock, Wendt et al. 1986; 307 Ma, U-Pb on zircon, Carl et al. 1989) are exposed 2 km E of the drilling site. Maier & Stöckhert (1992) estimated that the present level of erosion was at a depth of at least 9 km at the time of the intrusion of the Falkenberg Granite.

Subsequent to granite emplacement, the ZEV rocks underwent intense deformation in the semi-brittle and brittle field. Using cross-cutting relationships and index minerals, Zulauf (1990) has identified several generations of faults and veins in the cores of the KTB Vorbohrung (VB).

The most important faults belong to the Franconian Lineament (FL) which dips approximately 55° to the northeast. Along this reverse fault zone Variscan basement rocks have been thrust towards the southwest over the Permo-Mesozoic cover (Fig. B.1.1). This stage of reverse faulting as well as dextral strike-slip movements are attributed to the Cretaceous and lowermost Tertiary (Alpine) convergence (e.g. Ziegler 1987). Fission track studies (Coyle & Wagner 1994) have shown that the vertical displacement along this fault was more than 3 km. 3-D seismic images display the FL as a prominent reflector (SE-1) from the surface to at least 10 km depth (Hirschmann 1992). The KTB HB transsects this structure between 6850 and 7260 m depth.

Prior to drilling the tectonic models were based mainly on surface geology and conventionally migrated and interpreted 2-D seismic sections, suggesting the ZEV to be part of a shallow nappe complex that has been thrust over the low-pressure metamorphic rocks of the Moldanubian and Saxothuringian units (Franke 1989, Vollbrecht et al. 1989, Weber &

Vollbrecht 1989). Therefore, the KTB HB, which was placed within the ZEV, was expected to penetrate the ZEV-base at about 4 km depth and subsequently drill through different underlying units. However, down to the final depth of 9101 m, one and the same association of rocks form the ZEV has been drilled.

- The drilled crustal section essentially comprises paragneisses and metabasites; e.g. Röhr et al. 1990, Duyster et al. 1993, Kontny et al. 1994, Fig. B.1.1). The mineral associations indicate amphibolite facies conditions (Reinhardt 1992, Lich et al. 1992, Duyster et al. 1993, Kontny et al. 1994, Schulte & Blümel 1994).
- The foliation dips steeply (in most cases 60° - 80°) until the final depth with few exceptions.
- K-Ar and ^{39}Ar-^{40}Ar cooling ages of hornblende (around 380 Ma), muscovite (around 365 Ma), and biotite (around 317 Ma) are similar throughout the drilled sections of KTB VB and KTB HB down to at least 8300 m (Kreuzer et al. 1993, Wemmer & Ahrendt 1994, Henjes-Kunst et al. 1994).

B.2 Sampling

Cores

35 core runs with an overall core recovery of 83.6 m were performed in the KTB HB. Coring started below 4000 m, because the 4000 m deep KTB VB had been almost completely cored (core recovery ~90 %).

Cuttings sampler specimens

The „Cuttings Sampler" is a junk basket that was used to collect cm-sized rock fragments. These samples were collected from the whole depth interval of one bit run and also contained break out material from higher levels of the bore hole wall.

Cuttings

Cuttings were sampled in m-intervals, washed, sieved and dried. The fraction 0.063 -1 mm and 1-5 mm were visually examined under the binocular. The portions of the different lithologies were determined, and the degree of cataclastic overprint and alteration estimated. Mineralization (e.g graphite, sulfides), open fissures and drilling artifacts like „bit-metamorphism" (drilling induced microfracturing) and sample contamination by metal, rubber and plastic from the drilling process were identified.

Cuttings samples are frequently composed of a mixture of different rock types. This is partly due to mixing of samples because of time-dependant breakouts. For example, cuttings samples from the first few meter below cataclastic zones often contain a trail of cataclastic rocks from the fault zone above (e.g. 2810 m). Additional sample mixing can occur in the drill mud.

On the other hand, real intercalations between different lithologies exist (Table B.2.1). If the spacing of these intercalations is narrow (near or below the sampling interval of 1 m) cuttings samples cannot resolve intercalations and show a mixture between these lithologies. To distinguish between real intercalations and sample mixing the cuttings analyses were correlated with the bore hole logs. In particular the γ-ray log proved to be a useful tool to resolve intercalations between gneisses and amphibolites.

The depths of provenance cannot be determined precisely for cuttings samples. They are affected by drill string elongation which may vary within a range of several meters and by lag time computation uncertainties. The depths of all cuttings samples were corrected by comparison of well logging data with cuttings data, mainly by comparison with γ-ray logs.

Thin sections and **polished sections** of rock cuttings were prepared at regular intervals (4 and 20 m respectively). In zones of special interest, the sampling density was increased. For bulk geochemical analyses cuttings were hand picked under the binocular.

Table B.2.1 Nomenclature for alternating sequences with two different lithologies (*A* and *B*)

Relative proportion of lithology *B*	Name given to lithological unit in the cuttings profile (App. 9.2, 9.5)	Name given to lithological unit in the simplified cuttings profile (Fig. B.3.1)
< 5%	*A*	*A*
5- 20%	*A* with intercalations of *B*	*A*
20-35%	*A* dominated alternation of *A* and *B*	Alternation
>30 %	Alternation of *A* and *B*	Alternation

B.3 The geological profile of the KTB HB

Fig. B.3.1 shows the lithological profile of the KTB HB with major cataclastic fault zones. It comprises metagabbros, amphibolites, paragneisses, hornblende gneisses and alternations between these rocks. Subordinate are calcsilicate rocks, ultramafitites, lamprophyres and aplites. The lithological profile of the KTB HB is mainly based on cuttings analyses since core material is very rare (35 core runs with a core recovery of 83.6 m). Therefore, the names given to the rock units depend on the ratio of different rock types occurring in the mixed samples. The nomenclature, which is used for the different rock units in the simplified profile (Fig. B.3.1), in the detailed profile (appendix B.9.2) and the procedure of creating the lithological profile is explained in chapter B.2.

From 0 to 3200 m by paragneisses dominate with few intercalations of amphibolite. From 3200 m down to approximately 7300 m amphibolites with minor intercalations of metagabbros, hornblende gneisses and biotite gneisses prevail. In the depth interval 7260-7800 m an alternation of amphibolites (partly marble-bearing) and gneisses occurs. Below 7800 m to the final depth of 9101 m garnet sillimanite-biotite gneisses occur with the amount of amphibolite intercalations increasing below 8080 m.

Some of the major lithological boundaries are marked by cataclastic faults (e.g. at 7260 m and 7800 m), but unfaulted transitions between paragneiss series, alternating sequences and metabasite sequences are also observed in the profile. This holds true for the paragneiss series below 7800 m, where the amount of amphibolite intercalations increases with depth, and for the metabasite sequences between 6540 and 7260 m, where amphibolites alternate with hornblende gneisses and biotite gneisses (see appendix B.9.2). Table B.3.1 gives an overview of the rock types and their associations.

Paragneisses and hornblende gneisses show a penetrative foliation bearing a NNW-SSE oriented subhorizontal stretching lineation that developed during ductile deformation under upper amphibolite facies conditions. The metabasites, on the contrary, are deformed inhomogene ously: foliated amphibolites are observed close to almost undeformed metagabbros with preserved magmatic fabrics (Schalkwijk 1991).

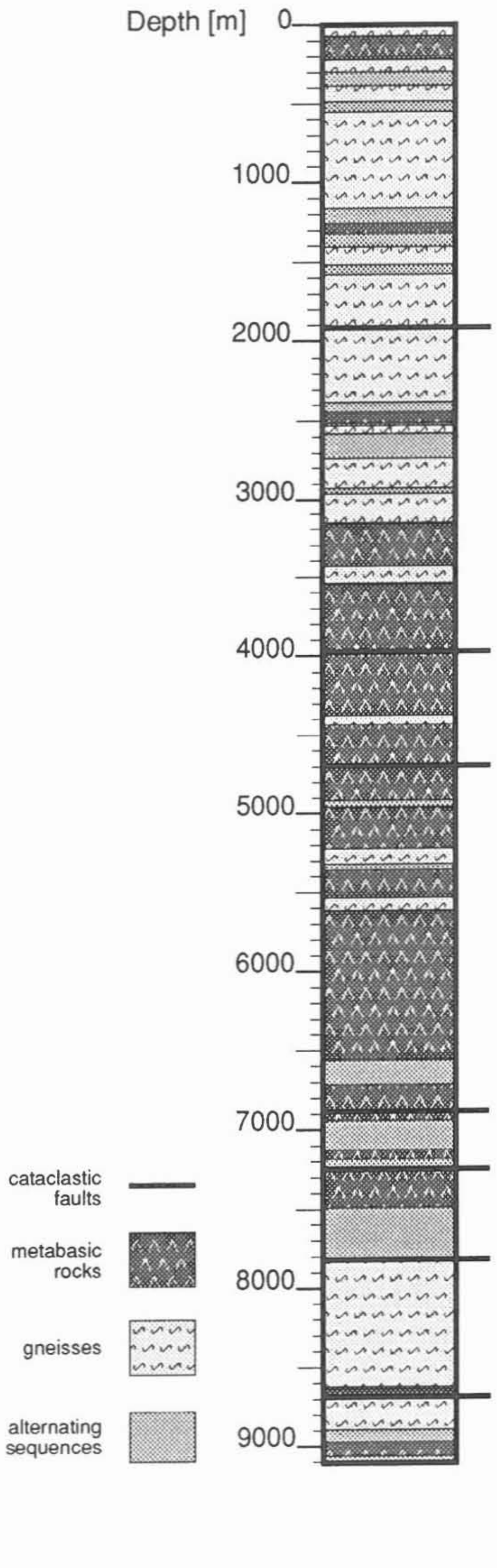

Fig. B.3.1 The simplified lithological profile of the KTB HB

Table B.3.1: Overview of rock types and associations encountered in the KTB bore holes with indication of the geochemical signature, peak-metamorphic conditions and radiometric ages.

	Metagabbros	Metabasalts	Metatuffites	Metasediments
	Ophitic fabrics, mostly strongly altered, undeformed	Fine-grained and coarse-grained types mobilisates inhomogeneous deformation	Bio-Hbl- and Hbl-Bio-gneiss with calksilicate layers	Gnt-Sill-(Ky)-Bio gneiss quartz-rich and mica-rich types
	Primitive tholeiitic composition	Transitional ocean-floor basalts to alkaline metatuffites		Graywackes to pelitic graywackes
Peak-metam. conditions	max. 750°C, 14 kbar (O´Brien et al. 1992)	max. 700°C,10 kbar (O´Brien et al. 1992)		max. 650°C, 8-10 kbar (Reinhard 1989)
Intrusion / Extrusion ages	485 ± 10 Ma v. Quadt, Hölzl, Köhler, Grauert (1994)		488 ± 3 Ma Söllner & Miller (1994)	
Peak-metam. ages	475 Ma Grauert (1994)		475 Ma Grauert (1994)	
Cooling after MP metam.	380-390 Ma (Hbl <500°C) 370 Ma (Mus <350°C) 320 Ma (Bio <300°C) Ar/Ar; K/Ar Henjes-Kunst et al. (1994), Wemmer & Ahrend (1994)			

In general the foliation dips steeply with angles between 60 and 80° to SW or NE. The foliation is folded to large scale folds with subhorizontal axial planes and NNW-SSE trending fold axes (e.g. Duyster et al. 1993, Hirschmann 1995).

The entire profile is transsected by cataclastic faults and mineralized fissures. Lamprophyres are observed predominantly in fault zones. The most extensive fault zone at a depth between 6850 and 7260 m is correlated with the Franconian Lineament, a large scale reverse fault.

Petrographically, the metabasites can be classified into three major groups: amphibolites, metagabbros and hornblende gneisses. These metabasic rocks are dominant in the amphibolite-metagabbro complexes which are interpreted as former ocean floor. Furthermore, metabasites occur in the variegated sequences, possibly representing ancient lavas and volcaniclastic rocks.

The paragneisses are derived from graywackes and pelitic graywackes and were probably formed as turbiditic layers at an active continental margin (e.g. Müller 1993).

Tectonic repetitions in the profile

In the KTB VB at 0-560 m and in the KTB HB at 7260-7812 m a particular gneiss-amphibolite alternation has been encountered. Both occurrences are strikingly similar with respect to rock association, petrography (Fig. B.3.2) and geochemical characteristics. In these sequences, transitional to alkaline metavolcanics appear which differ from the predominantly subalkaline to tholeiitic metabasites. The association comprises:

- marble- and calc-silicate-bearing amphibolites (Fig. B.3.2a and b), which are characterized by a high content of Fe-Ti oxides (magnetite, ilmenite, hematite). This rock type shows the highest magnetic susceptibilities measured in the KTB VB and HB (see chapter D 4.2),
- plagioclase-rich chlorite-(biotite) gneisses with a high amount of small rounded zircon grains (Fig. B.3.2g and h),
- microcline-bearing amphibolites and hornblende gneisses with allanite

These metavolcanics alternate with paragneisses. The kyanite-garnet-biotite gneisses mostly contain graphite and pyrrhotite (Fig. B.3.2c and d). Beside their petrographical and structural similarities, both series partially reveal a strong alteration (Fig. B.3.2e and f; see chapter B.4.2.2). This tectonic repetition is attributed reverse faulting along the Franconian Lineament (Duyster et al. 1995).

B.3.1 Amphibolite - metagabbro association

The distribution of metabasic series occurring in the KTB HB is shown in Fig. B.3.1 and in appendix B.9.2. Amphibolite is the dominating rock type, hornblende gneisses and biotite gneisses are intercalated. Metagabbros occur mainly between 5750 and 6300 m, meta-ultramafitites appear subordinately. The mineral chemistry of metagabbros and amphibolites of the KTB VB isdescribed in detail by Schalkwijk (1991), the mineral chemistry of ore minerals occurring in the metabasites by Grawinkel (1993) and Kontny (1994).

Fig. B.3.2 Comparison of microphotographs from associations found in the KTB VB, 0-560 m (right hand side) and KTB HB, 7260- 7812 m (left hand side).

a: marble-bearing amphibolite, KM14B4R, depth 116 m, one polarizer, width of view 4 mm;
b: marble-bearing amphibolite, HCS 7641-7712, depth 7641-7712 m, one polarizer, width of view 4 mm;
c: kyanite-garnet-biotite gneiss, KM72D16T, depth 474 m, one polarizer, width of view 4 mm;
d: kyanite-garnet-biotite gneiss, HC-K 7647, depth 7647 m, one polarizer, width of view 2.5 mm;
e: chlorite gneiss, KM22A1cT, depth 153 m, crossed polarizers, width of view 2 mm;
f: chlorite gneiss, HC 7700, depth 7700 m, crossed polarizers, width of view 2 mm;
g: zircon-rich chlorite gneiss, KM39A3R, depth 256 m, one polarizer, width of view 0.5 mm;
h: zircon-rich chlorite gneiss, HCS 7641-7712, depth 7641-771m, one polarizer, width of view 0.5 mm.

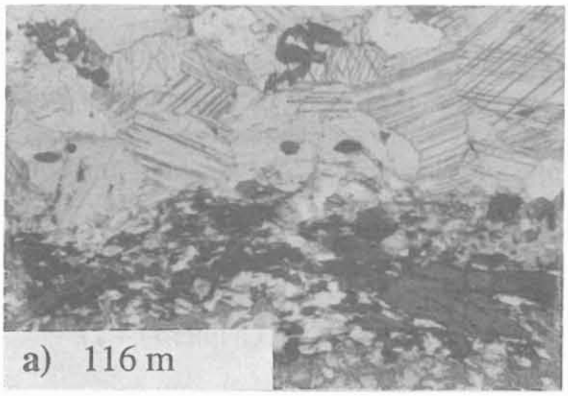
a) 116 m

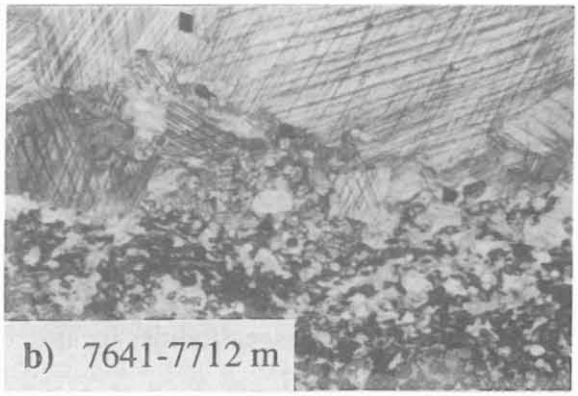
b) 7641-7712 m

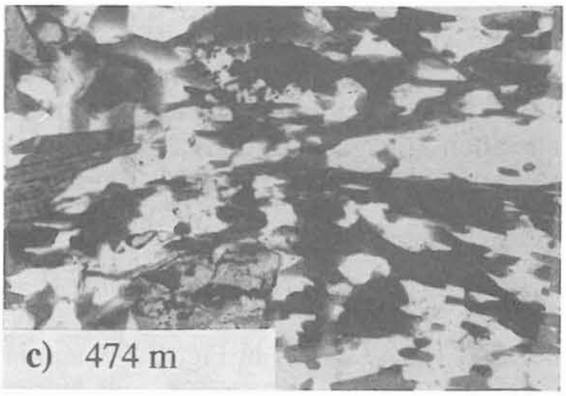
c) 474 m

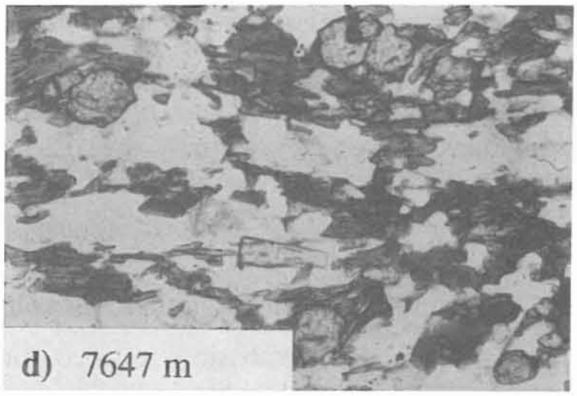
d) 7647 m

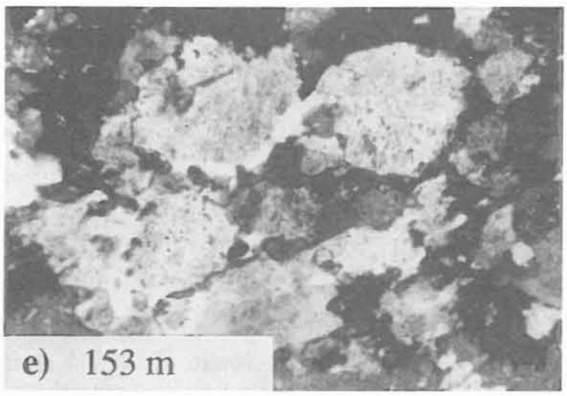
e) 153 m

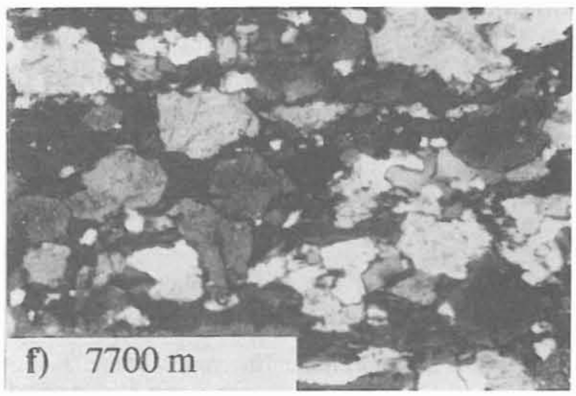
f) 7700 m

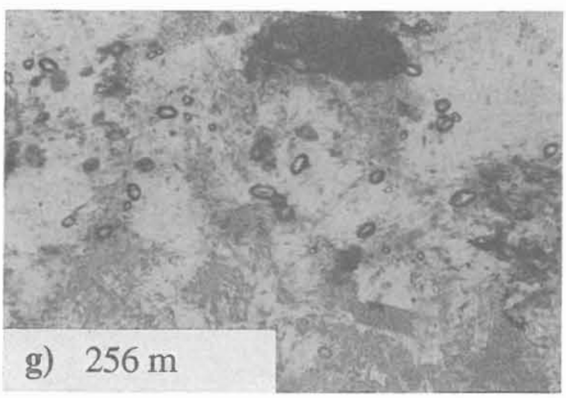
g) 256 m

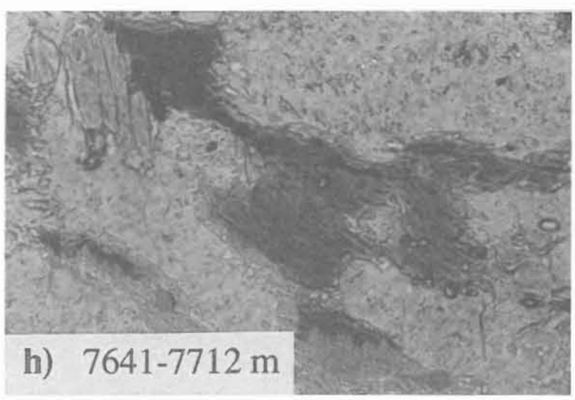
h) 7641-7712 m

Different types of **amphibolites** were observed in the amphibolite-metagabbro complexes (Lich et al. 1992):

- **fine-grained, homogeneous amphibolite**
- **coarse-grained amphibolite**
- **foliated amphibolite** with a pronounced compositional layering

The different fabrics are mainly due to a strongly inhomogeneous deformation. The close association of mafic cumulates, metagabbro and amphibolite is well demonstrated in core H006 (Fig. B.3.3).

The main rock forming minerals in all types are hornblende (tschermakite to magnesiohornblende), plagioclase and garnet (almandine-rich composition) as well as minor quartz and biotite (Fig. B.3.4). Accessories are K-feldspar, apatite, zircon, titanite, ilmenite, rutile and pyrrhotite. Garnet contents are highly variable and the grain sizes reach up to 5 mm. Quartz-feldspar mobilisates are common. Actinolite, chlorite, titanite and epidote are retrograde reaction products. Ore minerals are ilmenite, rutile, pyrrhotite, chalcopyrite and rarely pentlandite and sulfoarsenides (Fig. B.3.5). Depending on the whole rock alteration, the oxides are transformed to leucoxene and/or titanite (Fig. B.3.6). Magnetite occurs between 4000 and 5000 m as an alteration product of pyrite mostly in the vicinity of fault zones or as an alteration product in ilmenite together with rutile.

In fine-grained amphibolites, relics of clinopyroxene and clinopyroxene-plagioclase symplectites are common. This type frequently forms blocks enclosed in coarse-grained amphibolite and quartz-feldspar mobilisates. Fine grained amphibolites associated with mobilisates mostly display a well developed foliation. In general coarse-grained types are richer in felsic components than fine-grained types. Locally, fine-grained amphibolites are enriched in ore minerals (mainly ilmenite) compared to the coarse-grained amphibolites (e.g. garnet amphibolite of core H006).

The observed fabrics give evidence for a partial melting of the metabasic body whereby fine-grained amphibolites can be interpreted as „paleosome" and coarse-grained amphibolites as „neosome" (Schalkwijk 1991). Most structures suggest low mobility of the partially molten material, but sill-like injections crystallized to coarse-grained amphibolites along the preexisting foliation planes of fine grained amphibolites have been described (Schalkwijk 1991).

The amphibolites below 6450 m generally contain more homogeneously distributed quartz (Fig. B.3.7), compared to the amphibolites above 6540 m, where quartz is mainly restricted to quartz-feldspar mobilisates generated by partial melting (Duyster et al. 1993).

Coronitic metagabbros are massive and medium to coarse-grained rocks with preserved ophitic structures. No foliation is developed except for localized ductile shear zones. The metagabbros consist mainly of clinopyroxene, garnet, amphibole, and plagioclase with minor amounts of biotite and quartz. Rutile, ilmenite, apatite and occasionally zircon and pyrrhotite are accessories. Garnets have grown as coronas between plagioclase and clinopyroxene (O´Brien et al. 1992). The metagabbros show intense retrogressive overprint, especially below 6000 m (Fig. B.3.8).

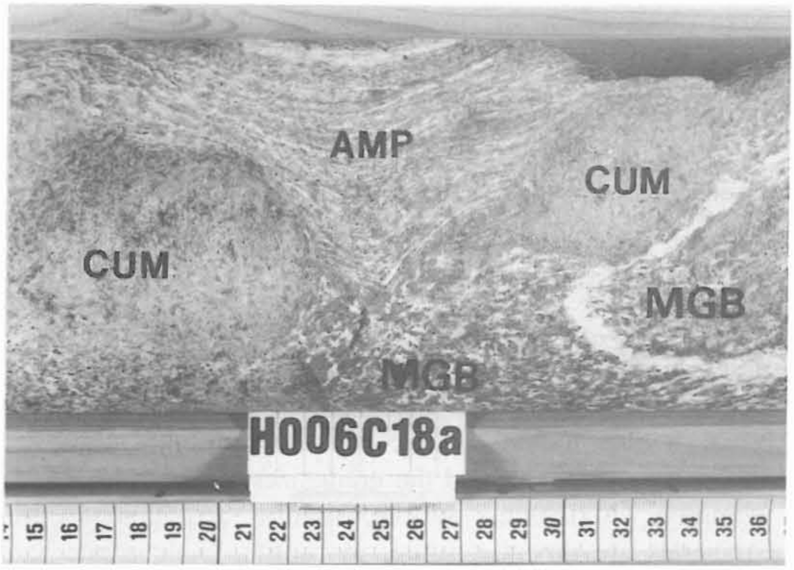

Fig. B.3.3: Lenses of mafic cumulates (CUM) as dislodged slices within strongly deformed metagabbro (MGB) with transitions to banded amphibolite (AMP).

(HB, 4513.4 m depth, sample H006C18a).

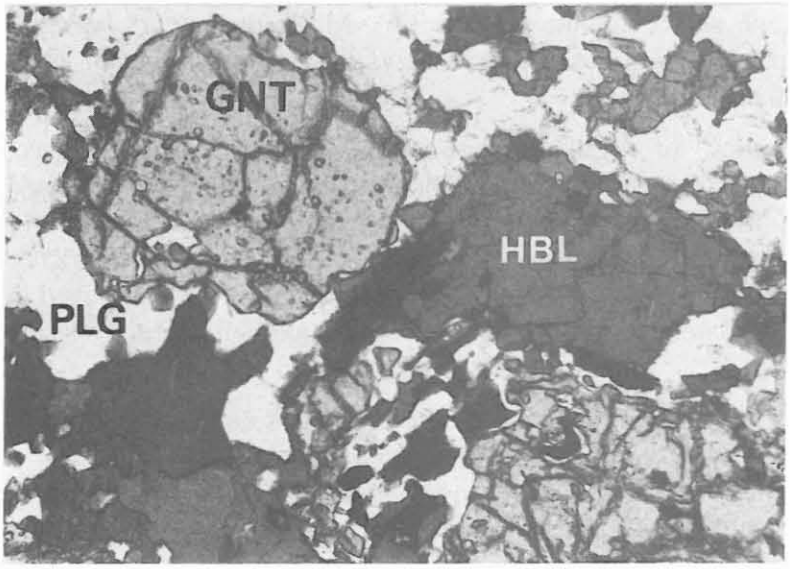

Fig. B.3.4: Amphibolite with hornblende (HBL), garnet (GNT) and plagioclase (PLG).

(HB, depth 4449.31 m, sample H015D30a, one polarizer, width of view 2.23 mm).

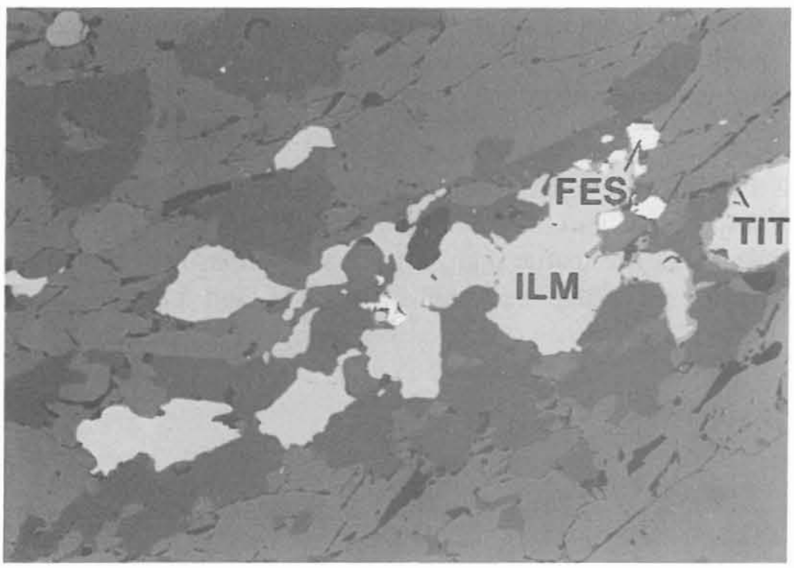

Fig. B.3.5: Typical ore mineral assemblage in amphibolite: ilmenite (ILM), with a small rim of titanite (TIT), few monoclinic pyrrhotite (FES).

(HB, depth 4251.22 m, sample H003A4, air, one polarizer, width of view 0.95 mm).

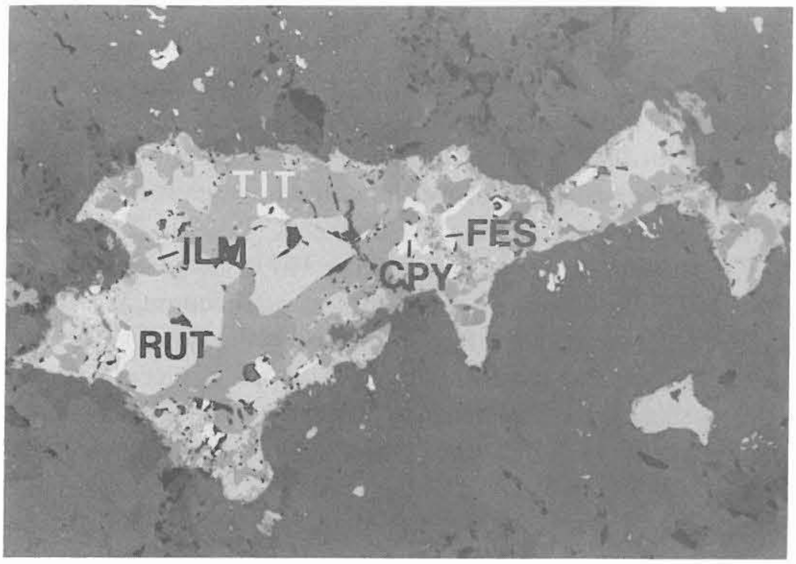

Fig. B.3.6: Ilmenite (ILM) is almost totally replaced by rutile (RUT), titanite (TIT) and pyrrhotite (FES) and contains inclusions of chalcopyrite (CPY) in strongly altered amphibolite.

(HB, depth 6242.45m, sample H024A2r, one polarizer, width of view 1.40 mm).

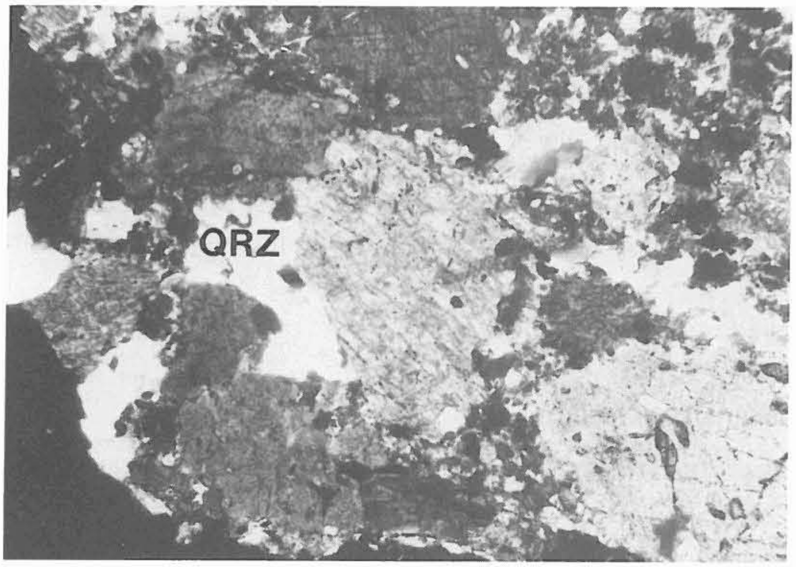

Fig. B.3.7: Quartz-rich amphibolite (QRZ).

(HB, depth 7190 m, sample HCK 7190, crossed polarizers, width of view 1.50 mm).

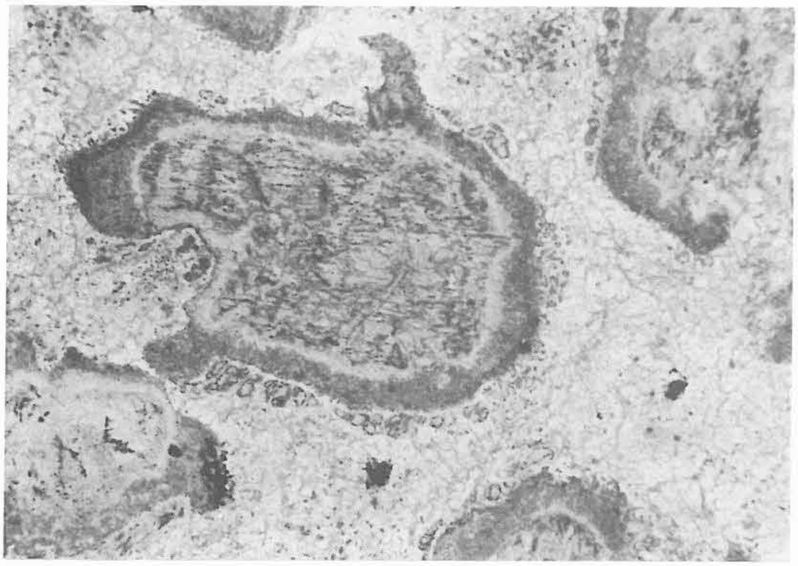

Fig. B.3.8: Metagabbro with intense retrograde overprint.

(HB, depth 6654 m, sample HCS 6654-1, one polarizer, width of view 7 mm).

Garnet is partially or completely replaced by chlorite. Clinopyroxene, clinopyroxene-plagioclase symplectites and brown Ti-rich hornblendes are replaced by several generations of Si-rich hornblendes (Mg-rich hornblende, actinolitic hornblende and actinolite; Duyster et al. 1993). Further descriptions of the fabric are found in Schalkwijk (1991) and Lich et al. (1992). The metagabbros of the KTB HB show a primitive tholeiitic composition with enriched MgO, Cr and Ni contents (chapter H) and low concentrations of incompatible trace elements (Zr, Y, Nb and P_2O_5; Hoffmann 1993). **Mafic cumulates** are rare in the KTB HB. They were observed at a depth of 182-184 m, 1268 m (cuttings), 4513.4 m (core H006 C18a, Fig. B.3.3), 4975 m (cuttings) and 5014 m (core H011). In cuttings, the amount of mafic cumulates is less than 2 vol.-% (e.g. Godizart et al. 1991). The main rock forming minerals are hornblende with inclusions of clinopyroxene, chlorite, actinolite and minor amounts of talc. Accessories are ilmenite, chromian spinels, magnetite, rutile, pyrrhotite, chalcopyrite and pentlandite. The mafic cumulates are classified as hornblendites and (talc-)chlorite-hornblende felses and correspond to the meta-ultramafitites found in the KTB VB (e.g. von Gehlen et al. 1990). The petrological observations as well as the composition of chromian spinels (Kontny 1994) confirm that hornblendites and chlorite-hornblende felses are gabbroic cumulates. The mafic cumulates are high in Cr (1160-2278 ppm), Ni (360-670 ppm) and MgO (15-22 wt-%) and low in incompatible elements (Godizart et al. 1991).

Hornblende gneisses (hornblende-biotite gneisses, biotite-hornblende gneisses) occur in association with amphibolite and/or biotite gneisses. They can be distinguished from amphibolites by higher contents of quartz and biotite and a distinct gneissic fabric. In cuttings samples the discrimination from mobilisate-rich amphibolites is difficult. According to geochemical data they are interpreted as magmatic differentiates of the precursor rocks of the amphibolites and metagabbros.

All metabasites are obviously derived from one magmatic suite.

B.3.2 Amphibolite - hornblende gneiss association

The alternating sequences are characterized by an alternation of metavolcanic and metasedimentary rocks.

Two different types of amphibolites are observed in these sequences.

- **Massive (garnet-)amphibolite**
- **Fine-grained banded amphibolite,** in places with calcsilicate and marble layers

Retrogression to greenschist facies grade and alteration is common in this sequence.

Massive amphibolites are mostly coarse-grained and contain olive-green to yellow-brown hornblende, plagioclase and garnet (Fig. B.3.9).

Fine-grained banded amphibolites show a pronounced stretching lineation. They contain yellow-brown to bluish-green hornblende (ferroan pargasitic to edenitic hornblende; Brätz 1994), plagioclase (oligoclase), epidote, titanite, garnet, actinolite, chlorite, clinozoisite, Fe-Ti-oxides, apatite, K-feldspar and minor clinopyroxene, biotite, quartz and sulfides (pyrrhotite, pyrite and chalcopyrite). Hornblende, rhombic grains of titanite and in some cases Fe-Ti-oxides are aligned parallel to the foliation. In places the fine-grained banded amphibolites contain higher amounts of microcline with cross-hatched twin pattern and varying amounts of apatite. The ore mineral assemblage consists mostly of titanite, ilmenite and pyrrhotite and/or pyrite with little chalcopyrite.

Marble-bearing amphibolite is a special type of fine-grained banded amphibolite occurring in the KTB profile and shows centimeter thick calc-silicate and marble layers (e.g. core H033, see appendix B.9.2, B.9.5 and Fig. B.3.10a and b). This rock type displays high amounts of Fe-Ti oxides (up to 2 vol-% in the hornblende-rich layers and up to 10 vol-% in the calc-silicate layers). The calc-silicate layers consist of clinopyroxene (diopside), plagioclase, epidote, clinozoisite, calcite, titanite, apatite, magnetite and rarely pyrite. Almandine-spessartine appears in the amphibolite and andradite in the marble layers. Numerous calcite-filled fissures crosscut the amphibolite. The contact between amphibolite and marble is marked by a distinct epidote mineralization. The main ore minerals are titanite, ilmenite, magnetite, rutile, ilmeno-hematite, pyrite and minor chalcopyrite. Pyrrhotite is completely absent in this rock type. The oxides reveil a shape preferred orientation parallel to the foliation (Fig. B.3.11).

This amphibolite type occurs in two depth intervals of the KTB drillings, in the VB between 81 and 168 m, and again in the HB between 7320 and 7490 m.

The chemical composition of amphibolites in the variegated sequences reveils transitions from tholeiitic to alkaline character (e.g. Hoffmann 1994), characterized by high contents of e.g. Nb, Zr and Ti.

Ore microscopy shows different replacement relations (Fig. B.3.12) reflecting the retrograde transformation of Fe-Ti-Oxides. The following stages can be distinguished (Kontny & de Wall 1994):

1. Fe^{3+}-bearing ilmenite with exsolution lamellae of Ti-bearing hematite and vice versa,
2. ilmenite with exsolutions of rutile and minor magnetite, recrystallized ilmenite with titanite rims,
3. magnetite and titanite with relics of ilmenite (ilmeno-hematite) and rutile

Stage 2 and 3 predominate, while stage 1 occurs only locally in less altered parts of the rocks.

Mineral chemistry:

The chemical composition of these Fe-Ti-oxides was investigated by microprobe:

- The ilmeno-hematite solid solution varies between $il_{81}hm_{19}$ and $il_{93}hm_7$ with MnO contents between 1.4 and 3.1 wt-%.
- Recrystallized ilmenite in assemblage with rutile and magnetite shows significantly higher MnO contents (8-8.5 wt-%). The Fe^{3+}content is only slightly decreased ($il_{89}hm_{11}$ to $il_{92}hm_8$).
- Magnetite shows no ulvöspinel component (Fe_2TiO_4) and is relativly poor in trace elements. However, Cr_2O_3 content of 0.4 to 1.7 wt-% was measured.

All Fe-Ti-phases show similar V_2O_3 contents (ca. 0.3 wt-%) indicating formation from one source mineral. The significant increase of MnO in recrystallized ilmenite is due to alteration with decreasing temperature. MnO enrichment during alteration is a typical phenomenon of ilmenite in the KTB profile (Kontny 1994). The lack of an ulvöspinel component in magnetite excludes a high temperature formation. The ilmenite component in hematite (0.3 mol-%) suggests an antiferromagnetic behaviour of the hemo-ilmenite solid solution (see chapter D.4.2).

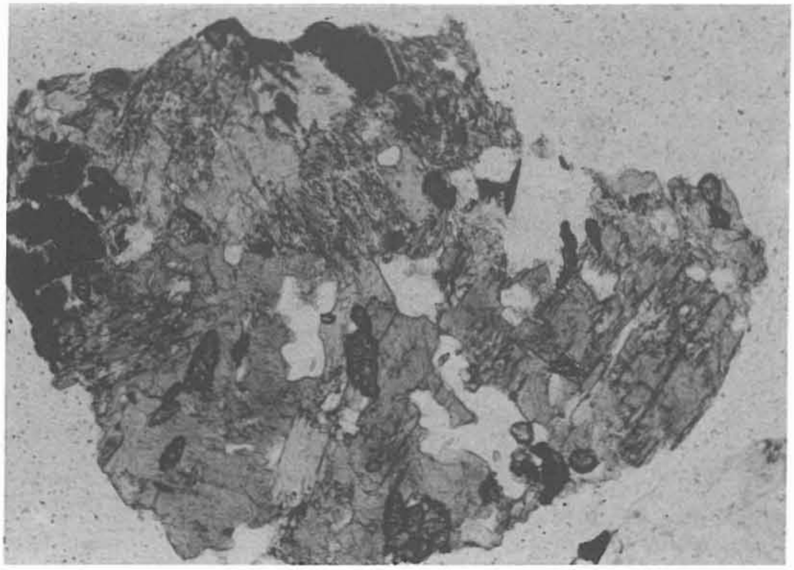

Fig. B.3.9: Massive amphibolite with pale-green hornblende, quartz, saussuritized plagioclase and titanite.

(HB, depth 8888 m, sample HC8888, one polarizer, width of view 1.78 mm).

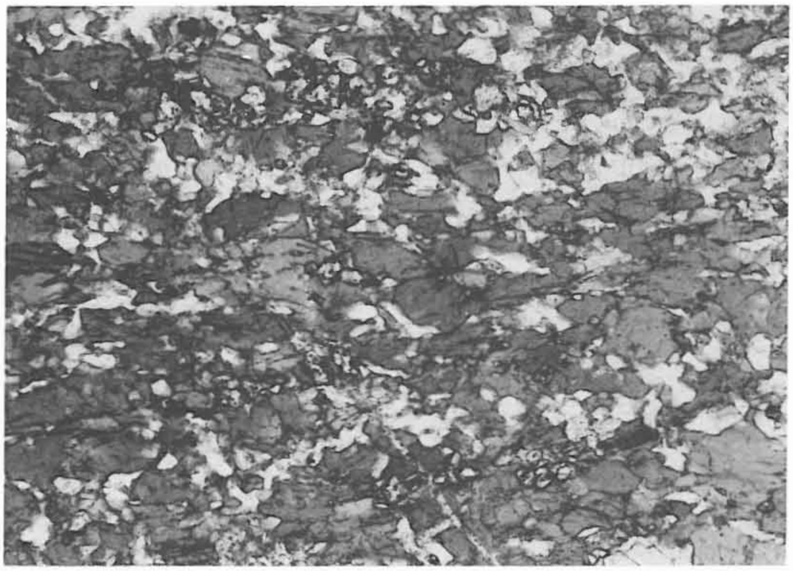

Fig. B.3.10: Fine-grained banded marble-bearing amphibolite with pronounced foliation.

a: amphibolite-rich layer with hornblende, chlorite, plagioclase, and relics of ilmenite and rutile in titanite,

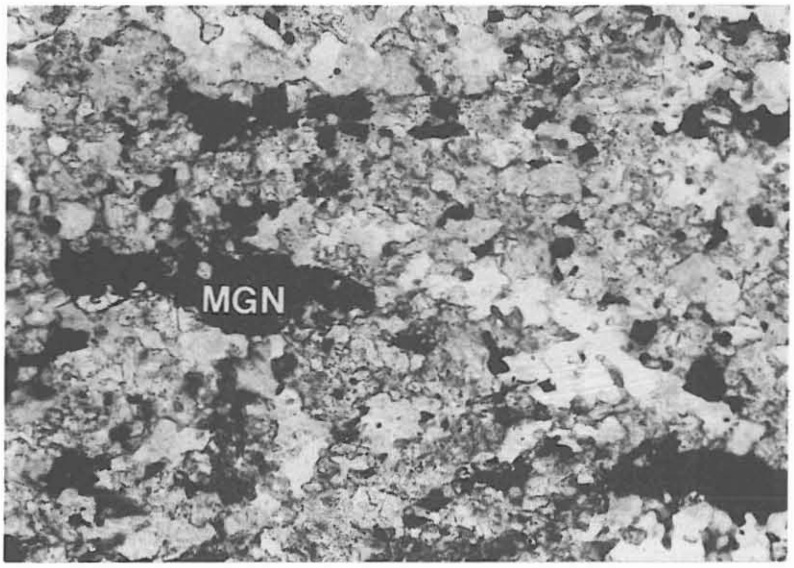

b: magnetite-rich (MGN) calc-silicate layer with plagioclase, hornblende, diopside and chlorite.

(HB, depth 7400.3 m, sample H033B8a, one polarizer, width of view 2.60 mm).

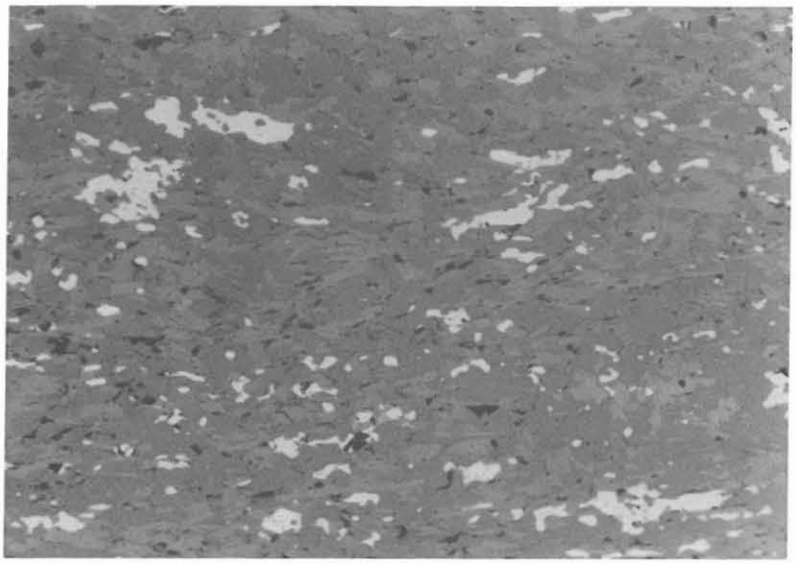

Fig. B.3.11: Fe-Ti-oxides (magnetite, ilmenite, rutile, see Fig. B.3.12) reveal a shape preferred orientation parallel to the foliation, marble-bearing amphibolite.

(HB, depth 7440 m, sample HC7440, air, one polarizer, width of view 1.50 mm).

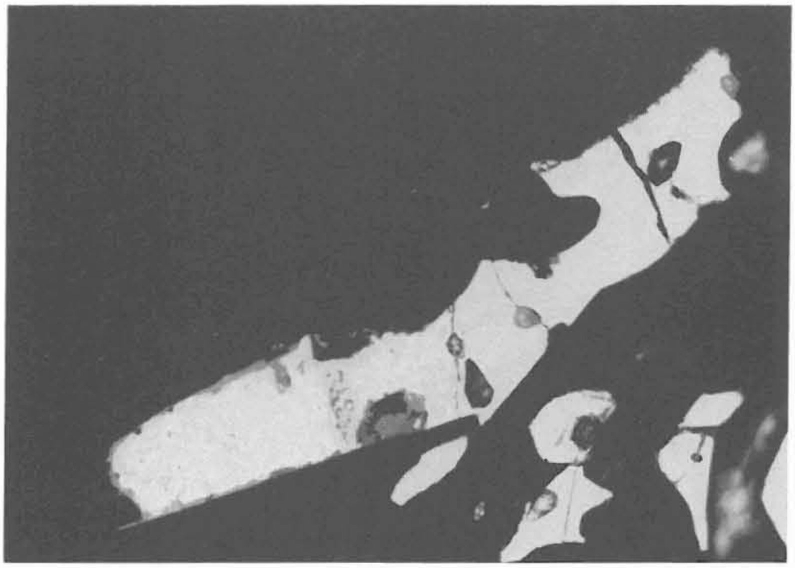

Fig. B.3.12: Alteration stages 1 and 2 of Fe-Ti-oxides in marble-bearing amphibolite (see text).

(HB, depth 7440 m, sample HC7440, oil immersion, one polarizer, width of view 0.35 mm).

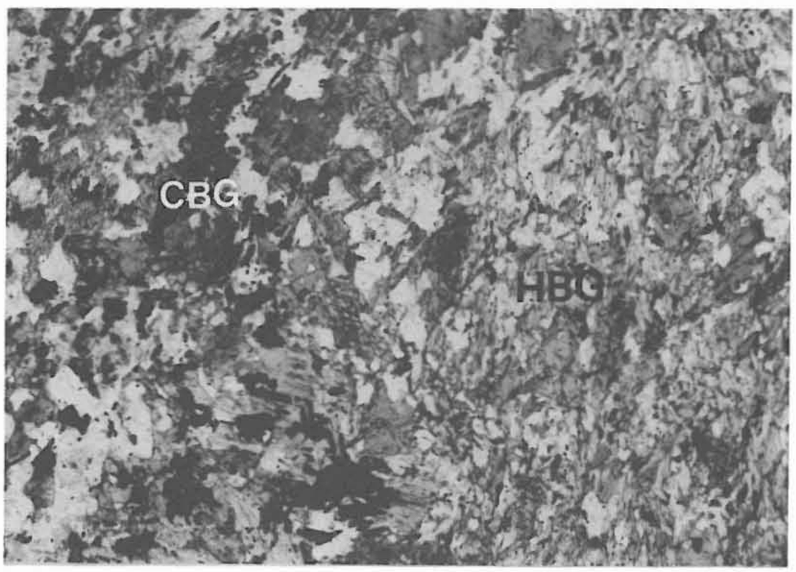

Fig. B.3.13: Contact zone of foliated hornblende-biotite gneiss (HBG) and chlorite-biotite gneiss (CBG) with high ore mineral content (pyrrhotite and graphite, see Fig. B.3.14).

(HB, depth about 9089 m, sample H035A3TII, one polarizer, width of view 5.62 mm).

Hornblende gneisses

Hornblende-biotite gneisses and biotite-hornblende gneisses are important rock types in the alternating sequences. Sometimes they show a close association with calcsilicate rocks. Plagioclase, quartz, potassium feldspar, hornblende and biotite are the main minerals (Fig. B.3.13). The titanite content is usually high and often layers enriched in pyrrhotite (and graphite) occur (e.g. in samples of core run H035 in layers up to 15 vol.-%, Fig. B.3.14). Oxides (ilmenite and rutile) mainly occur as inclusions in titanite. The hornblende gneisses show a pronounced foliation. Calcsilicate-rich layers contain hornblende, calcite, clinopyroxene, quartz, muscovite and some biotite.

The chemical composition (e.g. SiO_2 and TiO_2 contents) points to a volcano-sedimentary origin of this rock type. They are higher in TiO_2, FeO, MgO, CaO, Na_2O, Sr, V, Cr, Co and Ni and lower in SiO_2 than the paragneisses. Thus, they can be derived from basic detritus, volcaniclastic material or thin basaltic layers in a sedimentary protolith (e.g. Müller & Mingram 1993).

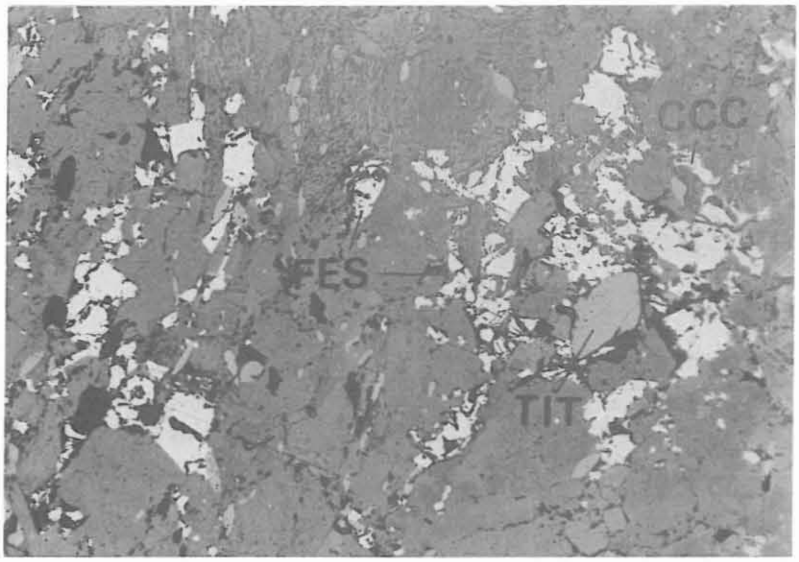

Fig. B.3.14: Titanite (TIT), pyrrhotite (FES) and few graphite (CCC) in hornblende-biotite gneiss.

(HB, depth about 9089 m, sample H035A6T1, air, one polarizer, width of view 1.41 mm.

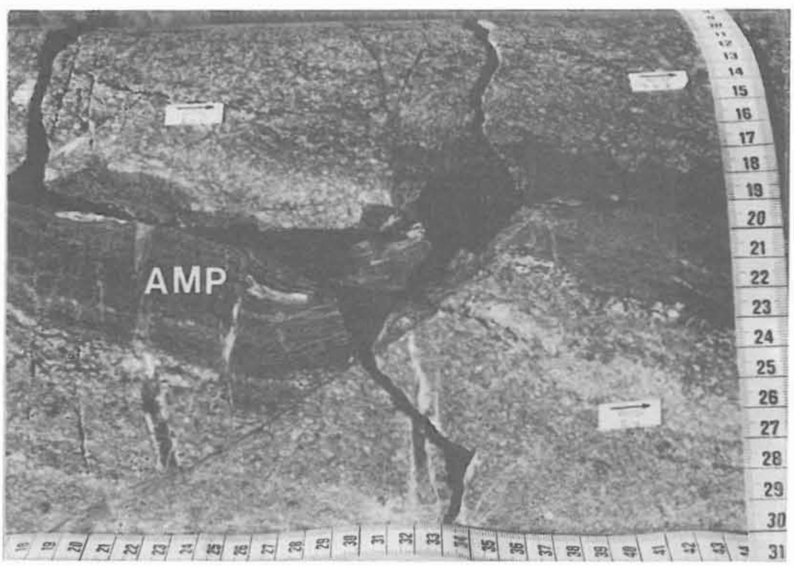

Fig. B.3.15: Macroscopic view of core-section H031B, showing an amphibolite intercalation (AMP) in hornblende gneiss.

(HB, depth 7011.3-7013.3 m)

The amphibolite-metagabbro complexes and the amphibolite - hornblende gneiss associations were probably formed in a single geotectonic setting. The close association of more tholeiitic and more alkaline metabasic types is well documented in core H031 (Fig. B.3.15). Here, a strongly foliated amphibolite intercalation enriched in Nb, typical for the alkaline series, occurs in garnet-bearing hornblende gneiss with tholeiitic composition. In the contact zone between both rock types the hornblende gneiss is significantly less altered. Geochronology has revealed similar ages for both rock types. Generally, the ages obtained for the alkaline series and the tholeiitic series in the KTB profile are 485 $\pm$ 5 Ma (Söllner & Miller 1994) and a more detailed differentiation between the two series is not possible.

B.3.3 Paragneisses

Paragneisses in the KTB HB occur

- **within massive biotite gneiss bodies, with minor intercalations of hornblende gneiss and amphibolite,**
- **as members of gneiss / amphibolite alternations,**
- **as minor intercalations in metabasic rocks.**

For details see appendix B.9.2 and chapter H.

The paragneisses consist of plagioclase (oligoclase), quartz, biotite, garnet, sillimanite and/or kyanite, muscovite and various products of retrogression: chlorite, rutile, sericite and others. Additional, staurolite-bearing gneisses have been described by Schulte & Blümel (1995). Typical ore minerals in the partly graphite-bearing paragneisses are pyrite, pyrrhotite, chalcopyrite, sphalerite, ilmenite and rutile (Fig. B.3.16). Locally, sulfoarsenides, molybdenite and rare minerals like argentian pentlandite occur (Kontny et al. 1994). Graphite occurs as flakes in the gneiss matrix and is enriched in cataclastic shear zones (see chapter B.3.2.1).

Biotite is dark brown and often contains rutile inclusions in the form of sagenite, especially in retrograded gneiss. Chlorite formed from biotite shows sagenite inherited from biotite.

Muscovite has formed at the expense of sillimanite and biotite.

Garnet centers are often rich in inclusions whereas rims are free of inclusions. In some cases, inclusion trails in garnet centers follow an older foliation oriented oblique to the external amphibolite facies foliation (Fig. B.3.17). According to Reinhard et al. (1989), these inclusions are interpreted as relics formed during progressive low-grade metamorphism. Smaller, often euhedral inclusion-free garnets also exist.

Two types of paragneisses occur (Müller 1990, Harms et al. 1993):

Type A gneiss is rich in mica and probably derived from pelitic graywacke. Fibrolite and biotite form anastomosing layers around large quartz- and plagioclase-blasts (Fig. B.3.18). These fibrolite-biotite layers were obviously formed at the expense of garnet during decompression. Fibrolite is often replaced by sericite.

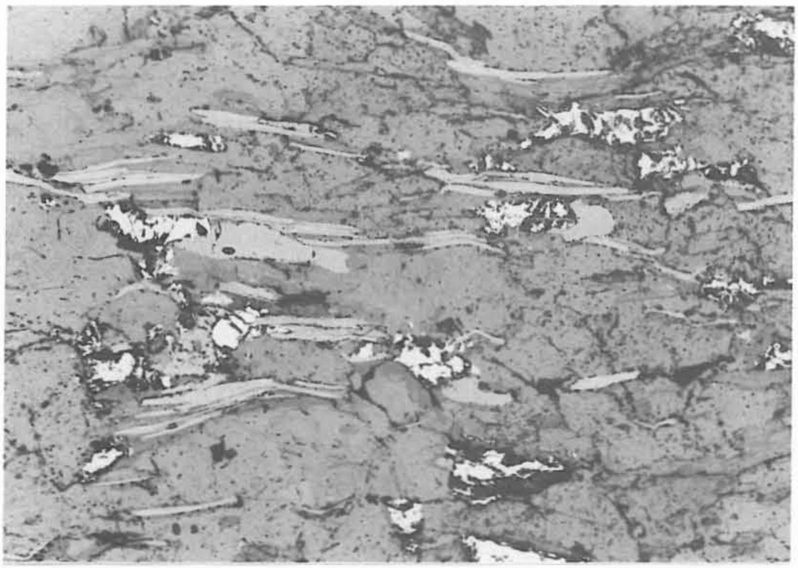

Fig. B.3.16: Typical ore mineral assemblage in paragneiss: pyrrhotite (FES) graphite (CCC) and rutile (RUT) are oriented parallel to the foliation.

(HB, depth about 9089 m, sample H035A6T, air, one polarizer, width of view 1.40 mm).

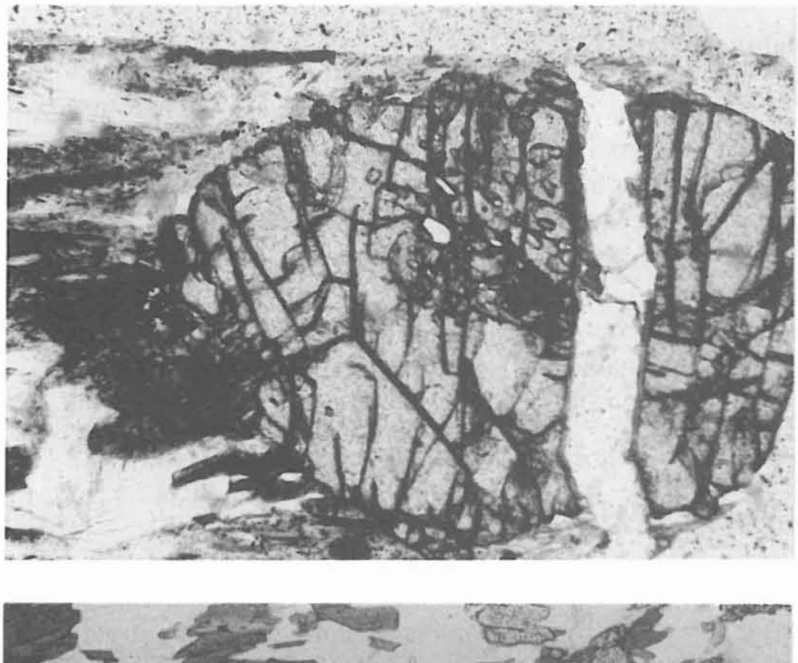

Fig. B.3.17: Garnet in (garnet-) sillimanite-biotite gneiss with inclusions displaying an older foliation oriented oblique to the amphibolite facies foliation.

(HB, depth 512 m, sample HC 0512, one polarizer, width of view 1.42 mm).

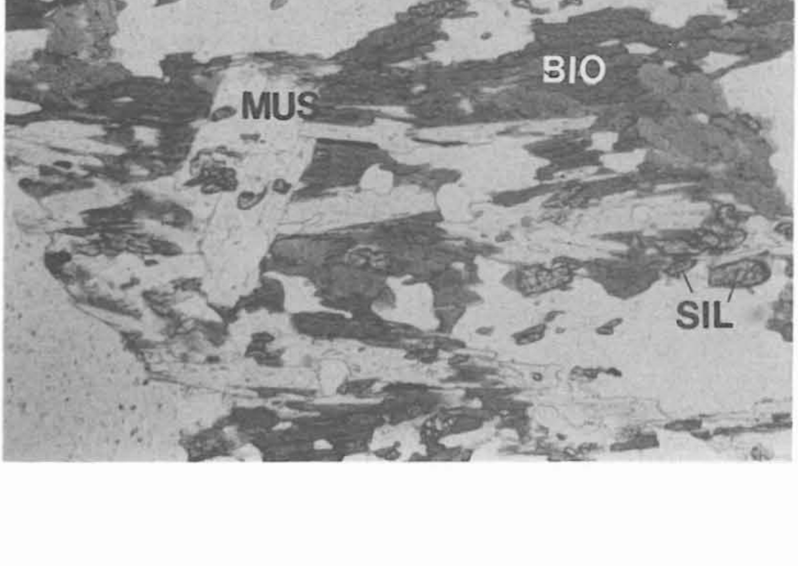

Fig. B.3.18: Biotite-rich (BIO) paragneiss with a distinct foliation of type A with sillimanite (SIL) and transverse muscovite (MUS).

(HB, depth 7952 m, sample HC7952, one polarizer, width of view 1.78 mm).

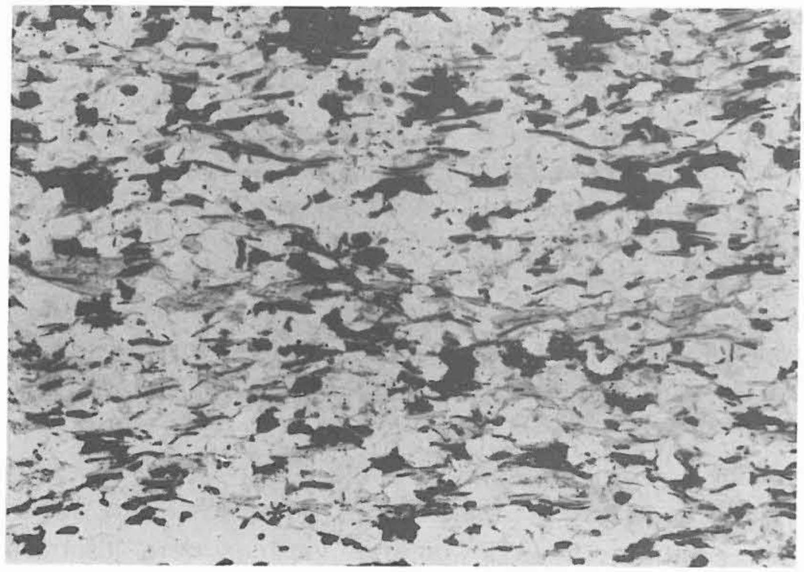

Fig. B.3.19: Quartz-rich paragneiss of type B with equigranular quartz/plagioclase fabric and disseminated fine-grained biotite.

(HB, H035A6T, depth about 9089 m, one polarizer, width of view 5.62 mm).

Type B is rich in quartz, has an equigranular quartz/feldspar matrix and biotite is disseminated (Fig. B.3.19). This rock is derived from graywackes.

In type A gneisses, sillimanite dominates over kyanite, whereas for type B gneisses the opposite holds true. Both gneiss-types are free of cordierite and potassium feldspar. Their mineral assemblage kyanite/sillimanite-garnet-biotite-muscovite-plagioclase-quartz indicates amphibolite facies conditions. Potassium feldspar was only observed in hornblende gneisses and gneisses from metavolcanic sequences.

The whole rock analyses (Müller 1994) suggest a uniform source for the paragneisses. The intimate interlayering of paragneisses and metabasites points to a primary sedimentary contact of paragneisses with tuffites and basalts in the alternating sequences.

B.3.4 Dykes

Different types of magmatic dykes crosscut the metamorphic rocks down to a depth of 7816 m. They can be classified as granitic aplites, calc-alkaline lamprophyres and intermediate types of (monzo-)dioritic composition.

B.3.4.1 Granitic aplite

Aplite occurs in the KTB HB between 3413-3427 m and at a depth of 3609 m. The main rock forming minerals are quartz and plagioclase; the latter is partially sericitized. Furthermore, biotite and sometimes chlorite occur. The identification of granitic aplite in cuttings samples is impeded because the constituent minerals do not differ significantly from those of the metamorphic host rock. The aplites are fine-grained equigranular rocks, which are strongly foliated (e.g. 3413-3427 m) and quite similar to aplites found in the KTB VB (Lich et al. 1992).

B.3.4.2 Calcalkaline lamprophyre

Lamprophyres crosscut the metamorphic rocks down to a depth of 7255 m. They form dykes of up to 5 m apparent thickness, and intruded along faults or lithological contacts (Fig. B.3.20). The macroscopically dense, brown to dark green colored rocks contain dark phenocrysts (< 0,5 mm) and carbonate nodes.

The main components of the lamprophyres are plagioclase, K-feldspar, hornblende and biotite. They are strongly to completely altered. Largely sericitized plagioclase laths and strongly altered hornblende crystals are embedded in a fine-grained groundmass of sericitized feldspar, chlorite, quartz and small leucoxene aggregates (Fig. B.3.21). Dark brown spinel, apatite, largely chloritized biotite and relics of brown hornblende belong to the primary minerals (Keyssner et al. 1988). The preferred orientation of the plagioclase phenocrysts reveals a flow structure (Godizart et al. 1991). Former olivine phenocrysts are totally altered to carbonates, chlorite, actinolite and fine-grained phyllosilicates. Enclosed in phenocrysts spinels and sometimes sulfides (pyrrhotite, chalcopyrite and Co-Ni-sulfides) occur. Along fissures actinolite, epidote/clinozoisite, prehnite, calcite, quartz and adularia have grown. The occurrence of both, extremely fine- grained beside coarser grained varieties, in some cuttings samples points to chilled margins.

The lamprophyres are characterized by a variable ore mineral content. The amount of ore is very small, however, and most of the disseminated ore minerals are difficult to identify due to their very small grain size (often $<10 \mu m$). The following ore minerals were identified (sometimes with help of a microprobe) in order of decreasing quantities:

chalcopyrite, pyrite, sphalerite, pyrrhotite, galenite, spinel (picotite), ilmenite, pentlandite, millerite, cobaltite, siegenite, molybdenite, argentian-pentlandite (?), anatas/rutile, magnetite and graphite.

Sporadically, the contact with the host rock and with gneiss xenoliths is mineralized with thin garlands of pyrite. This pyrite often shows strong cataclasis and is partially replaced by chalcopyrite and sphalerite along fractures. Two-phase inclusions of pyrrhotite and chalcopyrite in the cataclastic pyrite indicate formation temperatures (Sugaki et al. 1975) of $328 \pm 5°C$, if they are cogenetic.

According to their mineralogy the lamprophyres of the KTB HB can be classified as calc-alkaline types (e.g. Rock 1991 and Streckeisen 1979). In the KTB drillings mainly the two calc-alkaline varieties spessartite (predominant in the KTB HB) and kersantite (predominant in the KTB VB) occur.

The spessartites are marked by hornblende as the dominating mafic mineral. Plagioclase predominates over K-feldspar and quartz is lacking. Kersantites show a distinct quartz content, a dominance of plagioclase over K-feldspar, and biotite is the dominant mafic mineral.

Lamprophyres below 6000 m are extremely fine-grained and strongly altered (Duyster et al. 1993). Because of the small amount of lamprophyres in the cuttings samples no chemical analyses are available. In the cataclastic zone at 6700-7260 m, which is related to the Franconian Lineament, lamprophyres are common. Unfortunately none of the cores include lamprophyres in the KTB HB.

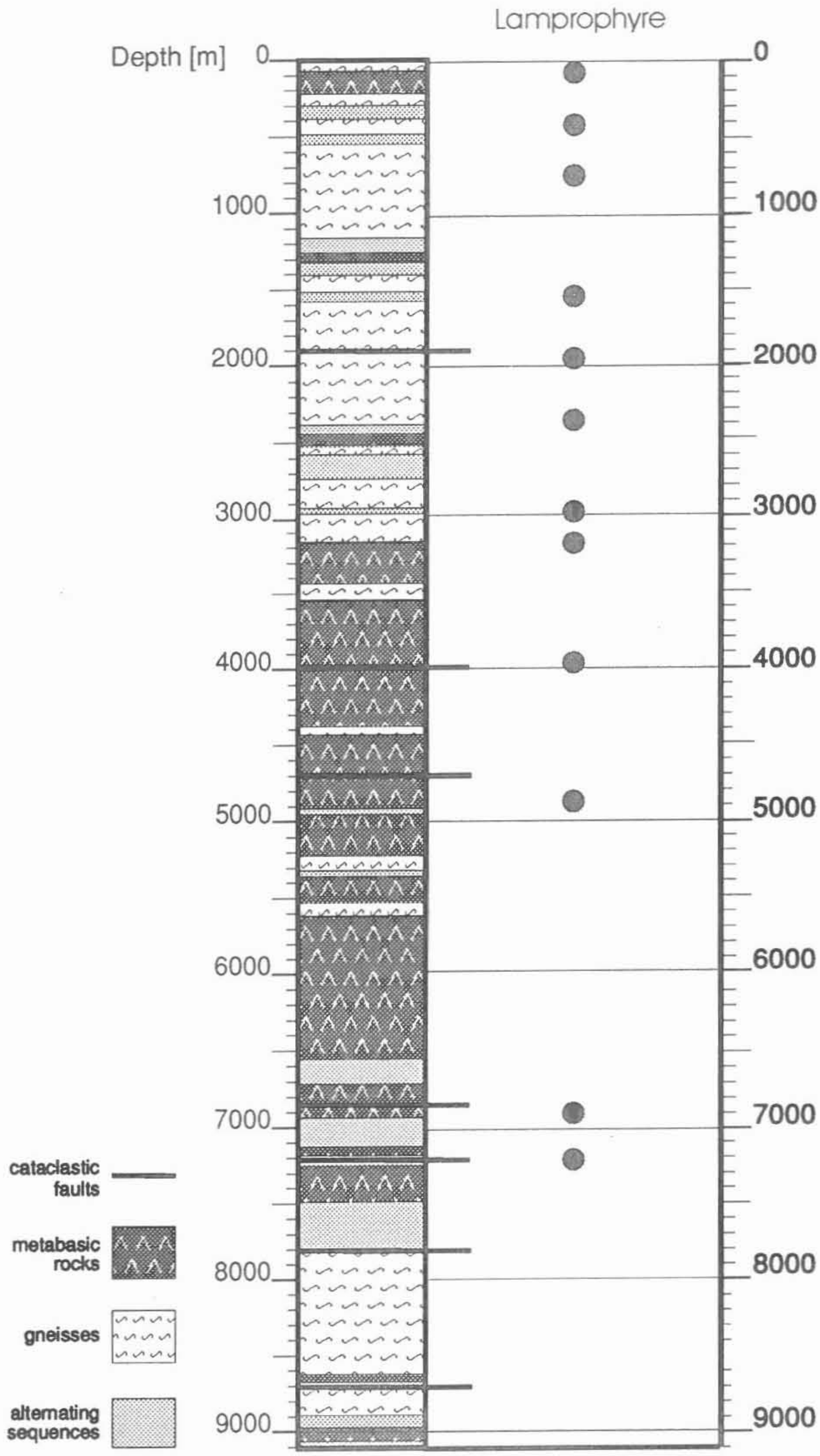

Fig. B.3.20 Occurrence of lamprophyre in the profile of the KTB HB

Besides the occurrence of lamprophyre fragments in the cuttings samples, a reliable indicator for the exact position is a significant increase of the natural γ-ray activity recorded by bore hole logging. For the HB, structural data of the dykes and their orientation to host rock are lacking. Lamprophyres from VB cores display xenoliths of cataclastically overprinted host rock. Therefore, the dykes are of the same age or younger than the cataclastic deformation of the rocks (Röhr et al. 1990). Ar-Ar age determinations (Kreuzer et al. 1993) of 306 Ma were corroborated by Rb-Sr whole rock analyses, which yielded a late Variscan intrusion age of about 306 ± 5 Ma (Henjes-Kunst, pers. com.). Earlier K-Ar determinations by Kreuzer et al. (1990) on lamprophyres from the western Bohemian massif yielded about 295 Ma.

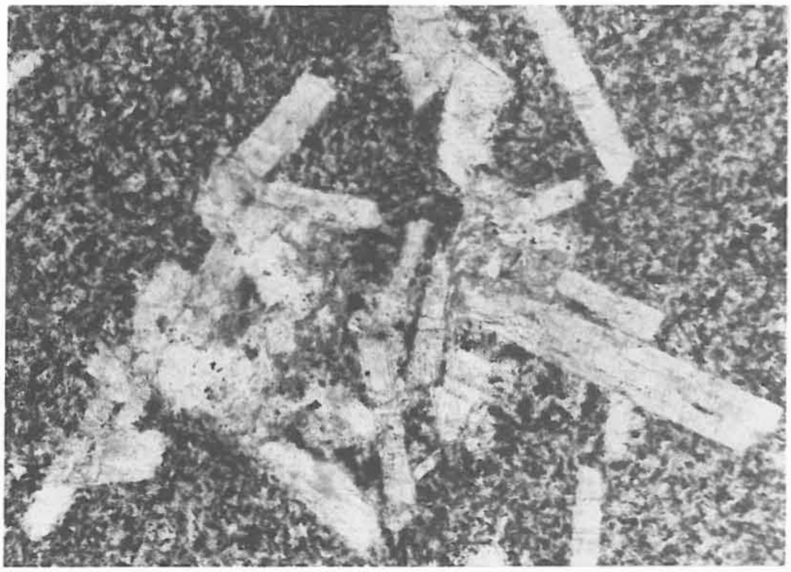

Fig. B.3.21: Sericitized plagioclase laths embedded in fine-grained matrix of sericitized feldspar, chlorite and quartz.

(HB, depth 756 m, sample HC0756, one polarizer, width of view 1.78 mm).

B.3.4.3 (Monzo-)Diorite

These rocks occur sporadically in small proportions in cuttings, especially in the range between 7663 and 7673 m and between 7812 and 7816 m. After the classification of Streckeisen (1976) for granitic rocks based upon modal composition in volume % the essential mineral composition corresponds to monzodiorite or diorite. Plagioclase constitutes about 85-90 %, K-feldspar 5-10 % and quartz < 5 % of the felsic minerals. Mafic minerals are chlorite, actinolite, biotite with rutile needles, epidote, calcite and titanite. Ore minerals are rare, sometimes euhedral pyrite can be found.

Medium- to coarse-grained subhedral to porphyritic microstructures can be observed in small cuttings (Fig. B.3.22). Some samples show radial to sheaf-like biotite-clots and very low quartz contents. The mineralogical composition and especially the microstructure resembles those of monzo-diorites, which are widespread in the area as small intrusions related to the Variscan granites. The diorites belong to a hybrid gabbroic to tonalitic rock suite, regionally termed Redwitzit. These compare to appinites and other mafic granitoids related to late-orogenic granites, but are usually known as sheet intrusions or stocks (Siebel 1993). Radiogenic isotope studies imply a genetic link to the lamprophyres (Harms & Hölzl 1994, Siebel 1994). The very rare occurrence of fragments of these monzo-diorites in the KTB HB cuttings points to very small intrusions or sills. More detailed studies requiring large samples are precluded.

Fig. B.3.22: Diorite with biotite phenocrysts pseudomorphically replaced by chlorite in a groundmass of plagioclase, chlorite and actinolite.

(HB, depth interval 7663-7673 m, sample HCK 7663-7673, one polarizer, width of view 2 mm).

B.4 Metamorphic history

The metabasites have recorded a polyphase metamorphic evolution from an early eclogitic to granulitic stage followed by an amphibolite facies and a late greenschist facies overprint (Fig. B.4.1, Röhr et al. 1990, O`Brien et al. 1992, Schalkwijk & Stöckhert 1992). On the contrary, the paragneisses reveal only the amphibolite facies stage and the late greenschist-facies overprint (Reinhard 1989).

B.4.1 High pressure and amphibolite facies metamorphism

B.4.1.1 P/T Conditions

High pressure metamorphism

Eclogite facies relics preserved in metagabbros are inclusions of zoisite, kyanite and omphacitic pyroxene in corona garnet, resulting from the high pressure plagioclase breakdown preceding garnet crystallization (Röhr et al. 1990, Schalkwijk 1991, O'Brien et al. 1992). Pressure estimates for this reaction yield a minimum of 14 kbar.

Garnet granulite facies metamorphism

In coronitic metagabbros the paragenesis garnet - clinopyroxene - plagiclase - hornblende -Ti-phase (ilmenite or rutile) is found in garnet coronas around clinopyroxene. This documents metamorphism under garnet granulite facies conditions. Thermobarometric calculations of Schalkwijk (1991) yielded temperatures around 750°C at a minimum pressure of 12 kbar.

Pervasive amphibolite facies metamorphism with partial melting

After eclogite and garnet granulite facies metamorphism, the metabasites suffered pervasive reequilibration under amphibolite facies conditions. The mineral assemblage hornblende - plagioclase - biotite - quartz - garnet - ilmenite ± titanite ± pyrrhotite was stable.

Leucocratic plagioclase-quartz layers are very common in the metabasites. Both, undeformed and strongly deformed layers can be observed. These layers are mobilisates formed by partial melting under amphibolite facies conditions. The mobilisates cross-cut an older foliation. Large, mm-sized hornblende clasts are characteristic for the mobilisates.

According to Reinhard (1989) the garnet zonation in the paragneisses reflects a prograde metamorphic evolution with maximum conditions of 650°C and 8-10 kbar. Eclogite facies and granulite facies metamorphic relics that have been preserved in the metabasites, were not observed in the paragneisses. Either, the paragneisses and the metabasites suffered a different early metamorphic history and were brought together on the retrograde path under amphibolite facies conditions, or the record of the first metamorphic stages is not preserved in the paragneisses.

B.4.1.2 Deformation during early high pressure and later amphibolite facies metamorphism

Schalkwijk (1991) differentiates two deformation events:

- „**first generation shear zones**“ are crosscut by mobilisates formed during the later partial melting event,
- „**second generation shear zones**“ locally deform these mobilisates.

In deformed mobilisates, quartz is concentrated in lenses and asymmetric pressure shadows around plagioclase clasts, their asymmetry reflects the sense of shear. Quartz c-axis distributions measured in deformed quartz-plagioclase aggregates display a pronounced preferred orientation (> 10 multiples of random distributon) with maxima at a small angle to the stretching lineation. This type of preferred orientation is interpreted to reflect the predominance of prism <c> slip (e.g Blumenfeld et al. 1986). Activation of this glide system requires high temperatures and consequently the related type of preffered orientation is exclusively observed in high temperature tectonites.

B.4.2 Deformation and alteration under greenschist and subgreenschist facies conditions

Except for local shear zones, greenschist facies overprint has never gone to completion. In the vicinity of fault zones the rocks show a strongly enhanced alteration. Hornblende and garnet are transformed partially or fully to chlorite, epidote, actinolite and clinozoisite. Biotite is replaced by chlorite and titanite. Plagioclase is sericitized and saussuritized. Formation of new quartz and sometimes of sulfides can be observed.

Alteration processes mainly lead to a redistribution of elements between main and accessory minerals whereby the metal content of the hole rock remains constant (Giese & Möller 1993). The strong alteration of ilmenite into leucoxene and/ or titanite correlates with the alteration of the host rock. The replacement of ilmenite by Ti-phases which do not incorporate Mn in their lattice causes an enrichment of Mn in ilmenite up to about 9 wt-%. With proceding alteration this Mn is released from the decaying ilmenite into solution and incorporated into newly formed minerals like chlorite. The Mn content of chlorites ranges up to 0.8 wt-% (Kontny 1994).

In contrast, cataclastic shear zones show a distinct chemical pattern compared to the host rock (Palm et al. 1994). Here, different strain rates and a higher fluid/rock ratio than in the less deformed host rocks cause an increased element mobility.

B.4.2.1 Graphite-bearing shear zones

Graphite occurrences in the VB and HB can broadly be classified into three groups:

- graphite formed from metamorphosed organic matter in paragneisses; here graphite crystallinity indicates temperatures of about 700°C (Reutel 1992) which is consistent with other geothermometers (see chapter B.4.1).
- graphitic cataclastic zones, where graphite was most probably deposited from a fluid (see below) and
- disseminated graphite flakes in some portions of metagabbros and amphibolites (e.g. Bartels 1994, Pasteris 1993)

Graphite enrichment along reverse faults is a characteristic feature in paragneisses and locally in the alternating sequences (e.g. 0-518 m, 2386-2718 m, 6600-7260 m, see appendix B.9.2). Graphitic reverse faults are very common and have caused break-outs in the bore hole wall. According to structural investigations of Zulauf (1992) the graphitized shear zones were formed in late Carboniferous times. Deformation mechanisms and mineral assemblages suggest formation temperatures of about 300°C.

Graphite in shear zones is predominately associated with chlorite, saussuritized plagioclase (Fig. B.4.1) and sometimes Fe-sulfides (mainly pyrite in the upper parts of the profile and pyrrhotite below about 8000 m). With the thermodynamic model of Walshe (1986) formation temperatures for chlorite, associated with graphite, were calculated (Table B.4.1). The mean temperatures range from 250-280°C. The Al^{IV}-thermometer of Catelineau (1988), systematically yields values higher by about 40-60°C (Kontny 1994).

Table B.4.1: Calculated formation temperatures of chlorite from graphitized shear zones of the VB and HB. The calculations are based on the thermodynamic model of Walshe (1986). T: mean temperature, (): T_{min}-T_{max}

Depth (m)	Lithology	n	T(°C)	Fe/(Fe+Mg)
VB 3039	paragneiss	11	264 (235-277)	0.557
VB 3191.4	paragneiss	6	250 (228-272)	0.519
VB 3386.4	paragneiss	12	258 (241-273)	0.563
HB 7012	alternating sequence	21	279 (246-340)	0.446

The deposition of graphite in cataclastic zones from a C-O-H fluid was discussed by Walther & Althaus (1989) and Ziegenbein et al. (1989) assuming a reaction $CO_2 + CH_4 = 2C + 2H_2O$. Although the $\Delta G(T)$ of this reaction is negative, the magnitude is very small and the progress of this reaction might be inhibited by a relatively high activation energy (Walther & Althaus 1993). Therefore, these authors suggested, that the activation energy for this process was provided by tectonic activity in the cataclastic shear zones.

Active enrichment of carbon in the graphitized shear zones is supported by models on volume change and mass transfer within shear zones (Palm et al. 1995). These authors have observed that the carbon content in shear zones is increased compared to the wall rock.

The association of graphite with Fe-sulfides (Fig. B.4.2) and the enrichment of both - C and S - in shear zones (see Fig. B.6.1) implies that the Fe-C-O-S system should be considered. Graphite-forming reactions involving sulfate and methane (e.g. $2FeS + 2SO_4 + 3CH_4 + 4H^+ =$

$3C + 2FeS_2 + 8H_2O$) are much more efficient concerning their $\Delta G(T)$ in the temperature range 250-350°C as the previously suggested reaction in the C-O-H system (Möller pers. com.).

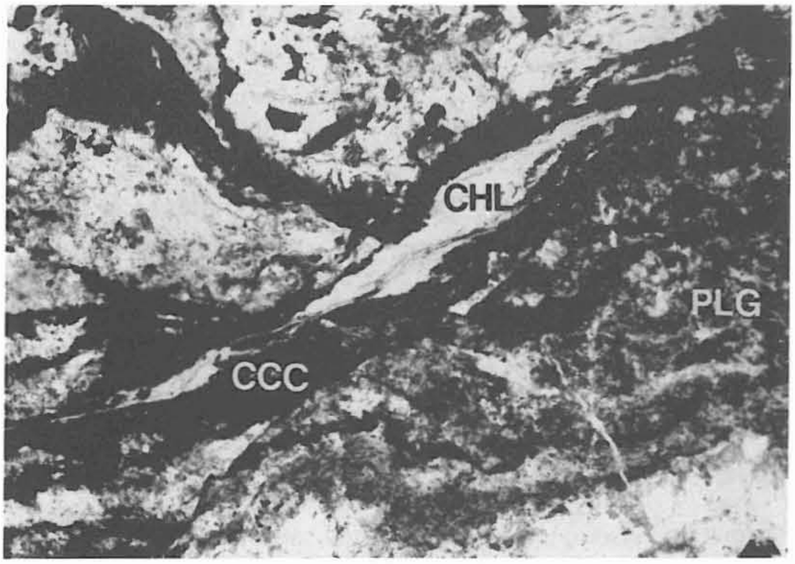

Fig. B.4.1: Shear zone with graphite (CCC), chlorite (CHL) and saussuritized plagioclase (PLG) in hornblende gneiss.

(HB, depth 7012 m, sample H031B4z, one polarizer, width of view 2.83 mm).

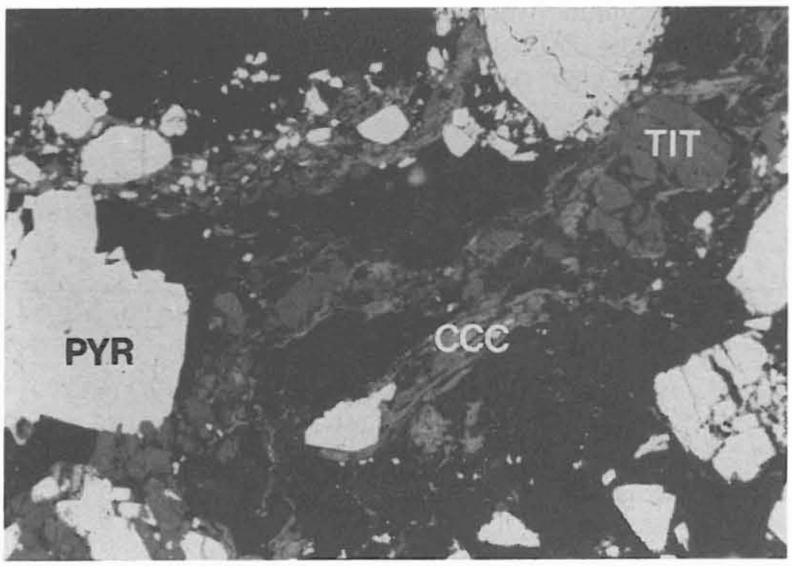

Fig. B.4.2 : Cataclastic pyrite (pyr) and titanite (TIT) with graphite (CCC), cataclastic amphibolite.

(HB, depth 6960 m, sample HC6960, air, one polarizer, width of view 0.7 mm).

B.4.2.2 Chloritization

The most intensely altered rocks were drilled in a gneiss-amphibolite intercalation at a depth of 7490-7650 m in the 4th borehole (see chapter A). The alteration has resulted in the formation of chlorite gneisses and chlorite felses. The metasomatic reaction is accompanied by a distinct depletion of Na, K, Rb, Sr and Si and a remarkable enrichment of Mg (Fig. B.4.3). The chlorite content of the metasomatized rocks, estimated from XRD bulk analyses, reaches up to 50 wt-% and the H_2O content up to 7.5 wt-%.

The composition of the chlorites is variable (Table B.4.2). Intermediate chlorites (type 1) predominate in the gneisses, Mg-rich chlorites(type 2 and 3) in the chlorite felses (Table B.4.2).

Table B.4.2 : Chemical analyses of different types of chlorites and calculated formation temperatures in the chlorite zone 7490-7650 m of the KTB HB.

Chlorite varieties	Chl 1	Chl 2	Chl 3
n	8	7	13
SiO_2	27.85	26.36	25.25
Al_2O_3	20.31	18.33	18.61
FeO	13.19	23.24	28.45
MgO	23.91	17.76	13.55
MnO	0.10	0.72	0.64
Total	85.39	86.45	86.57
Si	2.81	2.80	2.76
Al(IV)	1.18	1.20	1.24
tet	4	4	4
Al(VI)	1.24	1.10	1.24
Fe	1.12	2.07	2.60
Mg	3.61	2.81	2.21
Mn	0.01	0.07	0.06
okt	5.97	6.05	6.04
Fe/(Fe+Mg +Mn)	0.24	0.42	0.53
T(C°)C	319	324	337
T(C°)W	269	294	298
$\log(fO_2)$	-31.57	-32.01	-34.31
$\log(fS_2)$	-9.74	-10.21	-11.53

Chl 1 : Chlorite fels (Fe-clinochlore)
Chl 2 : Chlorite aggregates from fissures (Fe-clinochlore)
Chl 3 : Chlorite gneiss (Mg-chamosite)
T(C°) C : Temperature calculated after Cathelineau (1988)
T(C°) W : Temperature calculated after Walshe (1986)

Chlorites of type 1 and 2 form pseudomorphs after biotite and amphibole in the gneisses and amphibolites and enclose titanite along cleavage planes. The MnO contents range between 0.6 wt-% (type 1) and 0.7 wt-% (type 2). The Mg-rich chlorite (type 3) with low Mn contents has grown from hydrothermal fluids. Microscopically it is characterized by an irregular fabric.

The fluid involved in the metasomatism has been able to

- dissolve SiO_2 and remove it in solution
- supply Mg

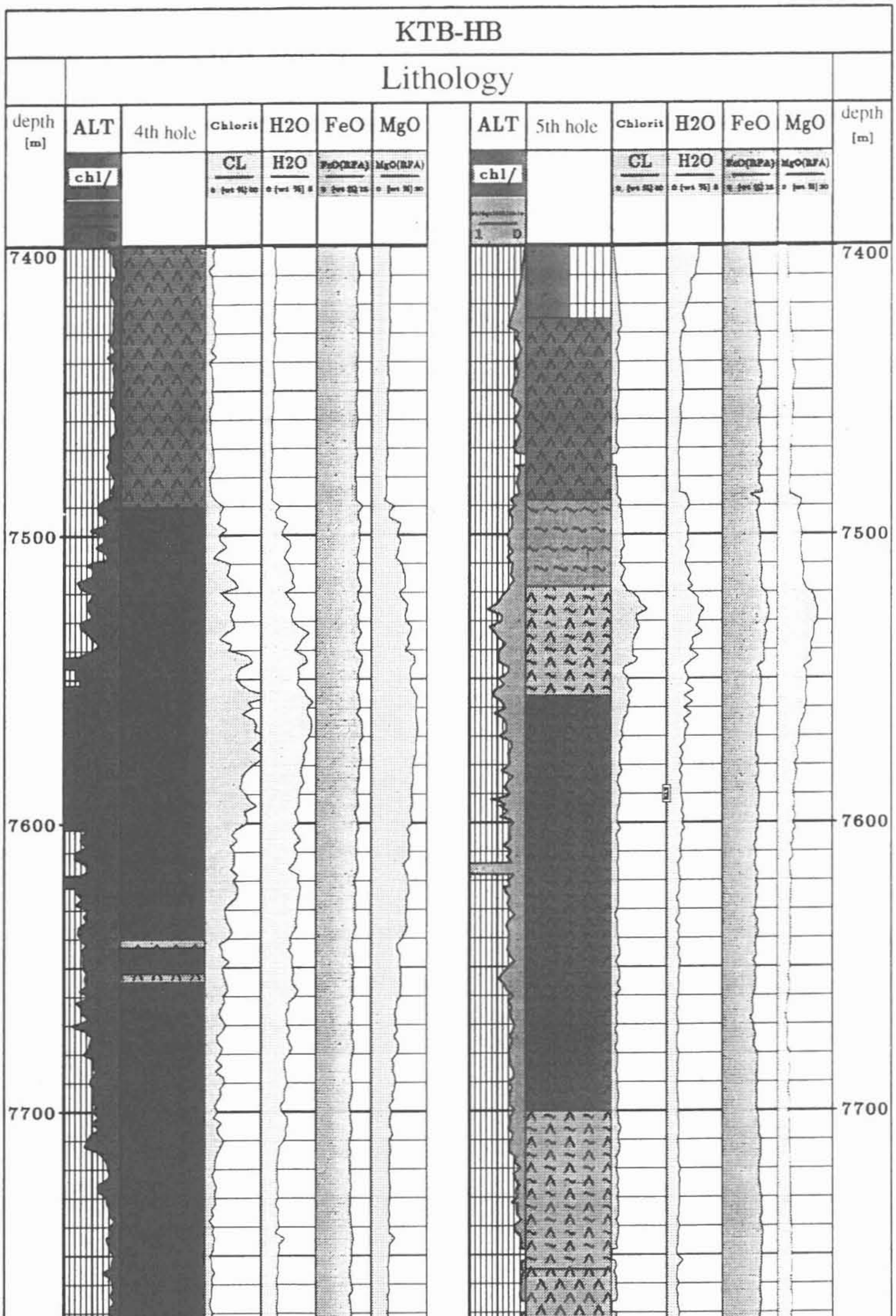

Fig. B.4.3: Chlorite-, H_2O-, FeO- and MgO-contents (XRD and XRF data) versus depth (4th and 5th borehole KTB HB, see chapter A).

- oxidize, as indicated by the chlorite chemistry (Table B.4.2 and Fig. B.4.4) and the associated minerals (new formation of pyrite and hematite)

The chlorite formation temperatures are calculated as 270-300°C, based on the thermodynamic model of Walshe (1986), Table B.4.2, and 320-330°C, based on the empiric Al^{IV}-thermometer of Cathelineau (1988).

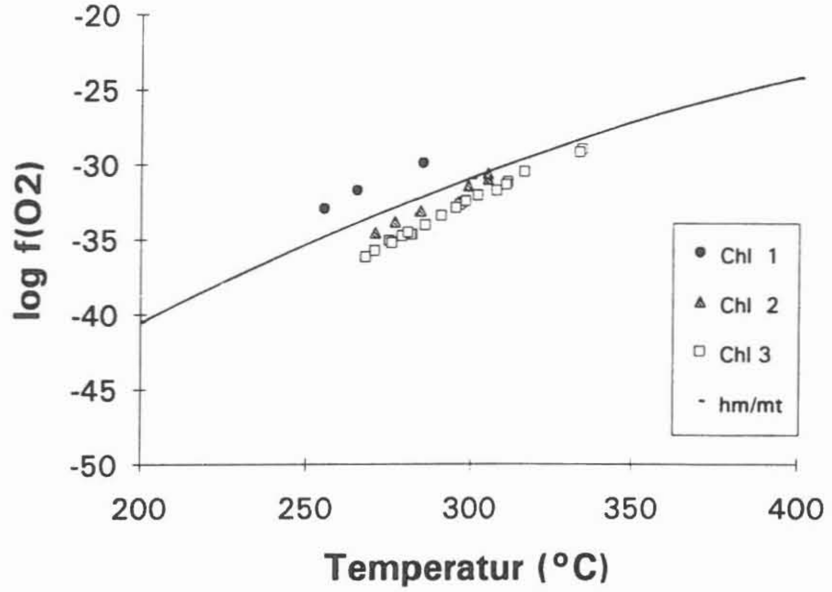

Fig. B.4.4: Log $f(O_2)$-temperature diagram of different types of chlorite (chl1 - chl3 see Table B.4.2, hm/mt: hematite-magnetite buffer). Temperatures and $f(O_2)$ values calculated from the thermodynamic model of Walshe (1986).

B.4.2.3 Faults and veins

Mineralization on fissures and fault-planes from cores of the KTB VB and HB were investigated by Zulauf (1990, 1992) and Borchardt (1993, 1994). In the KTB HB coring started below 4000 m depth. For additional information about the occurrence of vein minerals cuttings samples from 4800 m to the final depth of 9101 m were investigated in thin sections. A large quantity of data is available due to a maximum intervals of 4 m. However, information on the orientation or age-relations of joints cannot be obtained from cuttings. Therefore, these investigations rather complement the data gained from the cores.

Figure B.4.5 shows the frequency of veins and the kind of vein mineralization for the depth interval of 4800-9100 m. Idiomorphous crystals of prehnite, laumontite, epidote, clinozoisite, adularia, quartz, actinolite and tourmaline occur. The following vein mineral assemblages are observed:

- laumontite-epidote-calcite
- laumontite-calcite-quartz
- prehnite-calcite-quartz-chlorite
- prehnite-actinolite-clinozoisite/epidote-calcite-quartz
- prehnite-adularia-calcite
- epidote-calcite-quartz
- quartz-tourmaline-chlorite
- adularia-calcite-quartz

Fissures and pores are generally filled by vein minerals which are characterized by variable features (Zulauf & de Wall 1994). Euhedral shape of the minerals indicates crystal growth from solution into porous zones and open fissures.

Distinct mineral assemblages have formed in the different lithological units.

Metabasites: prehnite, epidote, clinozoisite, calcite, chlorite, adularia, quartz, sericite, actinolite and tourmaline

Gneisses: laumontite, calcite, quartz, chlorite, adularia, sericite.

Prehnite was observed in amphibolite-cuttings down to about 7650 m depth in aggregates of up to 2 mm size. Numerous mineralizations show an increase of grain size of up to 500 µm towards the centre of the fissure. *Epidote* occurs in veins in metabasites down to about 8000 m. Euhedral crystals occur as vein fillings in aggregates of up to 1 mm size. Epidote sometimes replaces plagioclase. *Clinozoisite*, often euhedral, increases with depths. It formed by the decay of hornblende to biotite and occurs until the final depth (Fig. B.4.6). *Adularia* was observed in metabasites as well as in gneisses and becomes more widespread with depth. It is often euhedral. Crystals have grow from the rim towards the centre of the vein. Frequently it can be found in cataclastic gneisses or in assemblage with prehnite in cataclastic amphibolites. *Laumontite* was observed in cores by Borchardt (1993) until 6250 m depth. Its shape is generally euhedral. Typically, laumontite is associated with prehnite, epidote and adularia. *Calcite* occurs in the whole HB, normally in monomineralic veins. Often calcite shows different twin lamellae. *Quartz* often occurs in monomineralic veins. In the neighbourhood of lamprophyres quartz gangues often occur parallel to the foliation (e.g. 428 m, 468 m, 1530-1550 m). Stalked *actinolite* often grows on hornblende (**Fig. B.4.7**) and can be observed until the final depth of the HB. *Chlorite* is sporadically found in association with prehnite, calcite, tourmaline, quartz and ore minerals until the final depth.

Between 5600 and 9101 m *tourmaline* occurs within the metabasites. The following mineral associations were observed (Duyster et al. 1993):

- Intergrowth of tourmaline-quartz-plagioclase in quartz-feldspar veins (e.g. H027)
- Monomineralic tourmaline veins, veins with tourmaline-actinolite, tourmaline-actinolite-clinozoisite and tourmaline-pyrrhotite-chalcopyrite (e.g. H019, H024, H028)
- Pseudomorphic replacement of hornblende by tourmaline or of garnet by tourmaline + chlorite occurs within alteration zones in the metabasites (e.g. H025).
- Assemblage of tourmaline-actinolite-chlorite in greenschist facies shear zones in.

The morphology of the tourmalines is euhedral to subhedral in forms of short columnar prisms or aggregates of needles (Fig. B.4.8). Tourmaline crystals show continuous and discontinuous zoning, enclose apatites and occasionally fluid inclusions. Grain rims are often corroded. Tourmaline veins are crosscut by cracks filled with prehnite or clinozoisite+prehnite. Sometimes prehnite replaces tourmaline pseudomorphically (Duyster et al. 1993). The aggregates show cataclastic overprint. The tourmalines belong to the schorl-dravit solid solution series (Schwarz 1993).

Generally the frequency of veins increases in fault zones. Below about 7650 m depth the vein frequency significantly decreases.

Zulauf (1992) distinguished four major deformation stages in cores of the KTB VB. These deformation stages could be confirmed in the KTB HB.

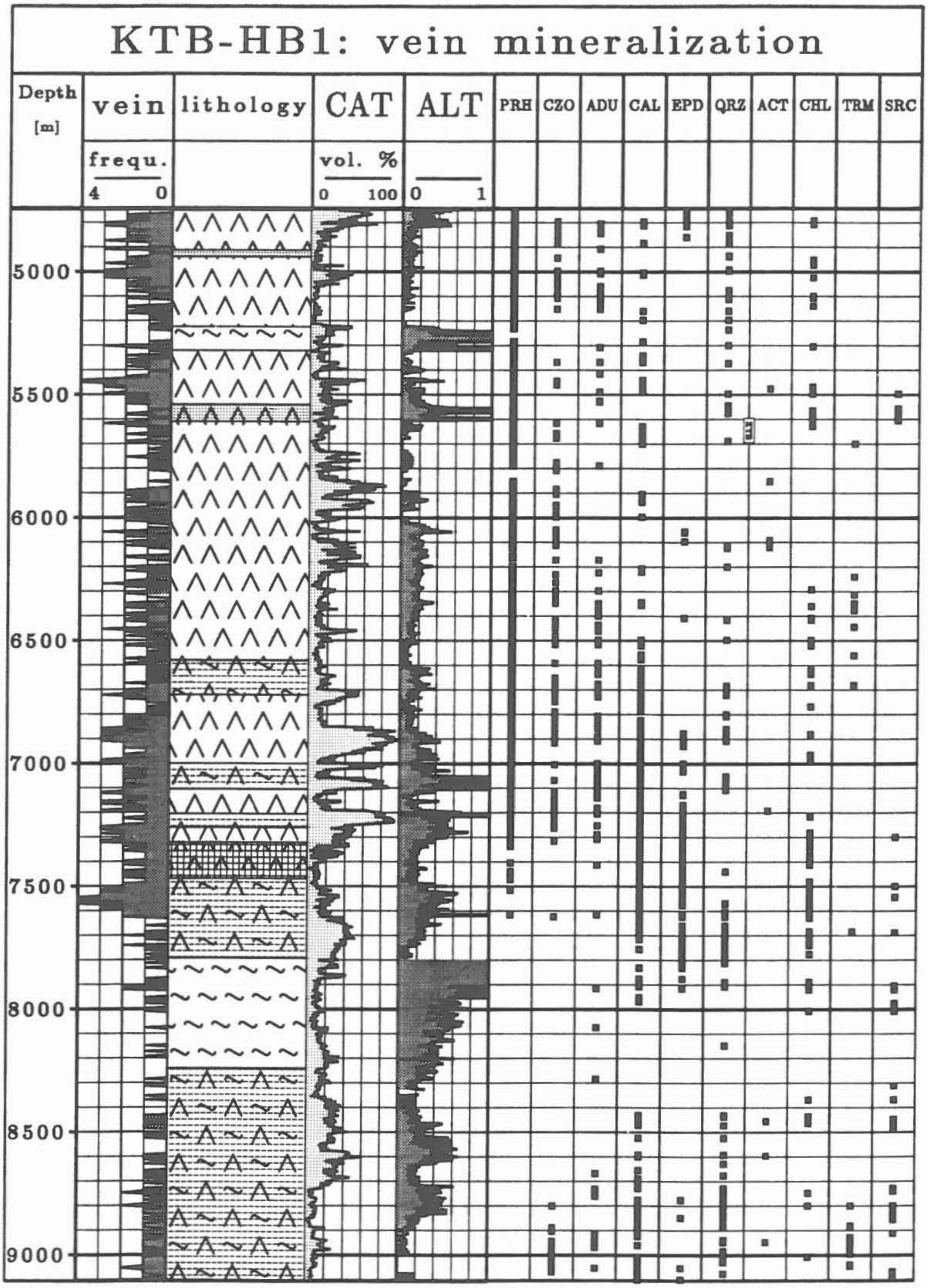

Fig. B.4.5: Vein minerals and frequency of veins of the KTB HB for the depth interval of 4800-9100 m.

The main phases are:

Subvertical extension gashes were mostly observed in metabasites down to 4300 m. The index minerals prehnite, epidote and actinolite indicate prehnite-actinolite facies conditions. Below this depth, only epidote, zoisite and actinolite were found, indicating that the conditions were beyond the limits of the prehnite-actinolite facies. Calcite, quartz and feldspar are abundant and tourmaline is rare.

The steep veins are displaced by *reverse faults bearing abundant graphite* in gneisses and alternating series. Lamprophyres containing fragments of graphite-bearing cataclasites could be observed in the KTB VB and in one case a graphite bearing shear zone cutting through a lamprophyre was observed. Hence the graphite bearing shear zones have probably formed at the same time. The lamprophyres are dated to 307 Ma (Harms & Hölzl 1994). In the KTB HB no cores containing lamprophyres were drilled.

The graphitized reverse faults are the most abundant brittle elements in the KTB bore holes. The characteristic quartz deformation features are fracturing and brecciation, and there is evidence for solution-precipitation creep. The quartz grains show undulatory extinction, polygonization and, below 1700 m, incipient recrystallization. Below 7500 m, the brittle features like brecciation diminish while the degree of recrystallization increases. All these deformation features indicate deformation of quartz around the brittle-ductile transition under temperatures around 300°C.

The graphite-bearing reverse faults are displaced by later *reverse graphite-free faults*, possibly of Cretaceous age (Wemmer & Ahrend 1992). Until 3200 m, laumontite and prehnite indicate zeolite facies conditions (temperature <240°C). Below this depth, prehnite-actinolite-epidote-zoisite mineralization indicate actinolite facies conditions for these faults.

The youngest structural elements are *steep normal faults* which Zulauf (1992) relates to the Tertiary Eger Graben rifting. Zulauf & de Wall (1994) observed laumontite until 4500 m in these normal faults.

For the deeper parts of the KTB HB an unequivocal discrimination of the different generations of faults is not possible due the lack of appropriate cores. Prehnite is completely absent below 7600 m. This indicates that greenschist facies conditions prevailed during formation af all faults.

The vertical extent of the prehnite-actinolite facies is considerably larger for the late Carboniferous reverse faults than for the younger, possibly Cretaceous reverse faults and the normal faults. For the Carboniferous reverse faults the vertical extent of the prehnite-actinolite facies is at least 7600 m. Prehnite actinolite facies mineralization are entirely absent below 7600 m. This indicates that also during the later faulting stages the metamorphic conditions should have been beyond the limits of the prehnite- actinolite facies below 7600 m. The upper limit of the prehnite- actinolite facies is 3200 m for the possibly Cretaceous reverse faults and 4500 m for the younger normal faults. This leaves a depth interval of ca 4400 m for the prehnite-actinolite facies during Cretaceous reverse faulting and 3100 m for the late normal faults.

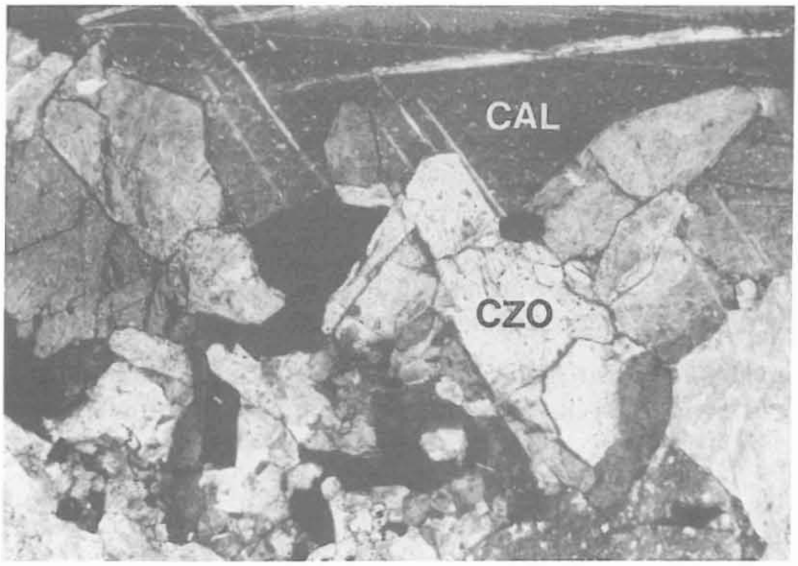

Fig. B.4.6: Vein mineralized with euhedral clinozoisite (CZO) and calcite (CAL) in marble-bearing amphibolite.

(HB, depth 7402.32 m, sample H033D8i, one polarizer, width of view 1.78 mm).

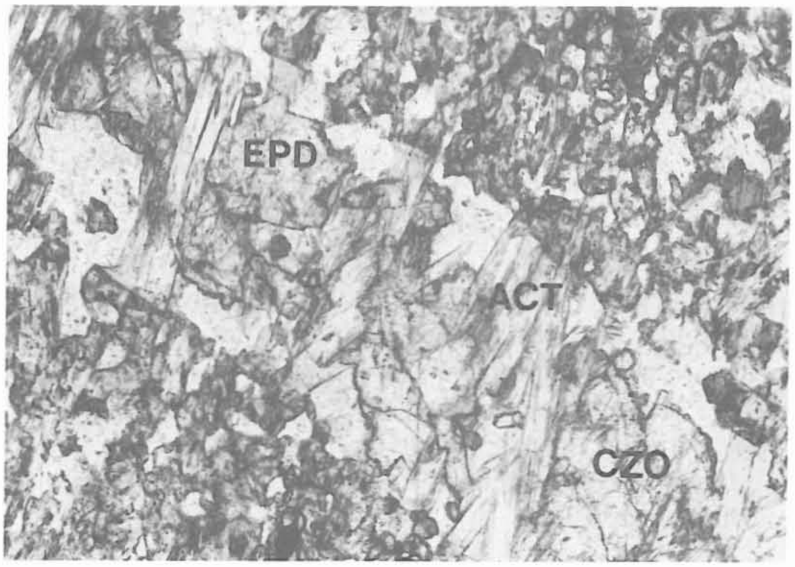

Fig. B.4.7 : Vein in marble-bearing amphibolite mineralized with stalked actinolite (ACT), epidote (EPD) and clinozoisite (CZO).

(HB, depth 7402.32 m, sample H033D8i, one polarizer, width of view 5.9 mm).

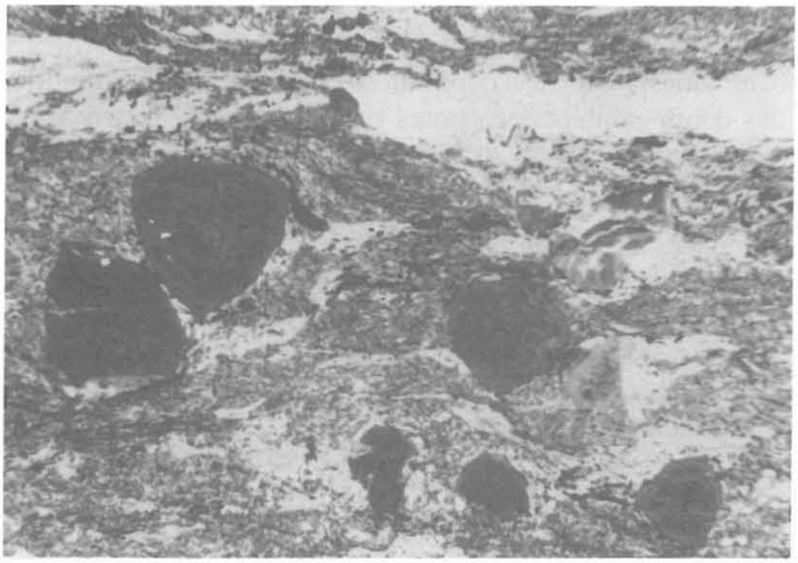

Fig. B.4.8 : Euhedral, zoned tourmaline in greenschist facies shear zone.

(HB, depth about 6546 m, sample HCS6546, one polarizer, width of view 6.7 mm).

B.4.2.4 Active mineralization processes - Observations from the borehole

Open fissures with euhedral mineralizations were observed down to 8700 m depth. The occurrence and distribution of open fissures is given in Fig. B.4.9. In the gneisses of the upper part of the profile open pores are very rare. First open fissures occur in metabasic rocks at 1200 m. In this metabasic sequence also the first fluid inflows are detected (see chapter C.2). The frequency of open fissures increases below about 3200 m in metabasites and open fissures filled with idiomorphic minerals are abundant. However, in the gneisses below 7800 m the frequency of open fissures decreases again. The lowermost open fissures in the profile were observed at a depth of 8698 m, where also the deepest fluid inflows were detected.

Open fissures occur mainly in amphibolites and metagabbros, probably due to their higher mechanical strength in comparison to geisses. Following minerals and mineral assemblages are seen in open fissures:

- quartz
- prehnite
- epidote
- prehnite-zeolite
- prehnite-quartz
- prehnite-quartz-epidote
- quartz-actinolite
- quartz-pyrrhotite-(chalcopyrite-pyrite)

A description of open fissures down to a depth of 6000 m in the KTB HB is given by Lich et al. (1992). Below this depth open fissures are mostly filled with euhedral quartz. Rarely prehnite or epidote crystals occur. The deepest pores at 8698 m depth in garnet-(sillimanite-) biotite gneiss contain euhedral quartz, hexagonal pyrrhotite, chalcopyrite and pyrite. The occurrence of hexagonal pyrrhotite + pyrite in open pores of the deep parts of the profile points to the existence of S-bearing fluids in (sub-)recent times and indicates that hexagonal pyrrhotite is formed at temperatures of about 250°C.

Open pores and fissure mineralizations show a distinct correlation with detected fluid inflows mainly in fault zones (Fig. B.4.9). This is documented e.g. in the prominent fault zone between 6850-7300 m where open fissures are widespread. At a depth of 7011 m, a strong fluid inflow was detected and the core from this depth exhibits open pores mineralized with quartz (Fig. B.4.10) and prehnite.

The final depth of KTB reached temperatures of about 270°C - a temperature regime in which most of the observed post-Variscan mineralizations in the KTB HB were formed. Whereas in the upper parts of the bore hole the rocks are not in equilibrium with their surroundings, especially with the fluids, with increasing depth an approach to equilibrium conditions is obvious. E.g. the Fe-sulfide assemblages attain equilibrium with its surrounding (hexagonal pyrrhotite + pyrite + fluid in open pores) and with increasing depth, sulfur isotopes between different sulfide phases attain isotopic equilibrium (Berner & Puchelt 1994). This interpretation is supported by isotopic data e.g. on noble gases (Drescher & Kirsten 1994) as well as by fluid inclusion data (Behr et al. 1994).

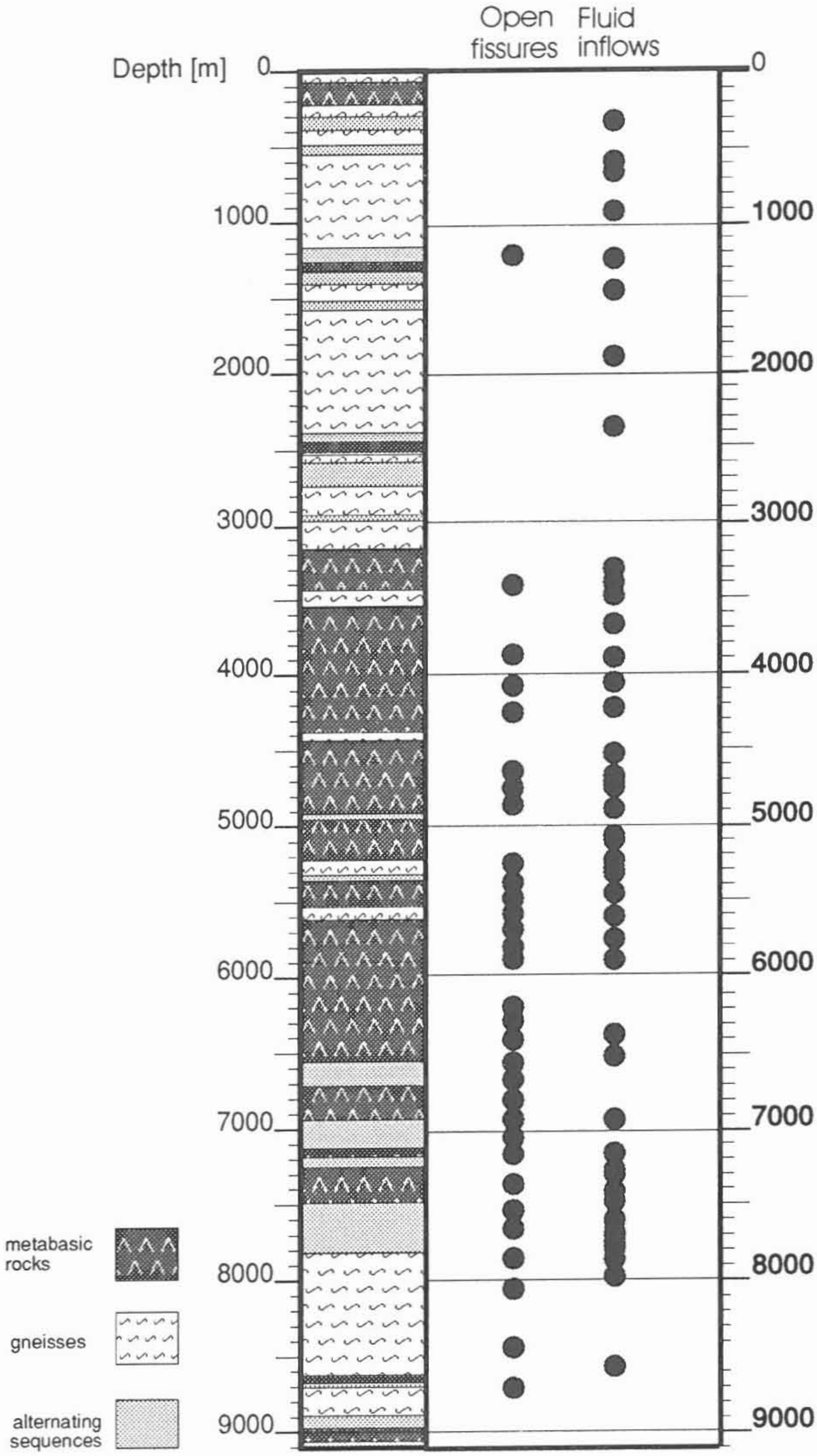

Fig. B.4.9: Occurrence of open pores in the lithological profile of the KTB HB and its correlation with fluid inflows

Fig. B.4.10: Open pore mineralized with euhedral quartz in amphibolite.

(HB, depth interval 7011.3-7013.3 m, sample H031T42, one polarizer, width of view 2,5 mm).

B.5 Structure

Based on the analysis of cores from the KTB VB and the interpretation of borehole measurements of the KTB VB and the KTB HB (Formation Micro Scanner, Formation Micro Imager) the following structural picture can be deduced (Duyster et al. 1993, Rust 1994, Lapp et al. 1994):

A predominantly steep foliation is characteristic for the whole drilled profile. In the upper section the foliation dips steeply or nearly vertical to SW and SSW, and to a smaller extent to the NE. From 2700 m (VB from 2900 m) to 3600 m the dip of the foliation decreases. The dip direction turns towards the E below 3000 m. Below 3600 m the foliation dips steeply again, with dip directions alternating between E and W. Between 5500 and 6500 m the foliation planes dip with about 60° to the E and ENE and further down to 7300 m the foliation dip direction again changes between E and W. Below 7400 m the foliation dips mainly to the W or SW with dip-angles around 60°.

The majority of the fault planes recognized in FMI and FMS logs follows the foliation.

B.6 The Franconian Lineament

The DEKORP/KTB ISO89 seismic experiment comprised a 3-D reflexion seismic study of the KTB surroundings. This seismic investigation revealed a number of strong, steeply inclined reflective zones, mainly dipping to the NE and the SW. The most prominent element, the SE-1 (steep element 1, Wiederhold 1992) is a large planar element dipping with about 55° to the NE. The SE-1 intersects the surface in the area of the large scale Franconian Lineament and is interpreted as the seismic image of this fault zone (Wiederholt & Hirschmann 1992). Reichard et al. (1993) predicted that the KTB HB would cut the upper limit of the SE-1 reflector at 6600-7000 m ± 140 m depth. In fact, in the depth interval 6850-7260 m the most prominent cataclastic fault bundle of the KTB profile was drilled. Fig. B.6.1 shows the amount of cataclastically overprinted rocks estimated by optical inspection of cuttings. Based on those analyses four major faults were mapped in the depth range 6850-6950 m, 7000-7020 m, 7060-7100 m and 7190 -7260 m. Between these faults more compact, less faulted rocks occur.

The macroscopic structure of the fault zone can be studied on core H031, which was recovered between 7011.3 - 7013.3 m depth. The core consists of a coarse-grained, strongly altered garnet-hornblende gneiss, with locally strong cataclastic overprint. Parallel to the steeply dipping and weakly developed foliation a 6 cm wide, fine-grained and foliated amphibolite is intercalated (see Fig. B.3.15). Different generations of faults crosscut each other. The oldest generation consists of subhorizontal approximately 1 cm wide quartz veins. Quartz in these veins is very rich in fluid inclusions, and shows incipient recrystallization. Locally, the quartz grains are stretched with their long axes aligned oblique to the vein boundary. A subvertical dip-slip fault parallel to the foliation, which is mineralized with a fine-grained matrix of chlorite, graphite, titanite and prehnite displaces the quartz gangues. The fault plane displays a subvertical slickenside striation. Numerous faults dipping at lower angles and without graphite, displace these faults.

Vein and fault mineralizations comprise adularia, clinozoisite, prehnite, calcite, graphite and sulfides. Euhedral prehnite, calcite and quartz have been formed in open faults and pores.

The microscopic images show numerous cross-cutting shear faults, partially with very finely ground material and brecciated rock- and mineral fragments (quartz, plagioclase, pyrite, clinozoisite, chlorite, graphite).

The shear faults are transsected by undeformed veins which are mineralized with euhedral prehnite, calcite, quartz, adularia, chlorite, clinozoisite and ore minerals. Graphite- and chlorite-bearing faults are mineralized by the *crack-seal* mechanism (Ramsay 1980) with prehnite, calcite, quartz and ore minerals (Fig. B.6.2).

Plagioclase is strongly sericitized, often kinked and broken and shows deformation twins. New grain nucleation on cracks is occasionally observed. Quartzes show sutured grain-boundaries, strong undulatory extinction, deformation lamellae and polygonization. Quartz clasts frequently reveal mica-quartz beards formed in their pressure shadows. All quartzes show abundant fluid inclusion trails. In tectonic breccia fracturing together with solution-precipitation creep is the most dominant deformation mechanism. In the oldest vein generations, quartz is stretched and partially recrystallized.

The conditions during deformation were in the brittle-ductile transition region for quartz. Penetrative recrystallization was not observed. The predominant prehnite-actinolite facies vein and fissure mineralization in accordance with the quartz deformation fabrics indicate temperatures between 250 and 350°C. This temperature range is also confirmed by chlorite thermometry (Schöps & Friedrich 1993).

The fault zone is characterized by increased contents of Fe-sulfide and graphite (Fig. B.6.1). The ore minerals and graphite occur disseminated in the rock matrix and as fault mineralization (Kontny et al. 1993). Graphite forms mm to cm long feather-like aggregates in cataclastic rocks, which often surrounds cataclastic pyrite. Occasionally, pyrrhotite, pyrite and chalcopyrite cement the intergranular space of quartz and feldspar.

The FMS-logs for this section of the profile shows planar structures with two orientation maxima (Fig. B.6.2). Moderately steep, preferably E dipping planes are probably foliation planes; some may be drilling induced fractures. A set of structures dipping with 50-60° to the NE are interpreted to represent fault planes.

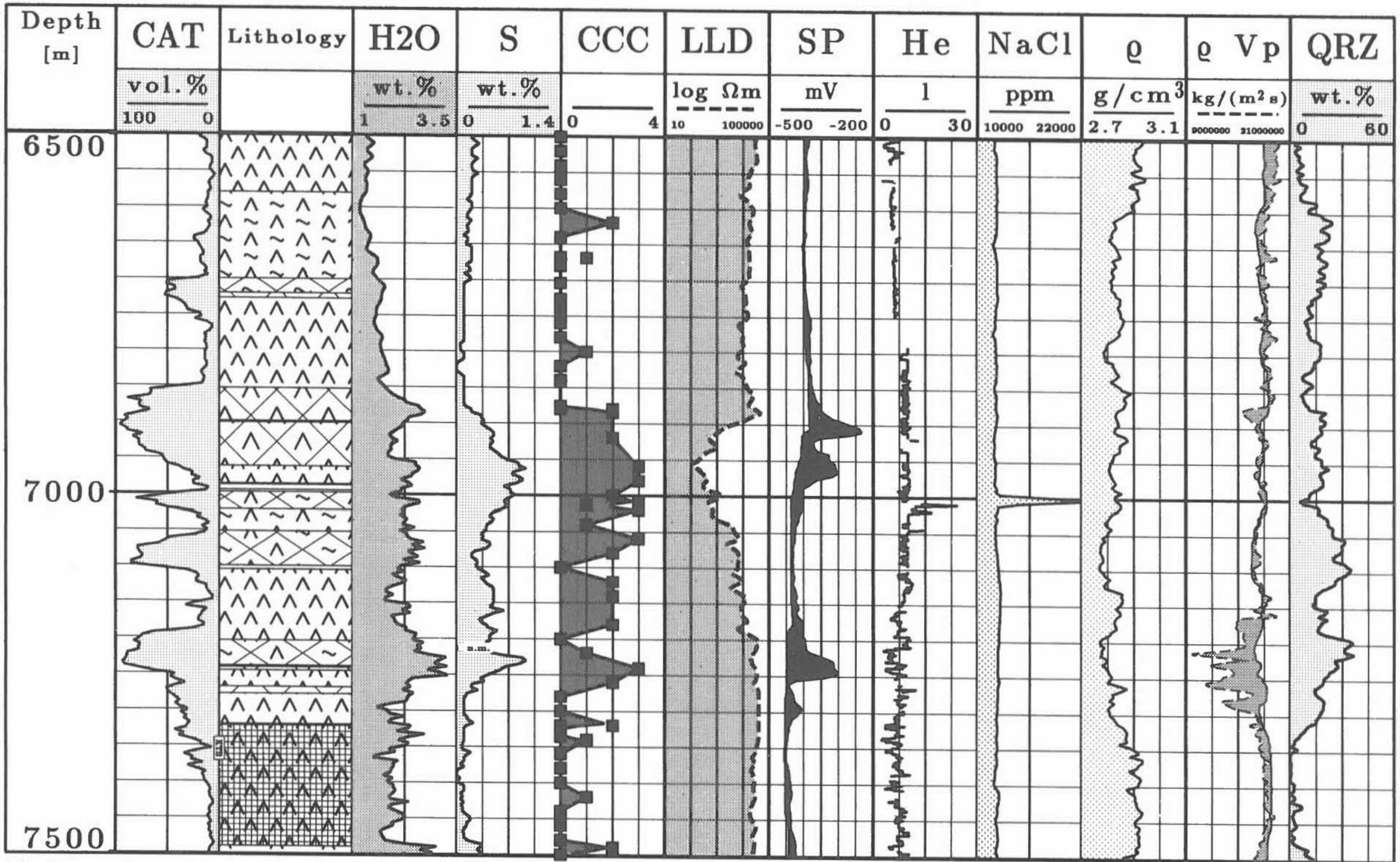

Fig. B.6.1 Selected parameters characterizing the fault zone between 6850 and 7260 m. Cat: amount of cataclastically overprinted rock, H_2O: indicator of alteration (IR-absorption), S: sulfur content (XRD), CCC: graphite content (semiquantitative microscopical determination, see also appendix B.8), LLD: latero log deep (electrical resistivity, bore hole measurement), SP: self-potential (bore hole measurement), He: helium content from mud-logging as indicator for fluid-inflows, NaCl: NaCl-equivalent computed from mud-resistivity (bore hole measurement), ρ: density (cuttings), ρVp: impedance, computed from sonic-log (solid line) impedance, computed from p-wave-velocities and mineral densities (dashed line), QRZ: quartz content (XRD)

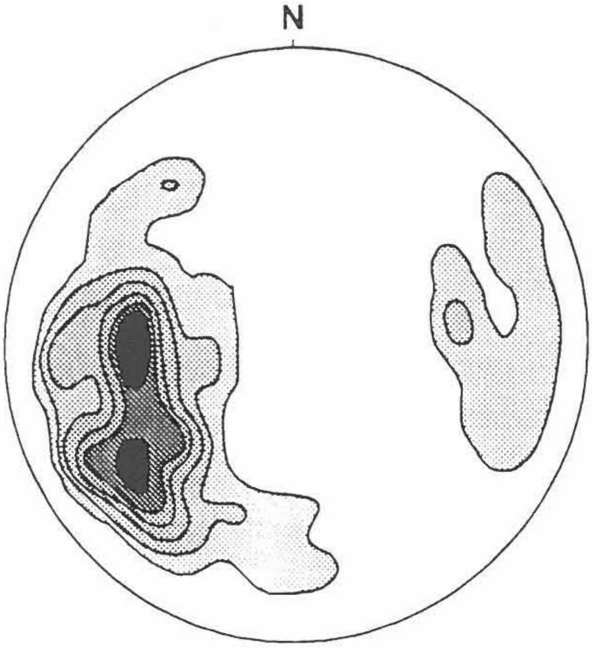

Fig. B.6.2: Planar elements, FMS-Log-Evaluation from the depth interval of the fault zone. Plane-pole densities; equal area projection, lower hemisphere.

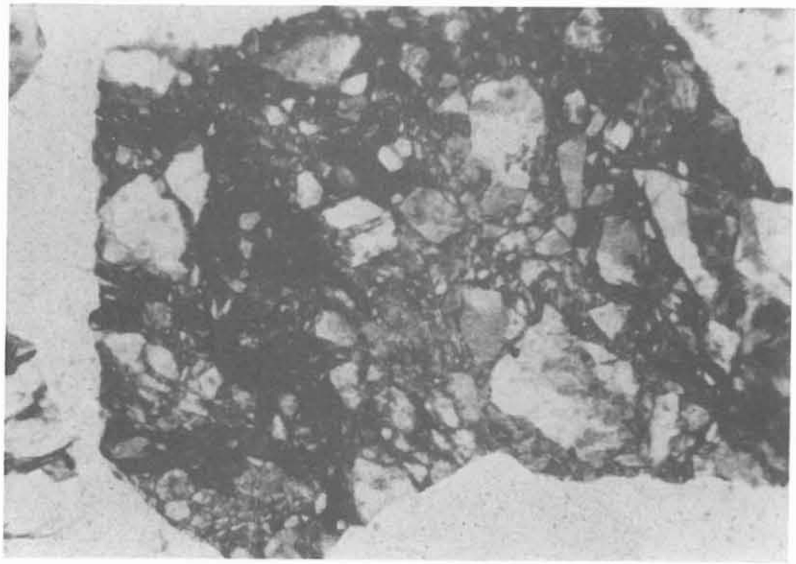

Fig. B.6.3 Fault related fabrics and mineralization

a)Cataclastic breccia with wall-rock fragments, HB, depth 7200 m, sample HC7200, crossed polarizers, width of view 3.5 mm.

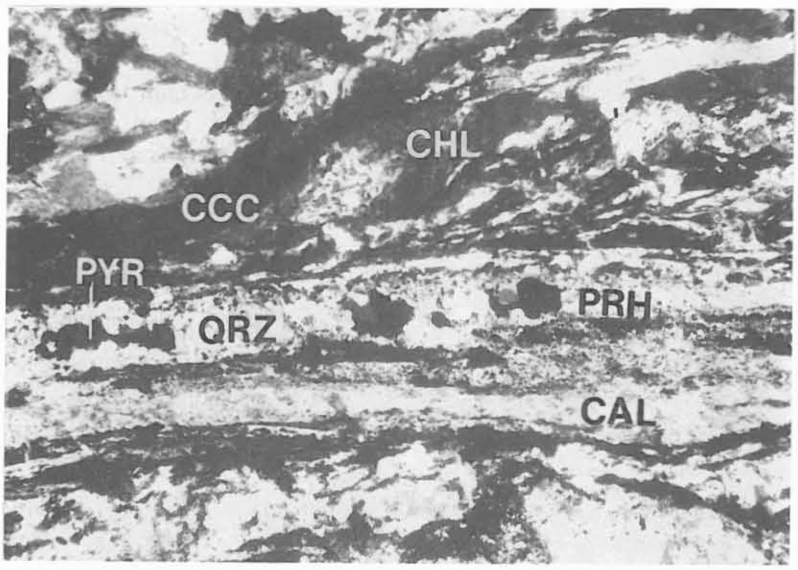

b) Graphite-(CCC) and chlorite-(CHL) bearing cataclastic fault zone with post-cataclastic crack-seal mineralization.

(HB, depth 7011-7013 m, sample H031B, one polarizer, width of view 2.2 mm).

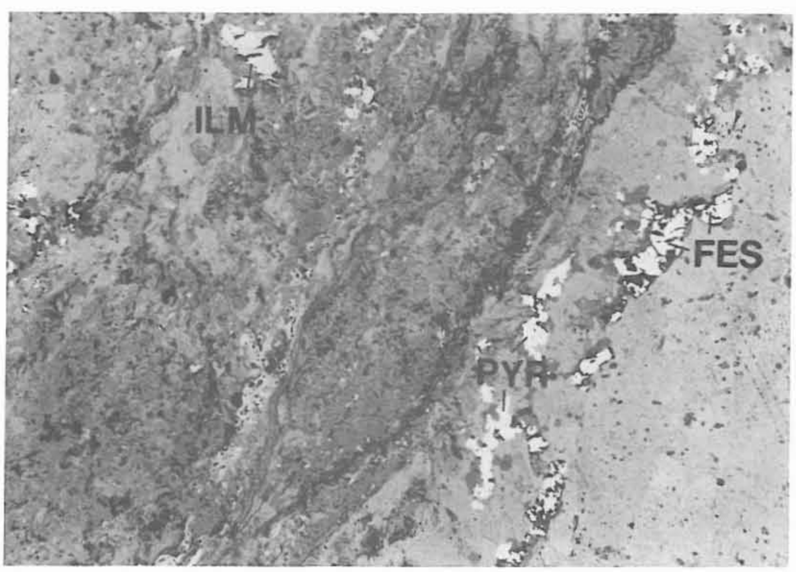

c) Quartz-vein (QRZ) with pyrite and pyrrhotite (FES), wall rock contains graphite and ilmenite (ILM), garnet-hornblende gneiss.

(HB, depth 7011-7013 m, sample H031B, air, one polarizer, width of view 1.4 mm).

B.7 Summary and Conclusion

The 9101 m deep bore hole KTB HB exclusively transsected metamorphic rock as exposed within the Zone of Erbendorf-Vohenstrauß (ZEV). The lithological profile is composed of three main units: paragneisses, metabasic rocks (amphibolite, metagabbro and meta-ultramafite) and alternating series (paragneiss, hornblende gneiss, amphibolite, subordinate calc-silicate and marble). Locally, dykes of granitic aplite, pegmatite, (monzo-)diorite and calc-alkaline lamprophyre crosscut the metamorphic rocks. With few exceptions, the foliation dips steeply with values between 60 and 80° towards the SW and NE. The foliation is folded. The large scale folds have near horizontal axial planes and NNW-SSE oriented fold axes.

Paragneisses, derived from graywackes and pelitic graywackes, are rather homogeneous in composition and are assumed to have deposited at an active continental margin (e.g. Müller 1993). The tholeiitic composition of amphibolites and metagabbros is similar to that of enriched mid-ocean ridge basalts (E-MORB). The intrusive and extrusive magmatites were formed during early Ordovician times (480 - 485 Ma, v. Quadt 1994). The amphibolites of the alternating series exhibit an alkaline-tholeiitic to alkali-basaltic composition. Their extrusion ages are likewise Ordovician (488 ± 3 Ma, Söllner & Miller 1994). The hornblende gneisses of these sequences are either more differentiated vulcanic products (trachybasaltic to trachyandesitic) or represent sedimentary mixtures of graywackes and tuffitic material (Harms 1994). The alternating series are of volcano-sedimentary origin. The close association of all rock types suggest formation in a single geotectonic setting whereby the geochemical environment of the intrusive and extrusive rocks most probably changed from an enriched to a more depleted mantle source (or vice versa), possibly in a marginal oceanic basin.

The ZEV rocks exhibit a multiphase complex metamorphic history. Relics of early high pressure stages (eclogite and granulite facies) are found within the metabasic rock units only (O'Brien et al. 1992), but are missing in the paragneisses. Later, paragneisses and metabasites suffered a penetrative amphibolite facies metamorphism. In the paragneisses, concomitant deformation resulted in a pervasive and a NNW-SSE oriented subhorizontal stretching lineation. The amphibolite facies mineral assemblage consists of plagioclase, quartz, biotite, garnet, sillimanite and/ or kyanite, muscovite, ± graphite, pyrrhotite and rutile. Deformation in the metabasites was inhomogenous. Therefore, metagabbros, fine-grained, coarse-grained and foliated amphibolites occur close together. The amphibolite facies mineral assemblage is hornblende - plagioclase - garnet - ilmenite ± titanite ± pyrrhotite. K-Ar and Ar-Ar ages of 370 and 380 Ma for muscovite and hornblende indicate that cooling after amphibolite facies overprint occurred in the Devonian (e.g. Henjes-Kunst et al. 1994).

Greenschist facies overprint has nowhere gone to completion except for local fault zones. The metamorphic rocks exhibit a multistage deformation history in the upper crust, resulting in abundant cataclasites. Graphite deposition from fluids along reverse faults is a characteristic feature mainly in paragneisses but also in alternating sequences. Mineral assemblages and microfabrics suggest formation temperatures of 240-350°C. Lamprophyres intruded into faults or follow lithological boundaries and are observed down to 7255 m. Hence, these faults predate the intrusion of these lamprophyre (306 ± 5 Ma, Henjes-Kunst, pers. com.).

Late to post-Variscan brittle faults and veins are very abundant deformation structures. Zulauf (1992) distinguished four major deformation stages in cores of the KTB VB. These deformation stages were also found in the KTB HB. Cataclastic deformation started in the upper Carboniferous and was particularly active in Cretaceous times (Zulauf 1992). The most prominent reverse fault of the KTB HB, which was predicted by seismic investigations, was drilled between 6850 and 7260 m and is part of the Franconian Lineament. According to the fission track data, the vertical displacement amounts to more than 3 km in Cretaceous time (Coyle & Wagner 1994). Open pores are mineralized with euhedral quartz and prehnite and correlate with salinar fluid inflows (see chapter C.2). The lowermost occurence of euhedral pore mineralization with by fluid inflows was observed in 8699 m depth. Cataclastic deformation is accompanied by multiple stages mineralization reflecting the complex history of the movements along the Franconian Lineament.

With respect to Carboniferous and earlier features the KTB HB revealed an anomalous crustal profile with a conspicious lack of gradients. This lack of gradients is explained by supracrustal stacking in late- to post-Variscan time (Duyster et al. 1995). This is also supported by fission-track data of apatite and titanite (Coyle & Wagner 1995).

B.8 Acknowledgements

We gratefully acknowledge G. Hirschmann´s contributions which helped to improve the definition of some lithological boundaries. B. Stöckhert provided a very constructive review which improved the text. U. Harms made helpful comments on dyke rocks and geochemistry. J. Häussinger, S. Keyssner, J. Kohl, G. Godizart, W. Hacker, S. Lich, H. Müller, C. Röhr, S. Rust & H. de Wall have worked in former geology groups of the KTB field-laboratory and contributed to the presented data.

B.9 Appendix

B.9.1 List of abbreviations

ACT	actinolite	**FDS**	feldspar	**PBS**	galenite
ADU	adularia	**GNS**	gneis	**PLG**	plagioclase
ALT	alteration	**GNT**	garnet	**PNT**	pentlandite
AMP	amphibolite	**HBG**	hbl-biotite gneiss	**PRH**	prehnite
BIO	biotite	**HBL**	hornblende	**PYR**	pyrite
CAL	calcite	**ILM**	ilmenite	**QRZ**	quartz
CAT	cataclasis	**KKL**	cataclasite	**RUT**	rutile
CBG	chlorite-biotite gneiss	**LAU**	laumontite	**SIL**	sillimanite
CCC	graphite	**LEX**	leucoxene	**SRC**	sericite
CCL	cataclasite	**MAC**	mafic cumulate	**SUL**	sulfides
CHL	chlorite	**MAG**	magnetite	**TIT**	titanite
CPY	chalcopyrite	**MGB**	metagabbro	**TUR**	turmaline
CZO	clinozoisite	**MGN**	magnetite	**ZNS**	sphalerite
EPD	epidote	**MOB**	mobilisate		
FES	pyrrhotite	**MUS**	muscovite		

Alteration:
1 fresh **2** weak **3** strong **4** complete.

Ore mineralization:
0 none **1** some **2** common **3** frequent **4** much.

B.9.2 Table of the geological profile

KTB HB, Lithological Units HC					
Depth (from m)	**Depth (to m)**	**Rocks**	**Remarks**	**Comments**	**Core Run**
0	16	Qrz-poor chl gns		idiomorphic epd/czo	
16	69	Mus-chl gns	30-35 m cataclastic		
69	73	Amp			
73	74	Lamprophyre			
74	206	(Gnt-)amp	180 m mafic cumulates		
206	243	Gnt-sil-bio gns			
243	247	Qrz-poor chl gns	cataclastic		
247	257	Cataclasite	256 m diorite		
257	294	Mus-chl gns, cataclastic	with qrz gangues, one lamprophyre		
294	306	Alternation of amp, mus-bio gns, hbl gns			
306	310	calc-silicate rocks			
310	312	Bio gns			
312	331	(Gnt-) amp with intercalations of calc-silicate			
331	370	Gnt-sil-bio gns			
370	389	Gns-dominated alternation of gnt-sil-bio gns, amp, hbl gns, calc-silicate rocks			
389	487	Gnt-sil-bio gns	from 405 m with intercalations of amp, hbl gns; 389-393 m calc-silicate rocks; 405-482 m cataclastic with gangues of lamprophyre		
487	518	Alternation of bio gns, hbl gns, amp			
518	530	Gnt-sil-bio gns with intercalations of bio-hbl gns and amp			
530	947	Gnt-sil-bio gns	570-575 m, 720-740 m cataclastic; 732-750 m gangues of lamprophyre, partially qrz-mobilisates	border after geochemistry	
947	994	Qrz-poor chl gns			
994	1183	Gnt-sil-bio gns	1002-1011 m, 1059-1080 m cataclastic; 1157-1172 m mus-bio gns, cataclastic		

Table B.9.2: Table of the geological profile KTB HB (HC= 4th bore hole, HHC= 5th bore hole, see chapter A), abbreviations see B.9.1

KTB HB, Lithological Units HC					
Depth (from m)	Depth (to m)	Rocks	Remarks	Comments	Core Run
1183	1206	Gnt-amp with intercalations of Gnt-sil-bio gns			
1206	1256	Gnt-amp with intercalations of sil-bio gns, cataclastic gns and hbl gns			
1256	1310	Gnt-amp			
1310	1412	Gnt-amp with intercalations of sil-bio gns, cataclastic gns and hbl gns bio gns			
1412	1515	Gnt-sillimanit-bio gns with intercalations of amp, hbl gns and mus-bio gns			
1515	1573	Alternation of amp, mus-bio gns, gnt-sil-bio gns	1537-1546 m lamprophyre; 1546-1573 m single gangues of lamprophyre		
1573	2382	Gnt-(sil-)bio gns	1940-2010 m, 2086-2096 m cataclastic		
2382	2386	Lamprophyre			
2386	2450	Alternation of bio gns, bio-hbl gns, amp	amp increases with depth		
2450	2506	Amp with intercalations of bio-hbl gns and bio gns			
2506	2528	Alternation of bio gns, amp, hbl gns			
2528	2570	Gnt-sil-bio gns			
2570	2595	Gns-dominated alternation of gnt-sil-bio gns, amp, hbl gns			
2595	2642	Alternation of amp, hbl gns, bio gns			
2642	2672	Amp-dominated alternation of amp, hbl gns, bio gns			
2672	2718	Alternation of amp, hbl gns, bio gns			
2718	2912	Gnt-(sil-)bio gns	2760-2770 m with less intercalations of amp; 2782-2812 m cataclastic		
2912	2944	Alternation of amp, hbl gns, bio gns			

Fig. B.9.2: Continuation

KTB HB, Lithological Units HC					
Depth (from m)	Depth (to m)	Rocks	Remarks	Comments	Core Run
2944	3160	Gnt-sil-bio gns to mus-bio gns	2944-2997 m mus-bio gns; 2997-3025 m gnt-sil-bio gns; 3025-3102 m mus-bio gns; 3102-3152 m gnt-sil-bio gns; 3152-3160 m mus-bio gns; 2970-2980 m cataclastic		
3160	3284	Amp	3180 m with intercalations of mus gns; 3185-3230 m single gangues of lamprophyre, amp is epd-bearing		
3284	3427	(Gnt-)amp			
3427	3537	Mus-bio gns	3532 -3536 m lamprophyre		
3537	3883	Amp, partially gnt-bearing	3610 m aplite, 3645 m mus-bio gns		
3883	3892	Amp-dominated alternation of amp, hbl-bio u. bio-hbl gns			
3892	3922	Amp with intercalations of hbl-bio u. bio-hbl gns	amp partially gnt-bearing	2 different types of amp	
3922	3950	Amp-dominated alternation of amp, hbl-bio, bio-hbl gns			
3950	3988	Amp with intercalations of hbl-bio u. bio-hbl gns			
3988	3996	Amp-dominated alternation of amp, cataclastical gns	3996 m lamprophyre		
3996	4016	Cataclastic amp	4010 m lamprophyre		
4016	4106	Amp, partially gnt-bearing	4017-4106 m many open pores		
4106	4165	Amp-dominated alternation of amp, bio-hbl gns, hbl-bio gns	4116-4124, 4144, 4147, 4150 m open pores with prehnite and quartz		H001
4165	4395	Amp	4180, 4190, 4210, 4235-4245, 4260, 4300 m intercalations of bio-hbl gns; 4175-4185 m, 4280-4284 m, 4348-4388 m qrz-fds mobilisates; 4374-4383 m gnt-rich; 4234, 4236, 4242, 4275 m open pores		H002-H004
4395	4426	Gnt-sil-bio gns	4419-4426 m many qrz-fds mobilisates		

Fig. B.9.2: Continuation

KTB HB, Lithological Units HC					
Depth (from m)	Depth (to m)	Rocks	Remarks	Comments	Core Run
4426	4520	Amp-dominated alternation of amp, bio-hbl gns	4512-4521 m with intercalations of metagabbro, mafic cumulates; from 4513 m gnt-amp, 4426-4434 m many qrz-fds mobilisates		H005-H006
4520	4550	Amp			
4550	4594	Amp with intercalations of hbl gns			H007
4594	4618	Amp-dominated alternation of amp, bio-hbl gns			
4618	4918	Amp	4835, 4845, 4855 m lamprophyre; 4714-4718, 4759-4775, 4807-4815m cataclastic		H008-H010
4918	4940	Alternation of gnt-bio gns, amp , hbl gns			
4940	5224	(Gnt-)amp	4974, 5014 m mafic cumulates; 5140 m intercalation of hbl gns		H011-H012
5224	5284	Mus-bio gns	5250 m intercalation of amp		H013
5284	5306	Gns with intercalations of amp			
5306	5320	Alternation of amp, gns			
5320	5540	Amp	5438-5446, 5454 m cataclastic; 5352, 5406 m intercalations of bio-hbl gns		H014-H016
5540	5554	Amp-dominated alternation of amp, bio gns			
5554	5576	Mus-bio gns			
5576	5590	Alternation of bio gns, gns			
5590	5606	Mus-bio gns			
5606	5636	Amp with intercalations of bio gns			
5636	6080	Amp	5757, 5779-5789, 5860-5864, 5928-5946 m cataclastic; 5680, 5690 m intercalations of bio-hbl gns; 5792-5812, 5855-5902, 5928-5940 metagabbro; 5860-5864 m metagabbro (very strong alteration)		H019-H024
6080	6285	Metagabbro	6120-6123 m cataclastic; 6148,2-6152,2 m intercalations of amp		H021-H025
6285	6598	Amp	6304-6307 m with intercalations of metagabbro; 6458-6462 m cataclastic		H026-H029

Fig. B.9.2: Continuation

KTB HB, Lithological Units HC

Depth (from m)	Depth (to m)	Rocks	Remarks	Comments	Core Run
6598	6720	Amp-dominated alternation of amp, bio gns, hbl-bio gns	6704-6720 m cataclastic; 6668-6672 m amp/metagabbro	border after gamma-ray and microscopy	H030
6720	6948	Amp	6780-6824, 6848-6948 m cataclastic; 6900 m lamprophyre; 6898-6948 m intercalations of mus-chl gns, partially CCC-bearing	border after microscopy	
6948	7120	Alternation of amp, hbl-bio gns, gns	6948-6960, 7000-7010, 7012-7020, 7056-7100m cataclastic; 7010-7012 m cataclasite; 6986, 6996 m lamprophyre	border after microscopy	H031
7120	7194	Amp		border after gamma-ray and microscopy	
7194	7260	Alternation of cataclastic gns, cataclastic Amp	7210, 7240, 7256 m lamprophyre; 7223-7248 m CCC-cataclasite		
7260	7320	Amp	7268-7277 m cataclastic		H033
7320	7490	Marble-bearing amp			
7490	7552	Alternation of amp, hbl gns, chl gns	7490-7640 m strongly chloritized zone		
7552	7628	Chl gns with intercalations of amp			
7628	7812	Alternation of chl gns, amp (partially marble-bearing), bio gns			
7812	7820	Mus-bio gns with intercalations of amp	7812-7816 diorite		
7820	7858	Gns-dominated alternation of bio gns, amp			
7858	8079	Gnt-sil-bio gns			
8079	8632	Gnt-sil-bio gns with intercalations of amp	8580-8596 m cataclastic		H034
8632	8664	Gns-dominated alternation of gnt-bio gns, amp (partially gnt-bearing)			
8664	8680	Amp-dominated alternation of amp (partially gnt-bearing),gnt-bio gns			

Fig. B.9.2: Continuation

KTB HB, Lithological Units HC

Depth (from m)	Depth (to m)	Rocks	Remarks	Comments	Core Run
8680	8698	Gns-dominated alternation of gnt-bio gns, amp (partially gnt-bearing)			
8698	8712	Gnt-(sil-)bio gns with intercalations of amp	8698 m open pore with qrz, sul		
8712	8796	Gnt-sil-bio gns			
8796	8844	Gnt-sil-bio gns with intercalations of amp		border after geochemistry (Zr/Nb-ratio)	
8844	8896	Gns-dominated alternation of gnt-(sil-)bio gns, bio-hbl gns, amp		amp-increase (RDA, density), not seen in microscope	
8896	9020	Alternation of gnt-(sil-)bio gns, bio-hbl gns, amp	from 8928 m graphite- and sulfide-rich gneisses; 8942 CCC-cataclasite	from here 2 different types of amp	
9020	9070	Amp-dominated alternation of gnt-amp, gnt-bio gns, bio-hbl gns			H035
9070	9101	Alternation of gnt-sil-bio gns, amp, bio-hbl gns			

Fig. B.9.2: Continuation

KTB HB, Lithological Units HHC

Depth (from m)	Depth (to m)	Rocks	Remarks	Comments	Core Run
7440	7488	Marble-bearing amphibolite	7485-7566 m chloritized zone (less pronounced than in HC-samples)		
7488	7750	Alternation of chl gns, bio-chl gns, amp	7488-7520 m hbl-bio gns, bio-chl gns, chl gns; 7520-7560 m amp, hbl gns, chl gns; 7560-7700 m chl gns, bio gns, amp (partially marble-, magnetite- and K-feldspar-bearing); 7700-7750 m bio-chl gns, epd-amp, amp	amp: calcite-, magnetite- and K-feldspar-bearing	
7750	7794	Amp with intercalations of bio-chl gns			
7794	8236	Gnt-(sil-)bio gns	7810-7866 m, 7820-7950 m cataclastic		
8236	8632	Gnt-sil-bio gns with intercalations of amp (see HC-profile)			
8632	8664	Gns-dominated alternation of gnt-bio gns, amp (partially gnt-bearing)			
8664	8680	Amp-dominated alternation of amp (partially gnt-bearing),gnt-bio gns			
8680	8698	Gns-dominated alternation of gnt-bio gns, amp (partially gnt-bearing)			
8698	8712	Gnt-(sil-)bio gns with intercalations of amp	8698 m open pore with qrz, sul		
8712	8796	Gnt-sil-bio gns			
8796	8844	Gnt-sil-bio gns with intercalations of amp		border after geochemistry (Zr/Nb-ratio)	
8844	8896	Gns-dominated alternation of gnt-(sil-)bio gns, bio-hbl gns, amp		amp-increase (RDA, density), not seen in microscope	

Fig. B.9.2: Continuation

KTB HB, Lithological Units HHC

Depth (from m)	Depth (to m)	Rocks	Remarks	Comments	Core Run
8896	9020	Alternation of gnt-(sil-)bio gns, bio-hbl gns, amp	from 8928 m graphite- and sulfide-rich gneisses; 8942 CCC-cataclasite	from here 2 different types of amp	
9020	9070	Amp-dominated alternation of gnt-amp, gnt-bio gns, bio-hbl gns			H035
9070	9101	Alternation of gnt-sil-bio gns, amp, bio-hbl gns			

Fig. B.9.2: Continuation

B.9.3 Short core descriptiäon, KTB HB (H001 - H035)

H001 (4149.0 - 4156.8 m): Amphibolite

Amphibolite, fine grained, well foliated with intercalations of strongly deformed **biotite-hornblende-gneiss**, laumontite mineralization on joints, dip of foliation 50-70°, core recovery 5.30 m.
Rock forming minerals: plagioclase, quartz, biotite, amphibole, chlorite, garnet, laumontite, calcite, adularia, titanite, zircone, opaque phases.
Ore minerals: ilmenite, rutile, titanite, monoclinic pyrrhotite, chalcopyrite, sphalerite.
Vein minerals: multiple mineralisations of quartz, adularia, laumontite, chlorite and calcite.

H002 (4195.0 - 4202.2 m): Amphibolite

Amphibolite, fine grained, well foliated locally massive, in the lower part of the core run strongly deformed **hornblende gneiss**, dip of foliation 40-85°, core recovery 3.90 m.
Rock forming minerals: amphibole, plagioclase, quartz, clinozoisite, biotite, garnet, chlorite, titanite, epidote, ore minerals.
Ore minerals: ($\leq$1 vol-%) ilmenite, rutile, titanite, monoclinic pyrrhotite.
Vein minerals: chlorite, quartz, adularia, calcite and prehnite.

H003 (4251.0 - 4260.3 m): Amphibolite

Amphibolite, fine grained, well foliated, alternating with strongly foliated **hornblende gneiss**, deformed biotite-bearing quartz-feldspar mobilisates, dip of foliation 40-80°, core recovery 4.05 m.
Rock forming minerals: amphibole, plagioclase, quartz, biotite, garnet, epidote, titanite
Ore minerals: ilmenite, titanite, rutile, monoclinic pyrrhotite, pyrite. Ore mineral content is about 2 vol-%, locally up to 5 vol-%.
Vein minerals: Chlorite, plagioclase, epidote and clinozoisite

H004 (4341.3 - 4350,6 m): Amphibolite

Amphibolite, medium grained, locally garnet-bearing, partially strongly altered, dip of foliation 35-70°, 2.30 m.
Rock forming minerals: amphibole, plagioclase, quartz, chlorite, garnet, epidot, actinolite, calcite
Ore minerals: ilmenite, titanite, rutile, leucoxene, pyrite, chalcopyrite. Ore mineral content is $\leq$1 vol-%.
Vein minerals: epidote, calcite, clinozoisite, prehnite and chlorite

H005 (4447.2 - 4456.2 m): Amphibolite

Ampibolite fine to medium grained, massive, locally well foliated, locally rich in deformed mobilisates with hornblende blasts, dip of foliation 50-70°, 2.90 m
Rock forming minerals: amphibole, plagioclase, quartz, garnet, biotite, chlorite, epidote, titanite, calcite, clinozoisite, ore minerals.
Ore minerals: ilmenite, titanite, magnetite, rutile, pyrite, pyrrhotite, chalcopyrite. The ore mineral content is about 2 vol-%.
Vein minerals: chlorite, clinozoisite, amphibole and epidote,

H006 (4512.0 - 4521.0 m): Garnet-amphibolite

Garnet Amphibolite fine to medium grained, with **metagabbro**-intercalations, locally well foliated with garnet rich boudins, partially strongly altered and **mafic cumulates**, dip of foliation 40-60°, 5.10 m
Rock forming minerals: amphibole, plagioclase, quartz, chlorite, biotite, garnet, titanite, clinozoisite, ore minerals
Ore minerals: ilmenite, rutile, titanite, pyrrhotite, pyrite, chalcopyrite
Vein minerals: clinozoisite, chlorite, quartz, epidote, adularia and calcite

H007 (4592.3 - 4601.6 m): Hornblende-gneiss / amphibolite

Hornblende-gneiss / amphibolite, locally strongly altered with epidote, open fissures, dip of foliation 50-60°, core recovery 3.84 m
Rock forming minerals: quartz, plagioclase, amphibole, biotite, chlorite, garnet, epidote.
Ore minerals: titanite, pyrite, ilmenite, pyrrhotite.
Vein minerals: calcite, chlorite, adularia, prehnite and amphibole

H008 (4646.2 - 4655.5 m): Amphibolite

Amphibolite, massive, locally strongly foliated, locally strongly altered, weakly jointed, dip of foliation 60-90°, core recovery 3.10 m
Rock forming minerals: amphibole, plagioclase, quartz, chlorite, epidote, titanite, ore minerals
Ore minerals: pyrite, leucoxene, titanite, goethite, rutile, magnetite, chalcopyrite, ilmenite
Vein minerals: chlorite, quartz, epidote and clinozoisite

H009 (4684.7 - 4692.4): (Garnet-)Amphibolite

Amphibolite / garnet-amphibolite, quartz/ feldspar mobilisates, steep ductile shear zone in the lower part of the core run, dip of foliation 60°, core recovery 4.15 m
Rock forming minerals: amphibole, plagioclase, quartz, chlorite, epidote, clinozoisite, actinolite.
Ore minerals: ilmenite, rutile, titanite, magnetite, pyrite, chalcopyrite. Due to alteration ilmenite decomposes into magnetite, rutile and titanite.
Vein minerals: clinozoisite and prehnite

H010 (4820.0 - 4826.6 m): (Garnet-)Amphibolite

Amphibolite, massive with quarz-feldspat mobilisates, locally garnet and titanite bearing, local cataclastic overprint, two **gneiss intercalations,** dip of foliation 35-65°, core recovery 3.50 m.
Rock forming minerals: amphibole, plagioclase, quartz, titanite, prehnite, clinozoisite, calcite.
Ore minerals: ilmenite, titanite, rutile, monoclinic pyrrhotite, pyrite, chalcopyrite.
Vein minerals: idiomorphic prehnite and younger calcite.

H011 (5012.0 - 5018.0 m): Amphibolite

Amphibolite, strongly to completely altered, cataclastic overprint, fault gouge in the lower part, **mafic cumulates,** dip of foliation 45-80°, core recovery 2.50 m.
Rock forming minerals: amphibole, plagioclase, quartz, prehnite, chlorite, clinozoisite, actinolite, ore minerals.
Ore minerals: titanite, rutile, ilmenite, leucoxene, pyrite, chalcopyrite, zircone.
Vein minerals: multiple mineralisation of prehnite, clinozoisite, calcite, chlorite, actinolite and adularia.

H012 (5082.0 - 5089.0 m): Garnet-amphibolite

Garnet-amphibolite, weakly altered, well foliated to massive, locally thin deformed mobilisate layers, dip of foliation 50-90°, core recovery 3.90 m.
Rock forming minerals: amphibole, plagioclase, biotite, garnet, quartz, epidote, titanite, chlorite, zircone., clinopyroxene / plagioclase symplecites, ore minerals.
Ore minerals: ilmenite, titanite, leucoxene, pyrrhotite, chalcopyrite, rutile. Symplectitic replacement of titanite by ilmenite.
Vein minerals: quartz, chlorite, calcite and prehnite

H013 (5282.0 - 5288.0 m): Muscovite-biotite-gneiss

Muscovite-biotite-gneiss, strongly altered and cataclastically overprinted, graphite-bearing shear zones, dip of foliation approx. 60°, core recovery 1.35 m.
Rock forming minerals: plagioclase, quartz, muscovite, biotite, chlorite, ore minerals.
Ore minerals: ilmenite, pyrrhotite, chalcopyrite, rutile, pyrite, zircone. Ferrimagnetic pyrrhotite transformed into pyrite and marcasite.
Vein minerals: quartz.

H014 (5378.0 - 5387.4 m): Amphibolite

Amphibolite, weakly to strongly altered with thin **hornblende-gneiss** intercalations, dip of foliation 20-30°, core recovery 4.70 m.
Rock forming minerals: amphibole, plagioclase, garnet, chlorite, quartz, ore minerals. Ophitic intergrowth of clinopyroxene (mostly replaced by brown hornblende) and completely saussuritized plagioclase, magmatic plagioclase is pseudomorphed by garnet.
Ore minerals: ilmenite, rutile, titanite, monoclinic pyrrhotite, chalcopyrite, sphalerite.
Vein minerals: prehnite, adularia and chlorite.

H015 (5502.5 - 5511.1 m): Amphibolite

Amphibolite, fine grained, cataclastic overprint, dip of foliation 55°, core recovery 0.15 m.
Rock forming minerals: plagioclase, quartz, garnet, chlorite, sericite, zircone, clinozoisite, biotite.
Ore minerals: ilmenite, pyrrhotite, titanite, leucoxene, chalcopyrite.
Vein minerals: prehnite, quartz and chlorite.

H016 (5523.2 - 5530.4 m): (Garnet)-amphibolite

(Garnet)-Amphibolite, fine grained, weakly foliated, with quartz feldspar mobilisates, dip of foliation 35-65°, core recovery 1.85 m
Rock forming minerals: amphibole, garnet, biotite, plagioclase, chlorite, ore minerals. Rims of hornblende altered to actinolite and chlorite.
Ore minerals: ilmenite, pyrrhotite, titanite, leucoxene, chalcopyrite. Xenomorphic ilmenite is altered to titanite or leucoxene.
Vein minerals: prehnite, quartz, calcite and sericite

H017 no core recovery

H018 no core recovery (Pilot Core System, test run)

H019 (5778.5 - 5782.5 m): Amphibolite

Amphibolite, partially strongly altered, massive to strongly foliated, dip of foliation 40-60°, core recovery 2.25 m.
Rock forming minerals: amphibole, plagioclase, quartz, chlorite, tourmaline, titanite, calcite, biotite, muscovite, clinozoisite, actinolite. Tourmaline occurs intergrown with quartz and feldspar, quartz/plagioclase symplectites, poiciloblastic hornblende.
Ore minerals: titanite, leucoxene, pyrrhotite, pyrite, chalcopyrite. Ilmenite is totally altered into titanite or leucoxene, pyrrhotite is intergrown with pyrite.
Vein minerals: calcite, chlorite, tourmaline and plagioclase

H020 (6016.0 - 6018.0 m) no core recovery

H021 (6112.0 - 6122.4 m) no core recovery

H022 (6143.0 - 6144.2 m) no core recovery

H023 (6148.2 - 6152.2 m): Amphibolite

Amphibolite, fine grained, foliated, strongly altered, mobilisate layers, concordant / discordant, many sealed subhorizontal faults. Dip of foliation 60-70°, core recovery 2.40 m.
Rock forming minerals: amphibole, plagioclase, biotite, chlorite, ore minerals, quartz.
Ore minerals: ilmenite, rutile, titanite, monoclinic and hexagonal pyrrhotite, chalcopyrite, pentlandite, sphalerite, graphite.
Vein minerals: clinozoisite and quartz.

H024 (6242.6 - 6244.7 m): Amphibolite / metagabbro

Amphibolite/metagabbro, coarse grained massive, at times weakly foliated, deformed mobilisate, dip of foliation 50-70°, core recovery 1.60 m (LDCS)
Rock forming minerals: hornblende, plagioclase, quartz, chlorite, clinozoisite, biotite, titanite, zircon, ore minerals.
Ore minerals: ilmenite, rutile, anatase, titanite, monoclinic and hexagonal pyrrhotite, chalcopyrite, pyrite, pentlandite, sphalerite
Vein minerals: clinozoisite, prehnite,chlorite and sulfides

H025 (6244.7 - 6250.7 m): Amphibolite / metagabbro

Amphibolite/metagabbro, coarse grained, massive, at times weakly foliated, weakly altered, with 10 cm thick, flat lying shear zone in metagabbro and mm thick vein mineralisation with actinolite, dip of foliation 50°, core recovery 4.95 m.
Microscopic: **Amphibolite,** coarse grained, weakly foliated, weakly to strongly altered with **metagabbro**, medium grained, massive, strongly chloritized.
Rock forming minerals: hornblende, plagioclase, quartz, tourmaline, chlorite, titanite, actinolite, muscovite, epidote, clinozoisite, ore minerals, prehnite, calcite and zircone. Tourmaline and quartz occur on fissures in strongly altered amphibolite, pseudomorphic replacement of hornblende by tourmaline.
Ore minerals: ilmenite, monoclinic and hexagonal pyrrhotite, rutile, titanite, pyrite, chalcopyrite, pentlandite, sphalerite.
Vein minerals: multiple mineralisation of prehnite and epidote.

H026 (6304.3 - 6307.3 m): Amphibolite / metagabbro

Amphibolite/metagabbro, fine grained, massive, few mobilisates, dip of foliation 35-55°, core recovery 1.30 m
Rock forming minerals: amphibole, plagioclase, quartz, chlorite, biotite, clinozoisite, titanite, zircon, ore minerals.
Ore minerals: ilmenite, monoclinic and mixed type pyrrhotite, titanite, rutile, chalcopyrite, pyrite, cobaltite
Few oxide aggregates of 2-3 mm grain size consist of rutile and ilmenite.
Vein minerals: clinozoisite and calcite

H027 (6355.0 - 6360.0 m): Amphibolite

Amphibolite, coarse grained, massive, at times weakly foliated. Coarse grained mobilisate layers, sometimes strongly deformed, dip of foliation 45-70°, core recovery 4.90 m (LDCS).
Rock forming minerals: amphibole, plagioclase, quartz, chlorite, garnet, ore minerals, tourmaline, prehnite
Tourmaline occurs in quartz/feldspar-mobolisates. Shearzones are characterized by strong cataclastic overprint and high ore mineral and chlorite content.
Ore minerals: ilmenite, titanite, rutile, monoclinic pyrrhotite, chalcopyrite, pyrite.
Vein minerals: multiple mineralisation of prehnite, epidote, clinozoisite, chlorite, calcite, quartz, adularia, pyrrhotite, chalcopyrite.

H028 (6434.5 - 6436.6 m): Amphibolite

Amphibolite, fine grained, dense, mainly weakly altered. Few mobilisate bands. Core disking, dip of foliation 45-60°, core recovery 1.70 m (LDCS).
Rock forming minerals: amphibole, plagioclase, quartz, garnet, chlorite, titanite, biotite, actinolite, zircon, ore minerals. Actinolite grows from brown amphibole, small garnets occur disseminated in garnet-amphibolite.
Ore minerals: ilmenite, hexagonal pyrrhotite, leucoxene, rutile, titanite, chalcopyrite. The high ore mineral content up to about 6 vol-% is caused by ilmenite and hexagonal pyrrhotite.
Vein minerals: epidote, clinozoisite and adularia.

H029 (6540.2 - 6546.0 m): Amphibolite

Amphibolite, coarse grained and very mobilisate rich. Dip of foliation -, core recovery 2.20 m.
Rock forming minerals: amphibole, plagioclase, quartz, actinolite, biotite, titanite, clinozoisite, prehnite, chlorite, zircon.
Ore minerals: ilmenite, monoclinic pyrrhotite, rutile, leucoxene, titanite, chalcopyrite, pyrite.
Vein minerals: idiomorphic clinozoisite with prehnite, epidote, calcit and actinolite, pyrrhotite.

H030 (6668.0 - 6672.4 m): Amphibolite

Amphibolite, mostly strongly altered, very mobilisate rich; upper part **hornblende-gneiss** (a cataclastic zone divides it from the metabasite), the strike of foliation above and below this cataclastic zone is different, dip of foliation 75-90°, core recovery 2.50 m (LCDS).
Rock forming minerals: amphibole, garnet, plagioclase, quartz, chlorite, prehnite, clinozoisite, titanite, calcite, zircon, ore minerals
Ore minerals: ilmenite, monoclinic (and hexagonal) pyrrhotite, leucoxene, titanite, chalcopyrite, pyrite, marcasite, sphalerite, graphite, molybdenite
Vein minerals: multiple vein mineralisation with prehnite (margin coarse grained, centre fine grained), chlorite, clinozoisite, actinolite, quartz, pyrrhotite, chalcopyrite.

H031 (7011.3 - 7013.3 m): Hornblende-gneiss with amphibolite intercalation

Hornblende gneiss, coarse grained with a steeply dipping basic dyke (**amphibolite**), strongly altered. Different generations of sometimes graphitized and mineralized (prehnite, quartz, titanite, sulfides) shear zones. Intense cataclasis, showing transitions to ductile deformation in oldest quartz veins Open pores with quartz and prehnite, dip of foliation 80°, core recovery 2.20 m (LDCS).
Rock forming minerals: plagioclase, quartz, amphibole, chlorite, graphite, prehnite, ore minerals.
Ore minerals: pyrite, ilmenite, titanite, graphite, pyrrhotite, sphalerite, chalcopyrite, leucoxene, rutile, galena.
Vein minerals: quartz, chlorite, prehnite, graphite, clinozoisite, sulfides (pyrite, pyrrhotite, sphalerite, chalcopyrite), calcite and adularia.

H032 (7271.8 - 7272.6 m) no core recovery.

H033 (7400.3 - 7405.0 m): Marble-bearing amphibolite

Marble-bearing amphibolite, fine grained, folded marble layers, rich in epidote, numerous calcite fissures, horizontal pronounced stretching lineation, dip of foliation 80°, core recovery 3.05 m (LDCS)
Rock forming minerals: amphibole, plagioclase, quartz, calcite, epidote, ore minerals, actinolite, clinopyroxene (diopside), garnet, clinozoisite, chlorite, apatite,
Ore minerals: titanite, magnetite, ilmenite, ilmeno-hematite, hemo-ilmenite, rutile, pyrite, chalcopyrite
vein minerals: epidote, calcite, hornblende, adularia, quartz and clinozoisite. Cracks filled with calcite and epidote, sometimes with newly formed hornblende and adularia crosscut the foliation

H034 (8079.1 - 8085.1 m): Garnet-biotite-gneiss / amphibolite

Garnet-biotite-gneiss, weakly altered, with fine intercalations of **amphibolite**, sulfide mineralizations on fault planes. Core disking , dip of foliation 20-60°, core recovery 1.95 m.
Rock forming minerals: plagioclase, biotite, quartz, muscovite, garnet, ore minerals, calcite.
Ore minerals: hexagonal (monoclinic) pyrrhotite, graphite, titanite, ilmenite, chalcopyrite.
Vein minerals: no veins observed.

H035 (fragments from the depth range 9050-9080 m): Hornblende-biotite-gneiss

Hornblende-biotite-gneiss, fine grained, well foliated, weakly altered, with thin calcsilicate layers, graphite in hornblende-and biotite-free layers, high pyrrhotite contents.
Rock forming minerals: plagioclase, quartz, amphibole, biotite, calcite, clinopyroxene, potassium feldspar (microcline), chlorite, muscovite, titanite, ore minerals, graphite, zircon.
Ore minerals: hexagonal, (monoclinic) pyrrhotite, titanite, graphite, rutile, sphalerite, chalcopyrite
Ore minerals are enriched in layers (mainly pyrrhotite and titanite up to 20%). Graphite occurs in biotite-dominated gneiss layers and is rare in hornblende-rich layers.
Vein minerals: chlorite and actinolite.

B.9.4 Distribution of ore mineralization 0 -9101 m (scale 1:10.000)

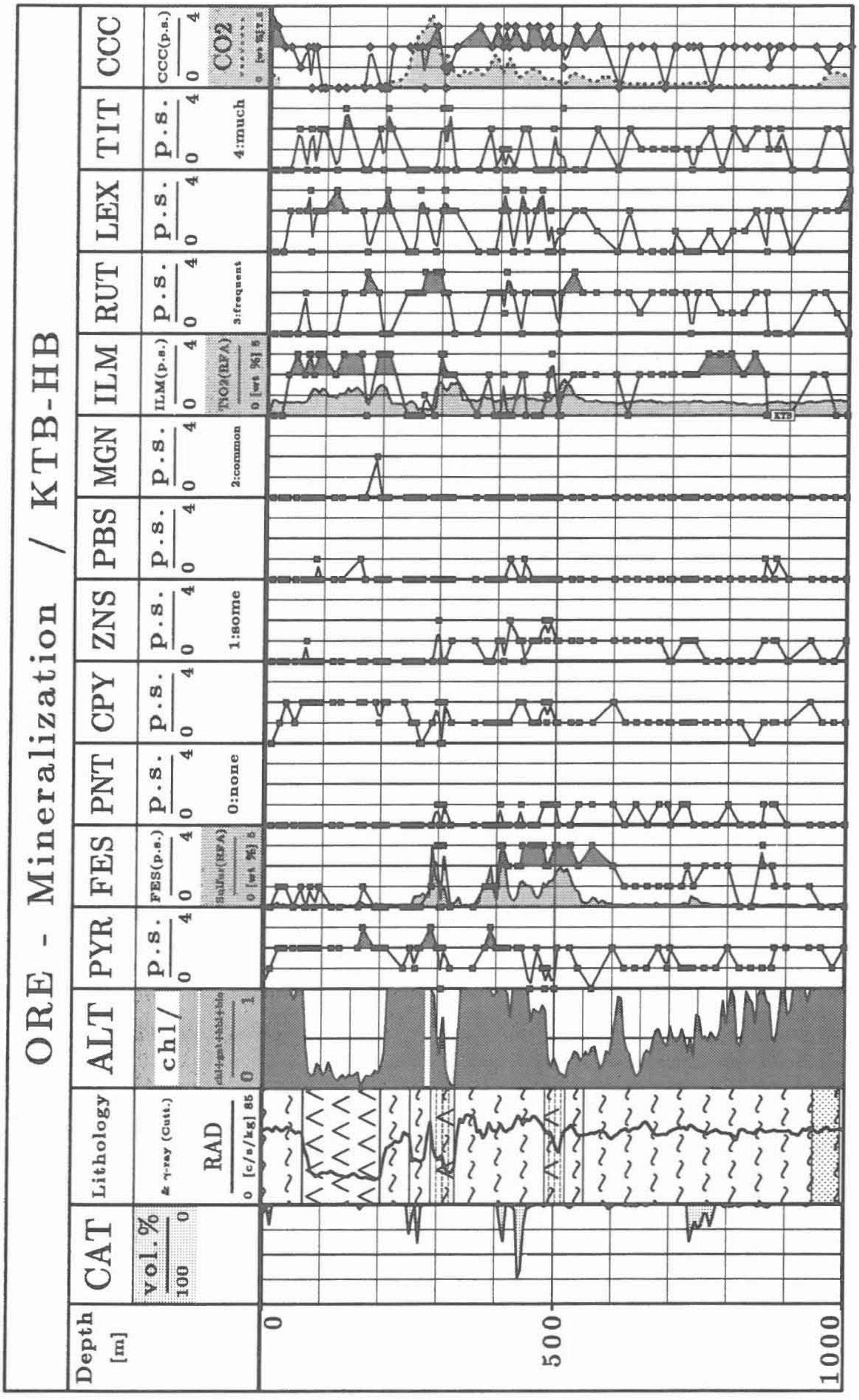

Fig. B.9.4: Distribution of ore mineralization 0-9101 m HB (scale 1 : 10.000), abbreviations see B.9.1

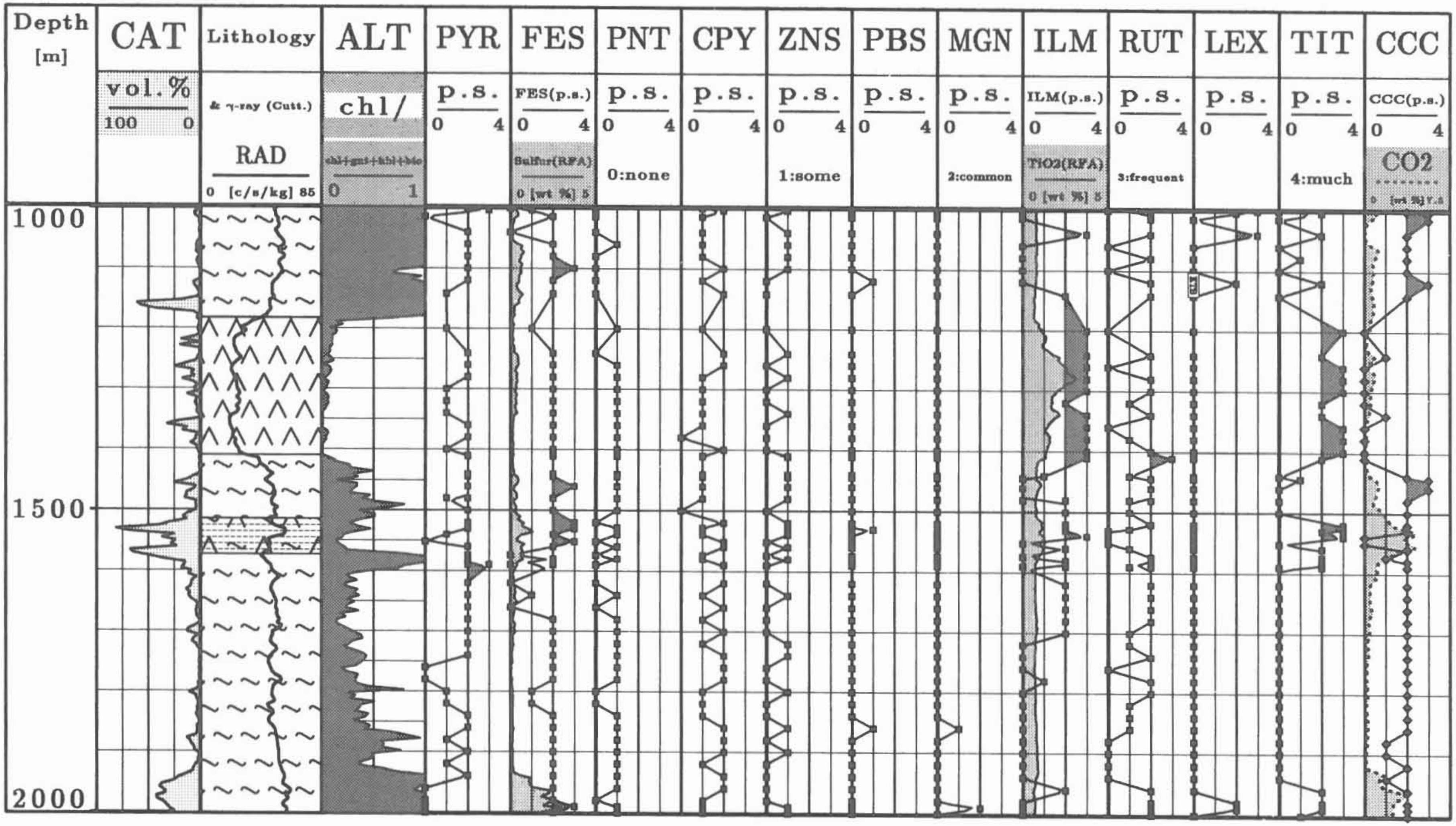

Fig. B.9.4: Continuation

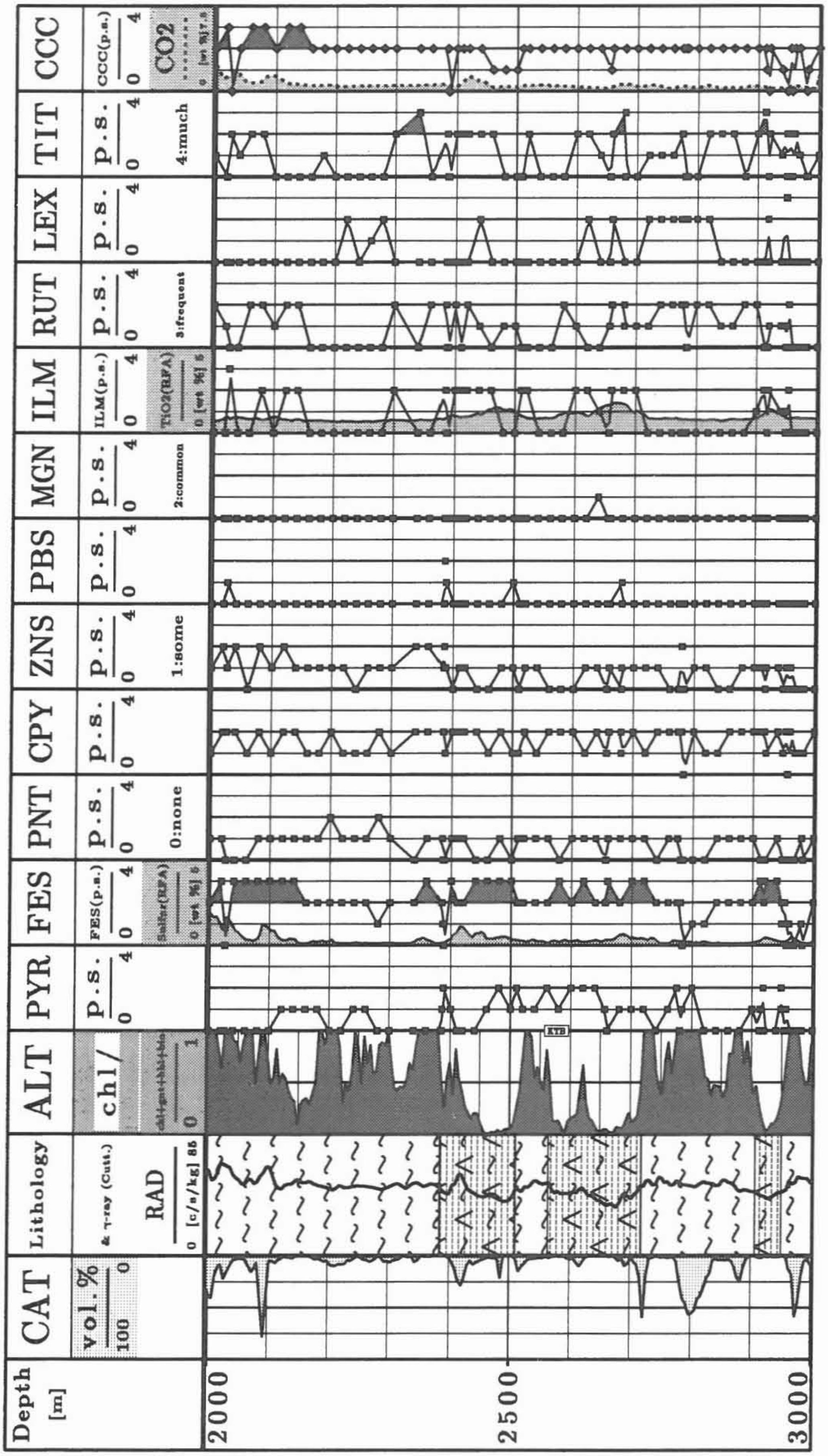

Fig. B.9.4: Continuation

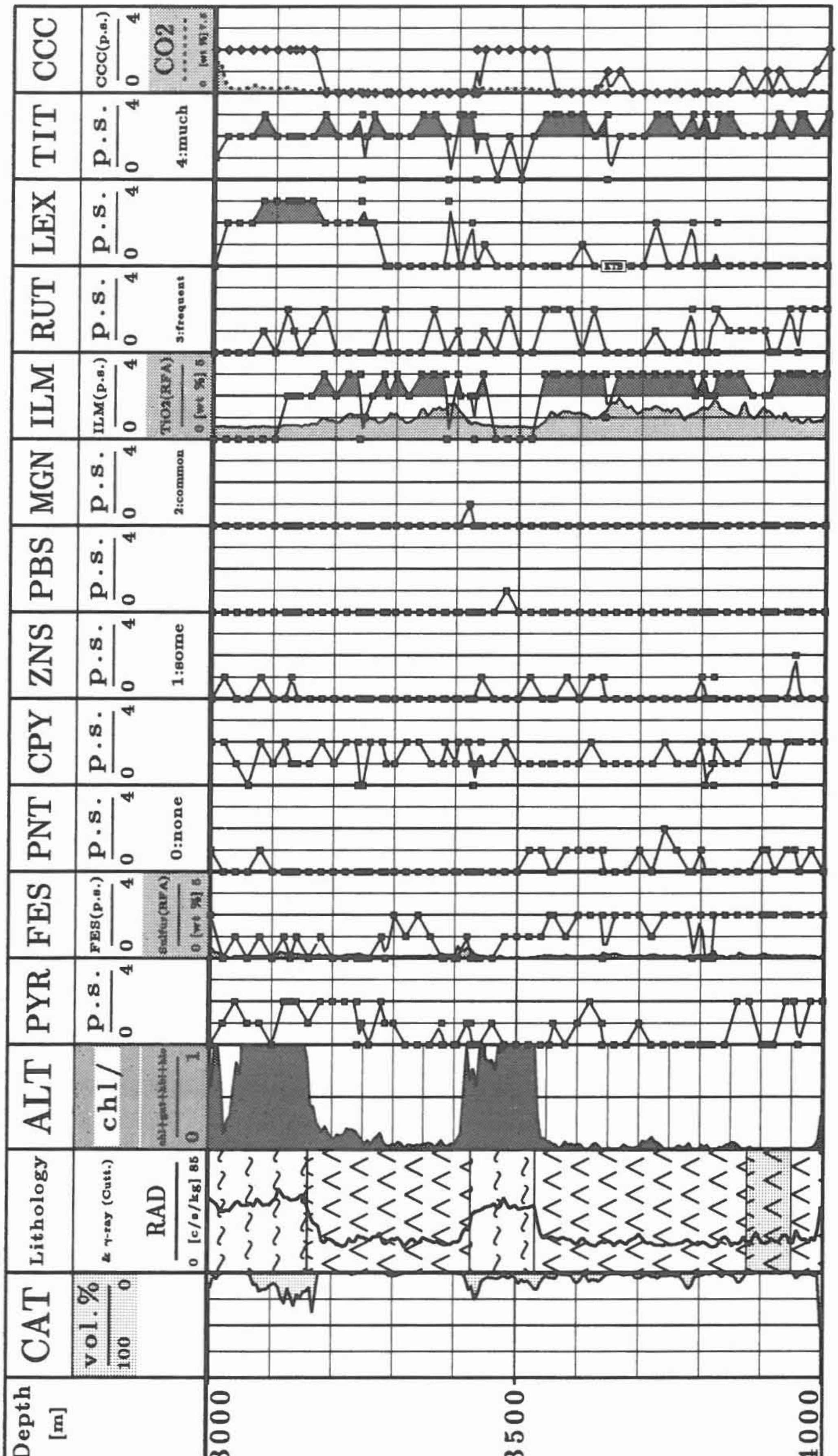

Fig. B.9.4: Continuation

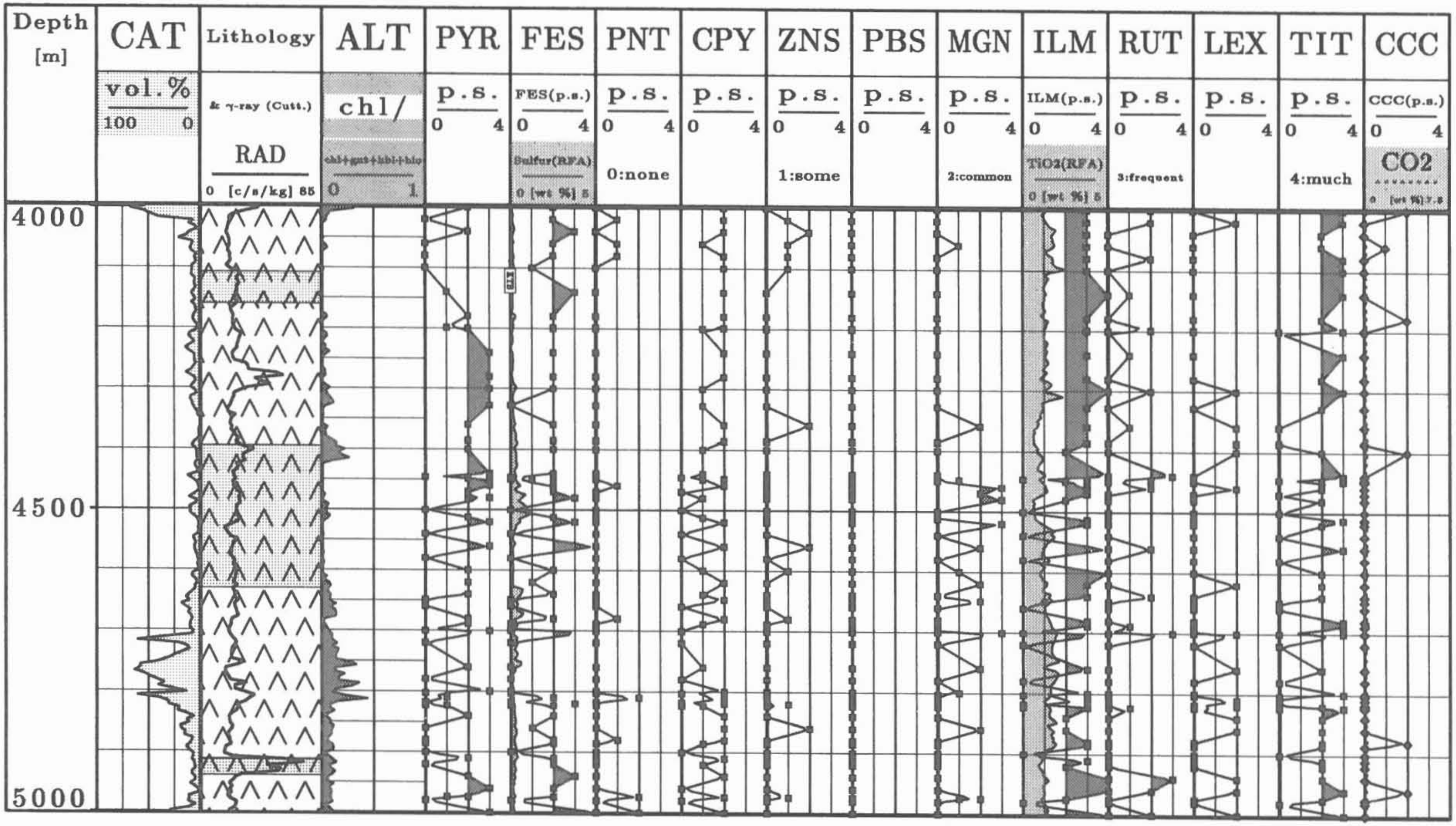

Fig. B.9.4: Continuation

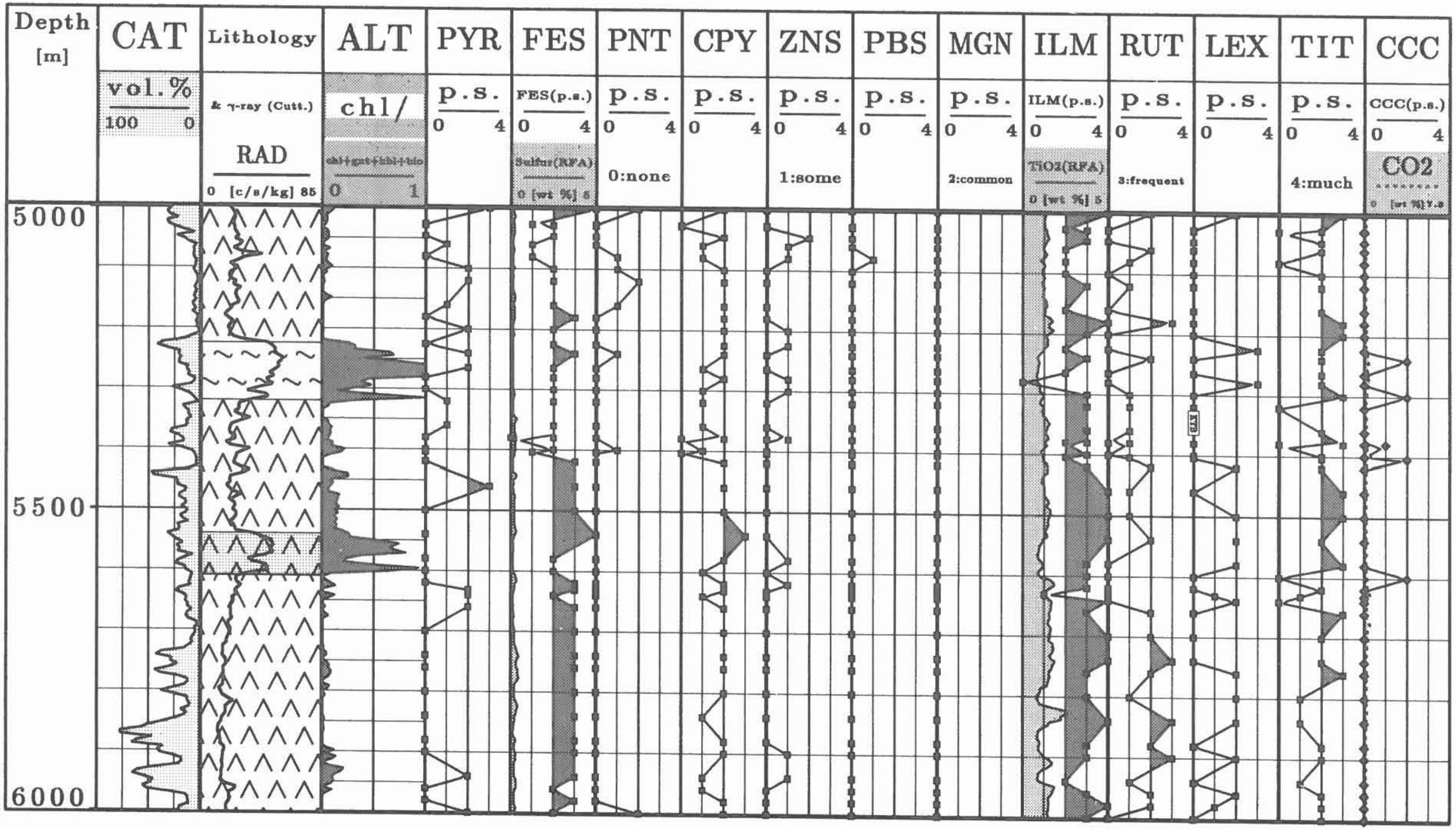

Fig. B.9.4: Continuation

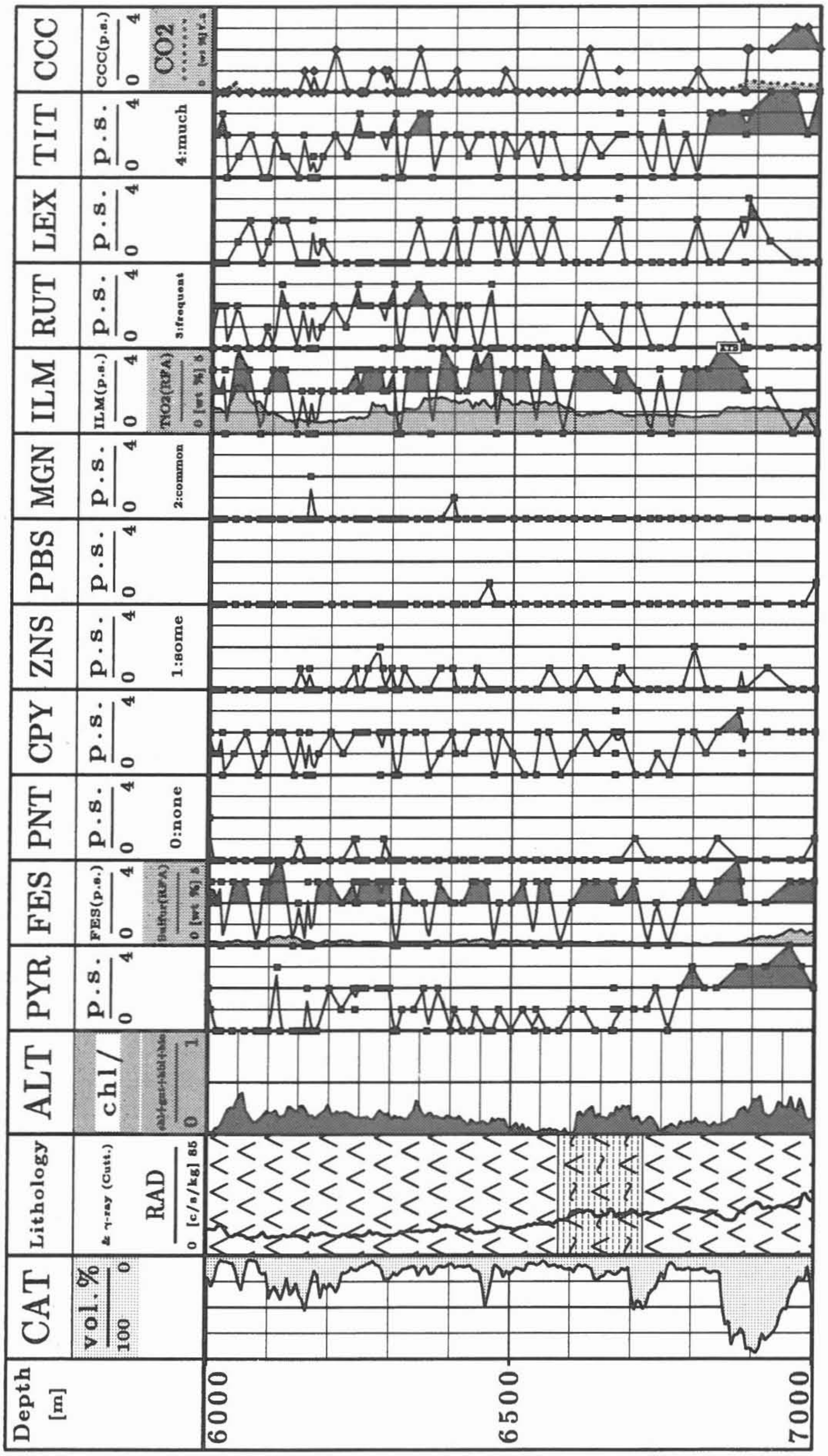

Fig. B.9.4: Continuation

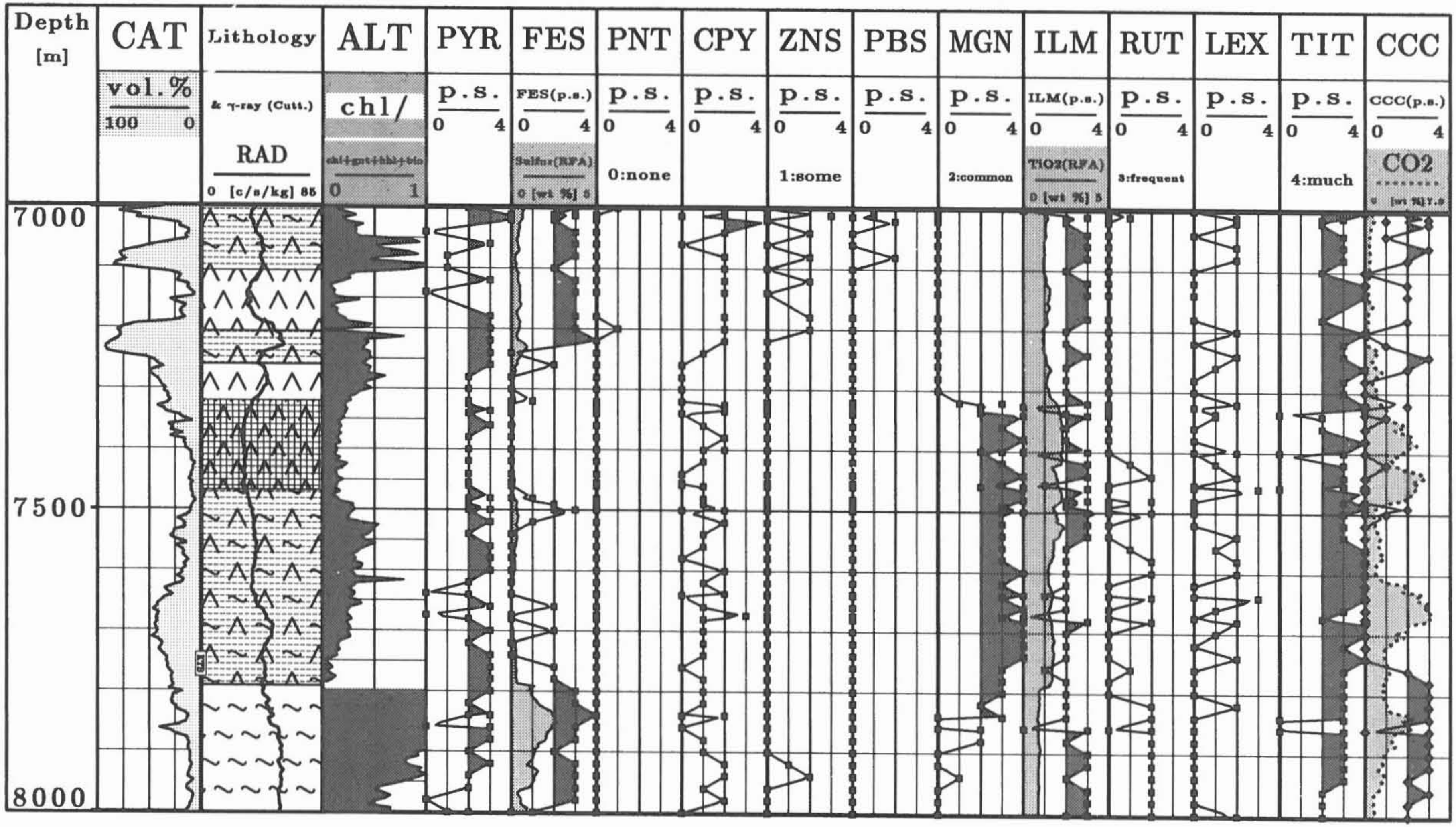

Fig. B.9.4: Continuation

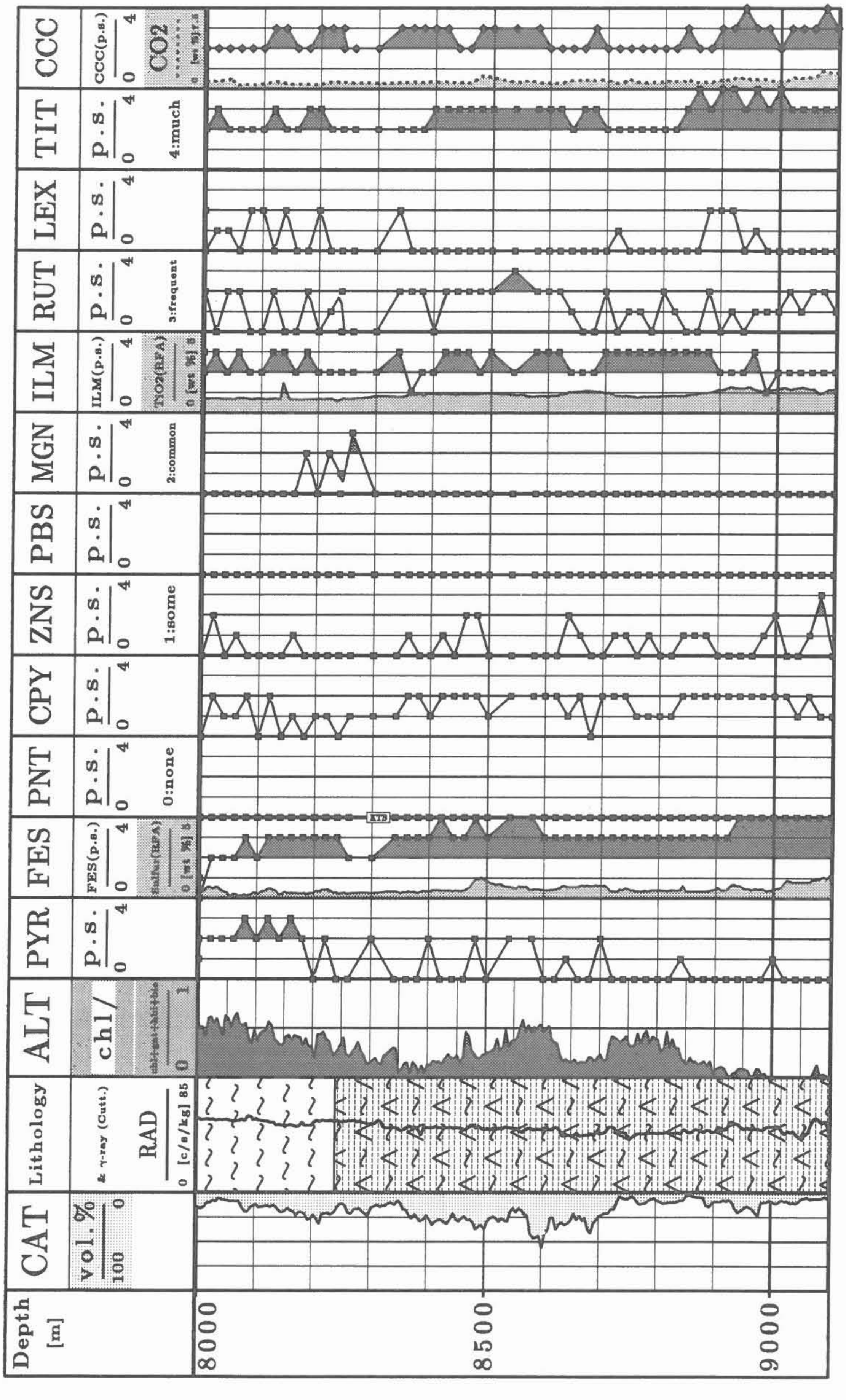

Fig. B.9.4: Continuation

B.9.5 Cuttings profile 6000 - 9101 m

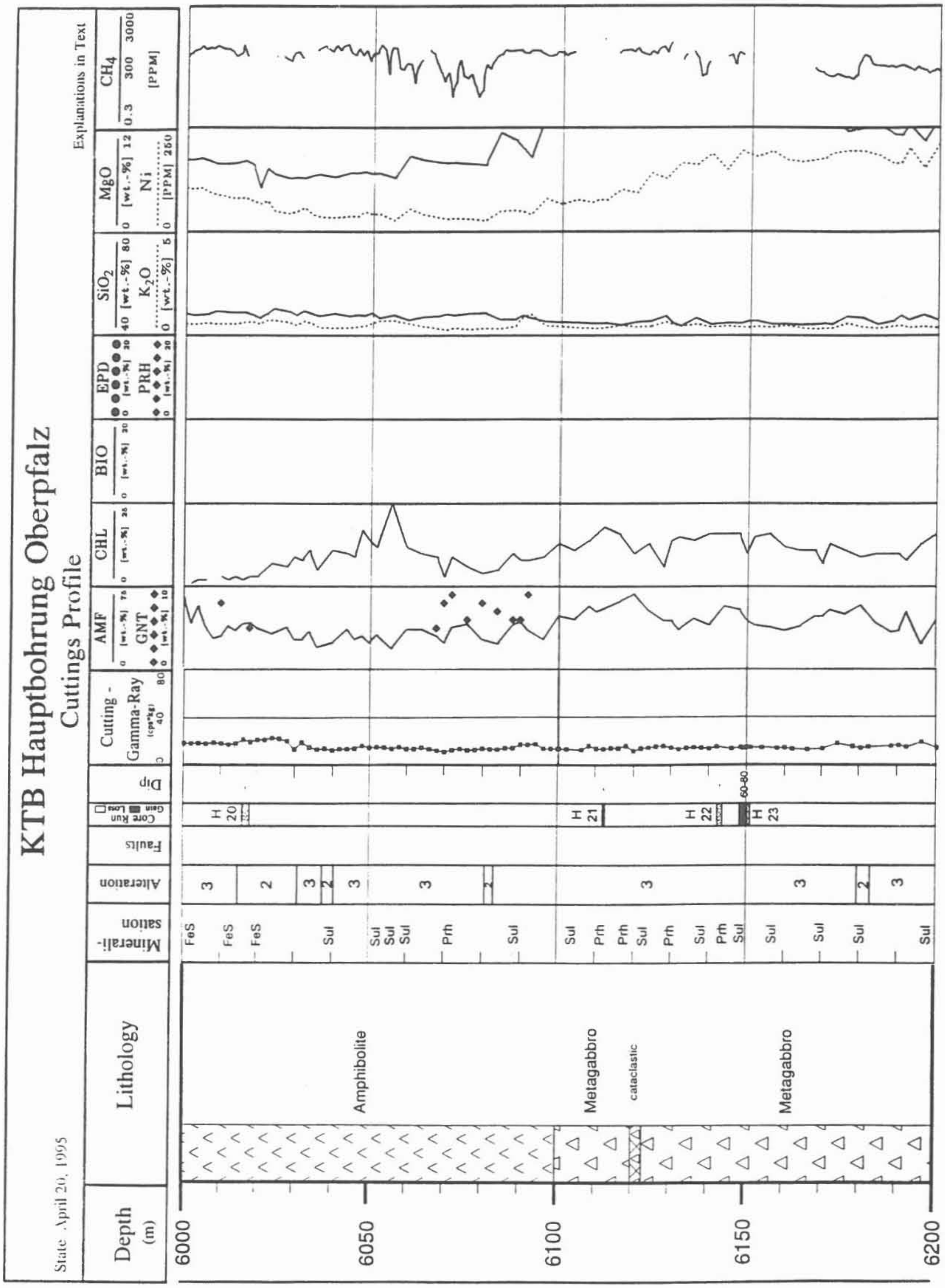

Fig. B.9.5: Cuttings profile with selected parameters of the KTB HB (6000 -9101 m, data from working groups geology, geophysics and geochemistry), abbreviations see B.9.1.

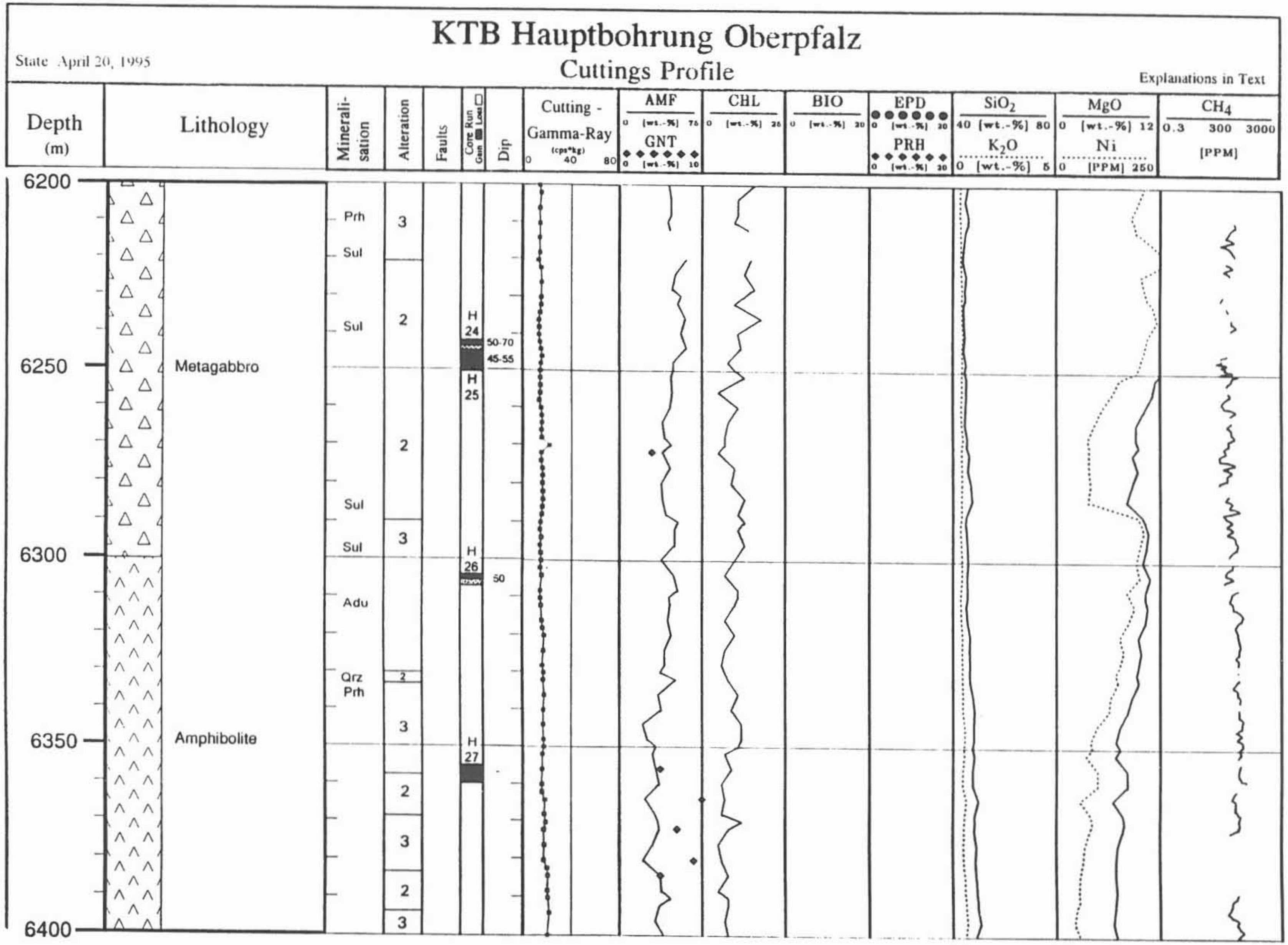

Fig. B.9.5: Continuation

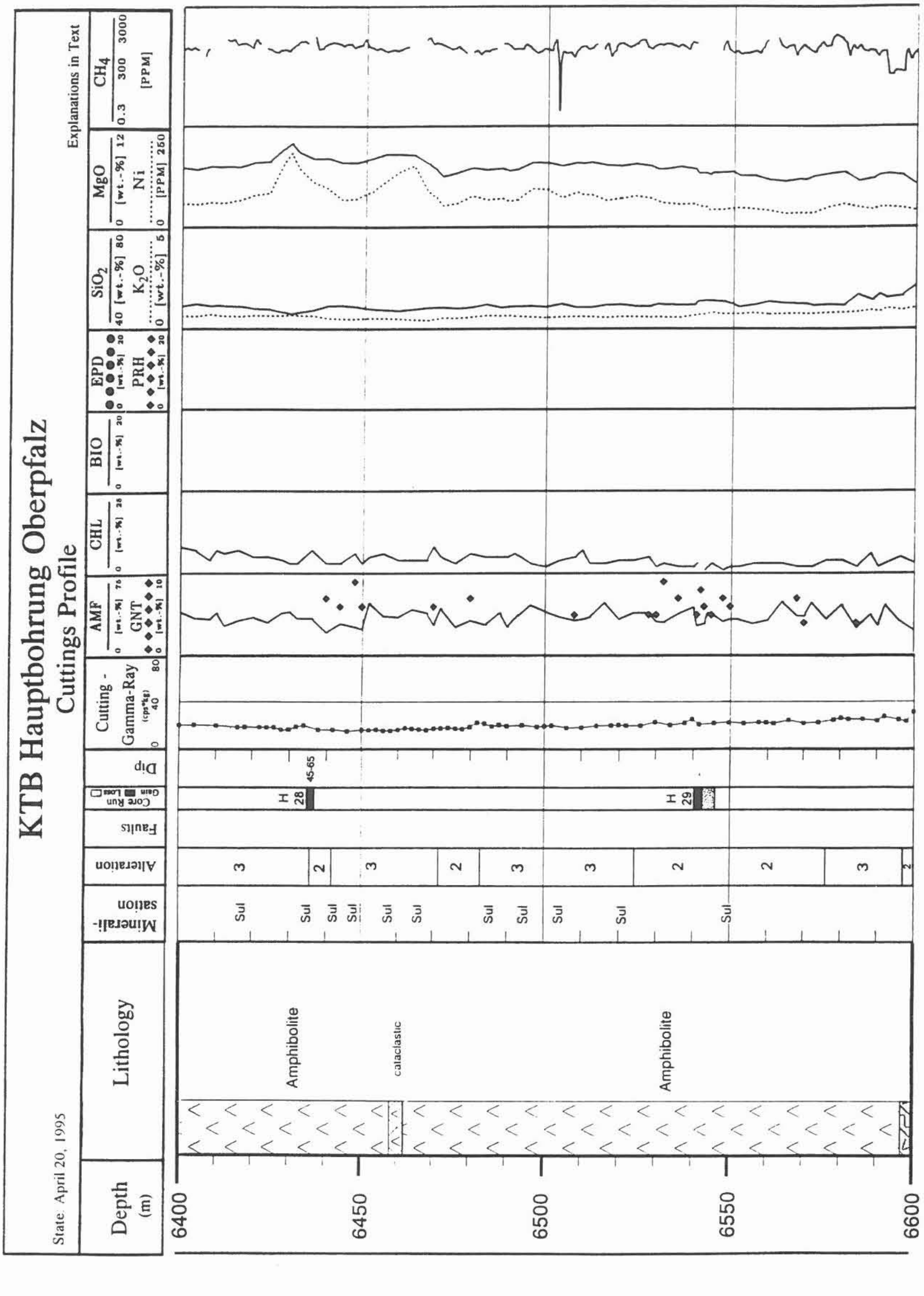

Fig. B.9.5: Continuation

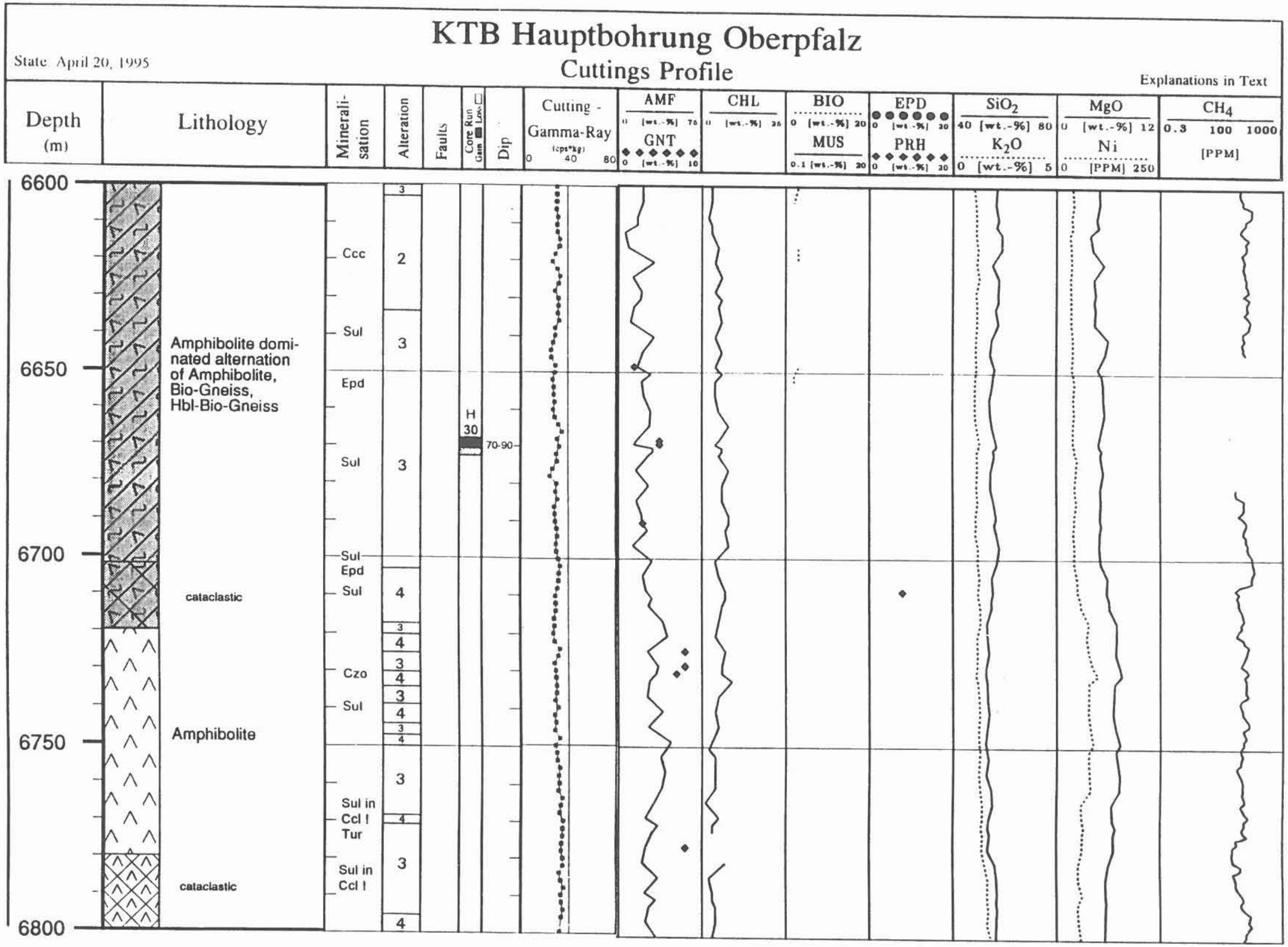

Fig. B.9.5: Continuation

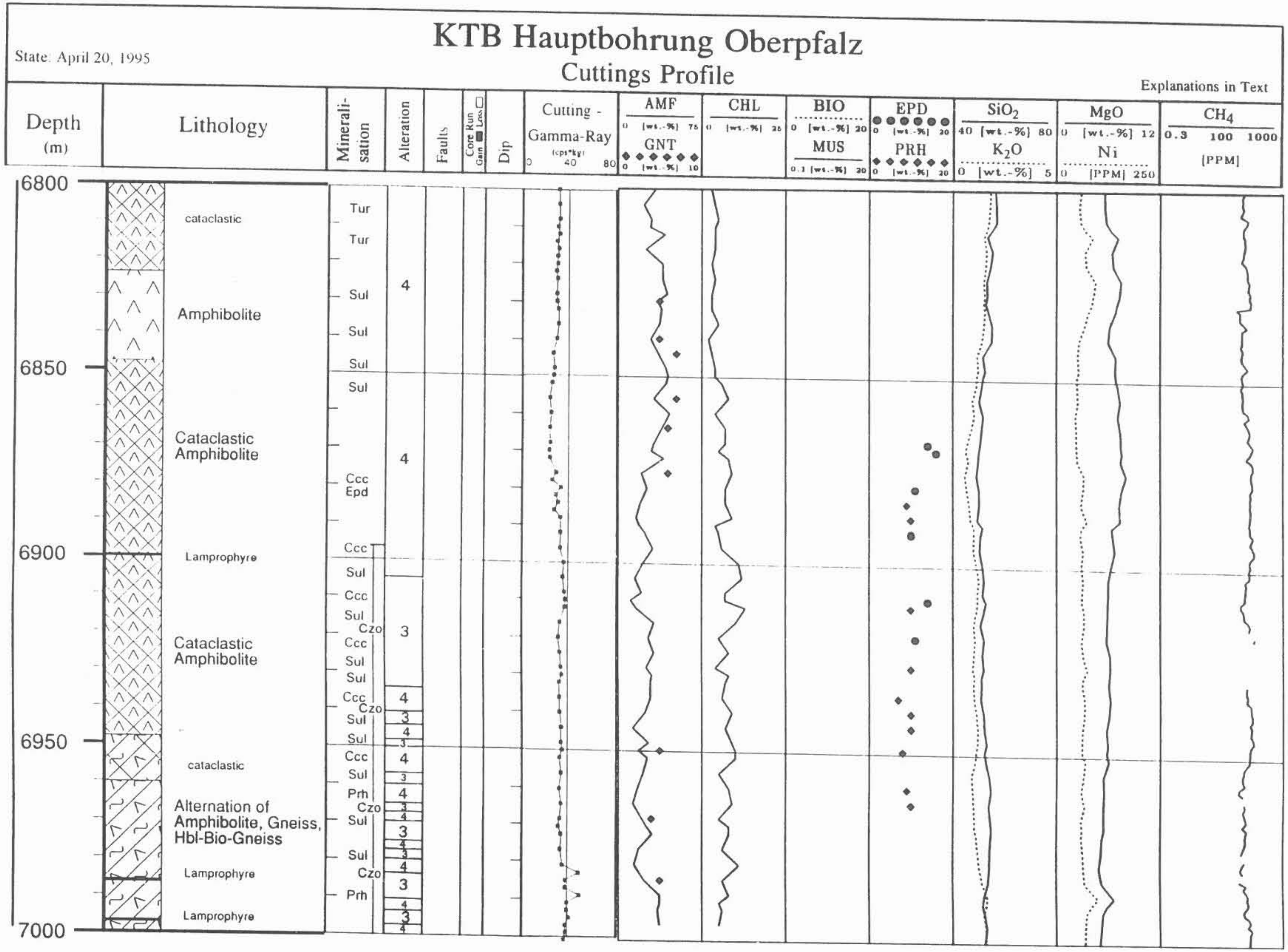

Fig. B.9.5: Continuation

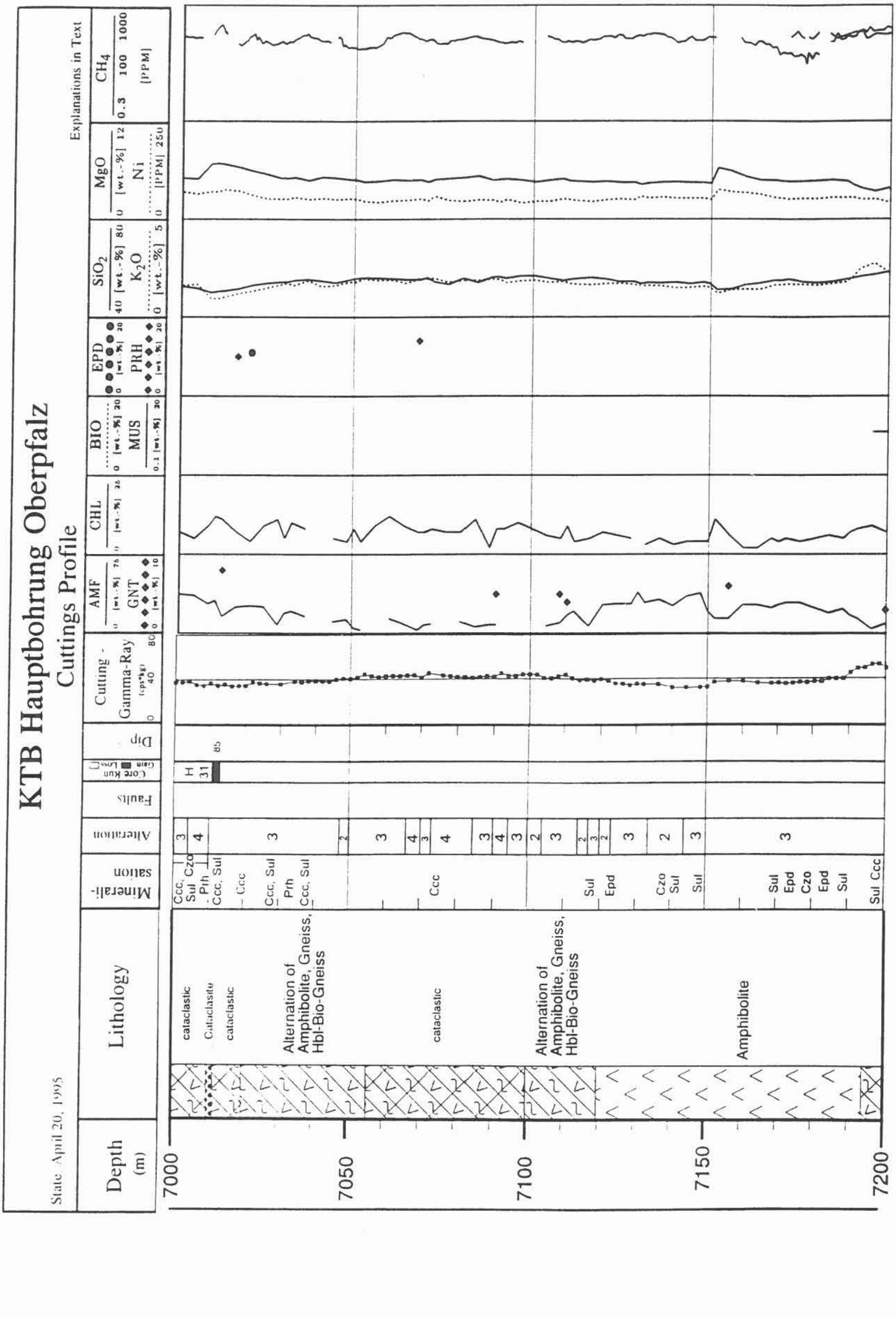

Fig. B.9.5: Continuation

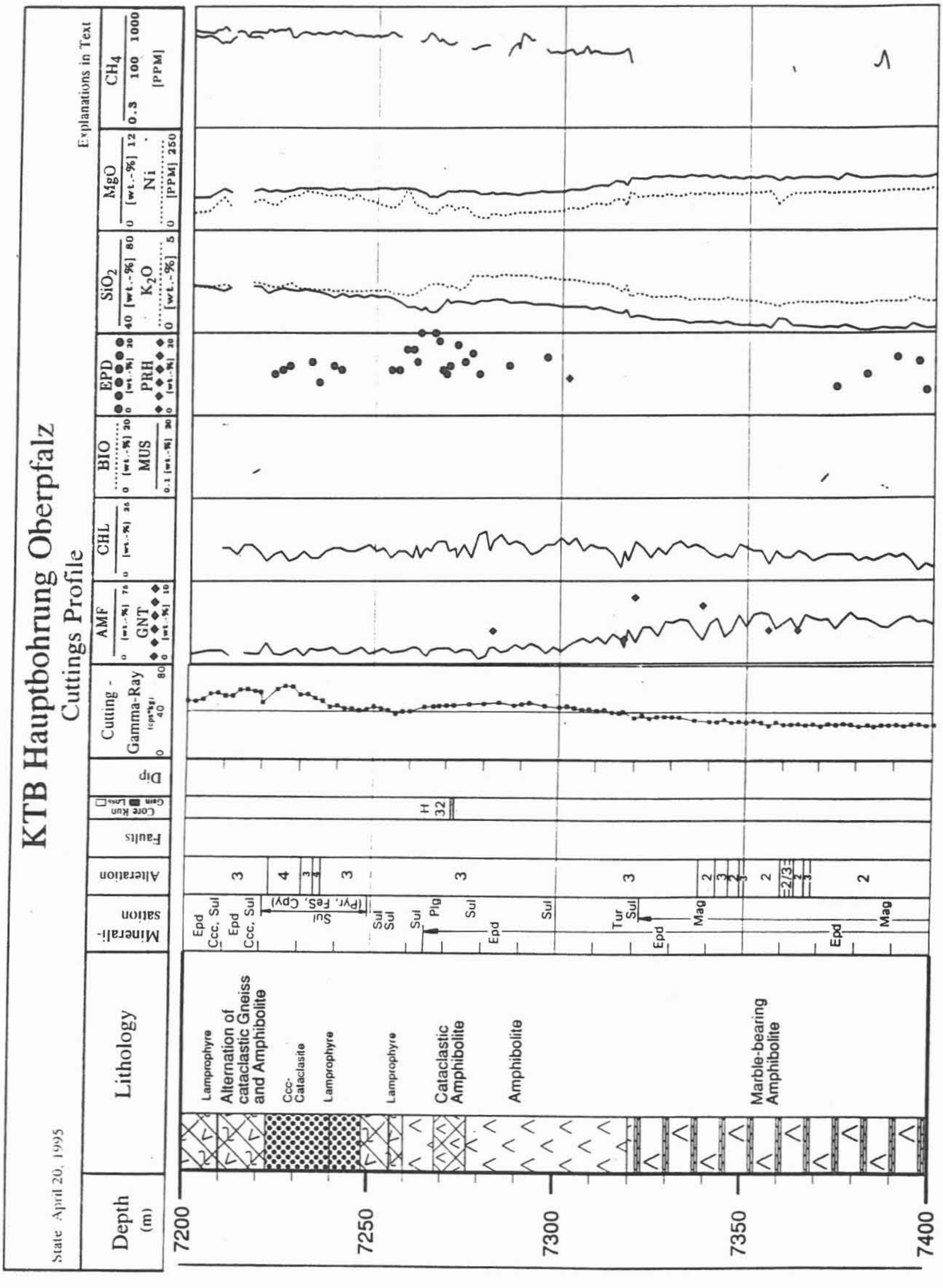

Fig. B.9.5: Continuation

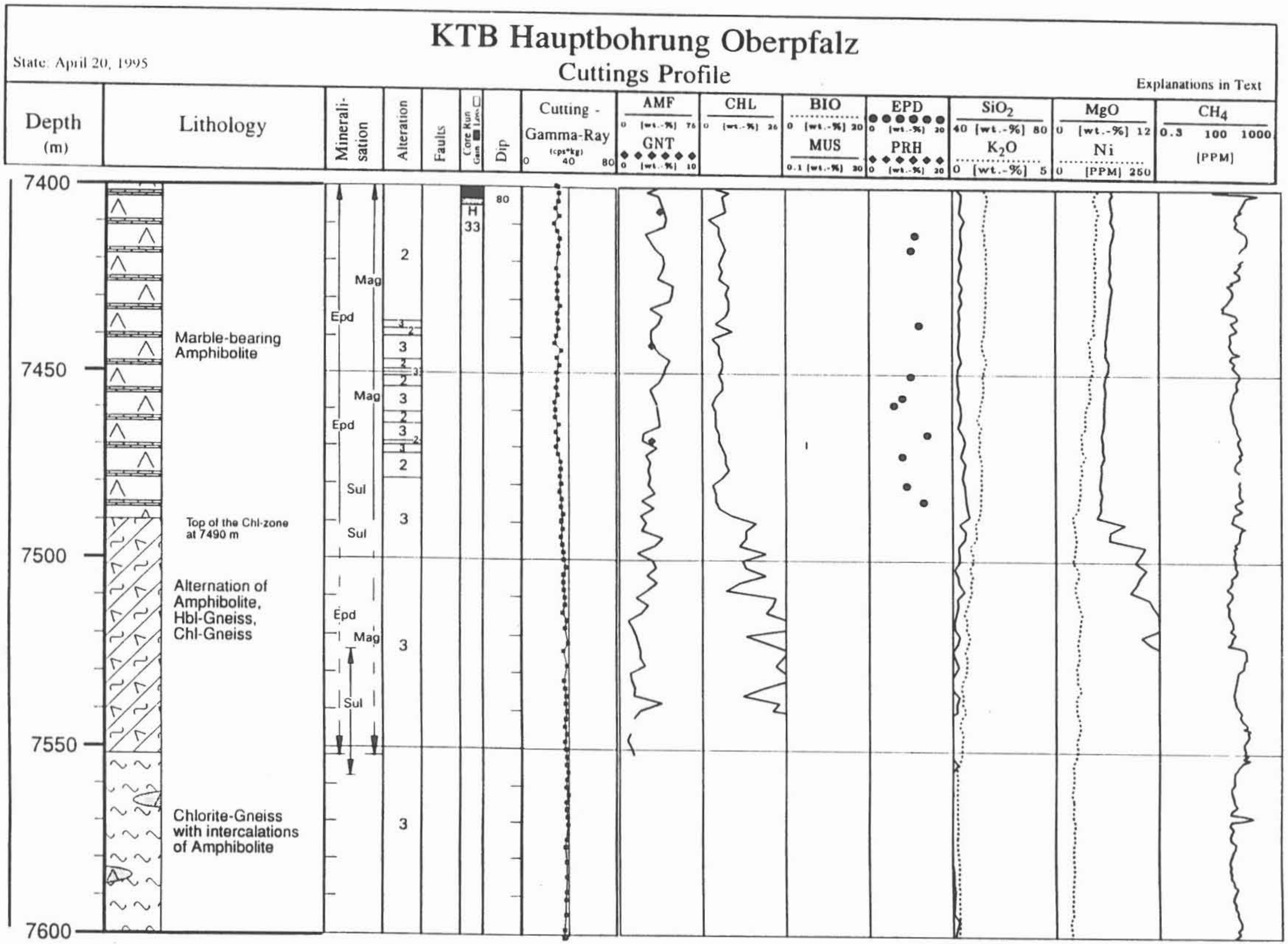

Fig. B.9.5: Continuation

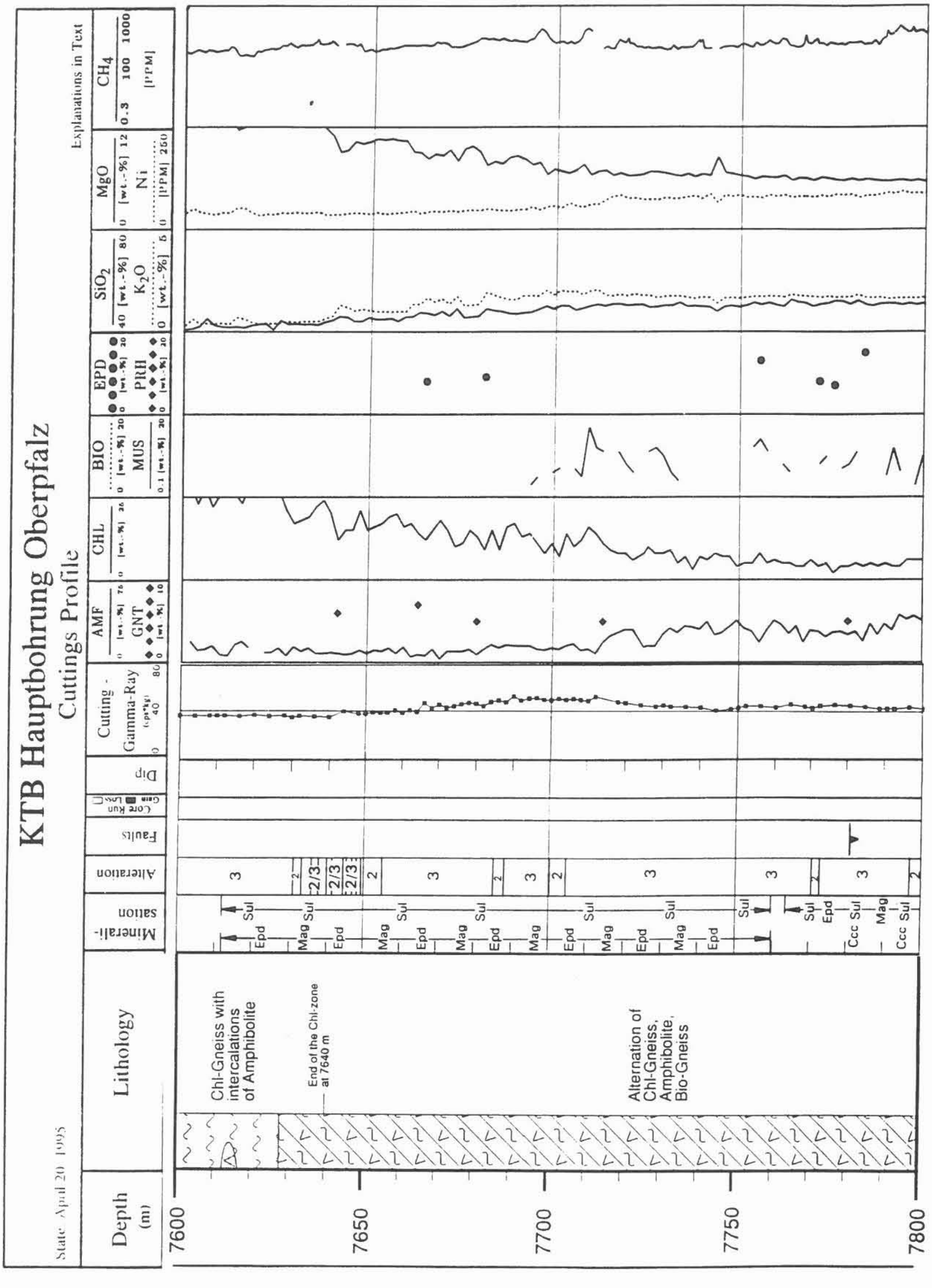

Fig. B.9.5: Continuation

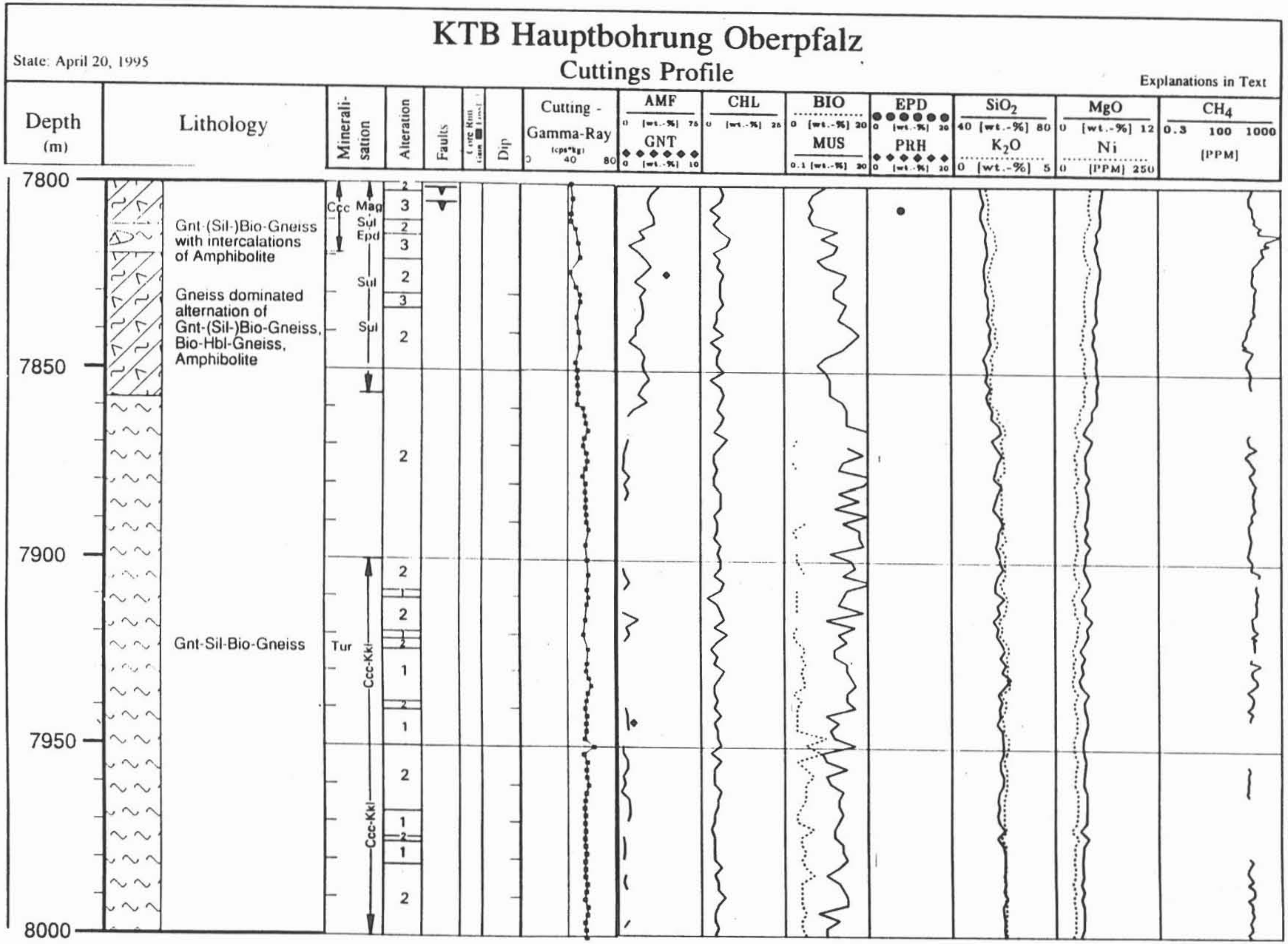

Fig. B.9.5: Continuation

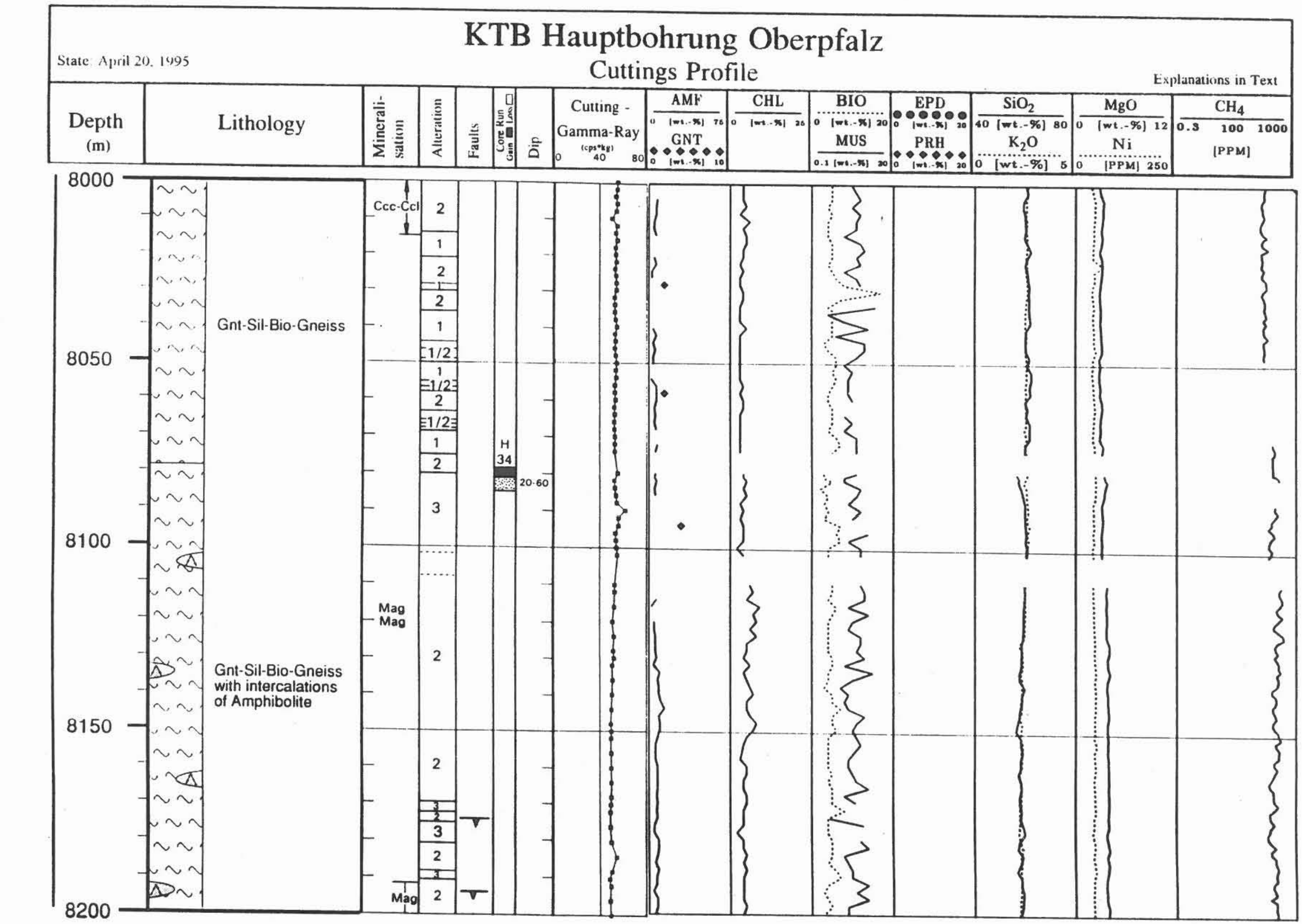

Fig. B.9.5: Continuation

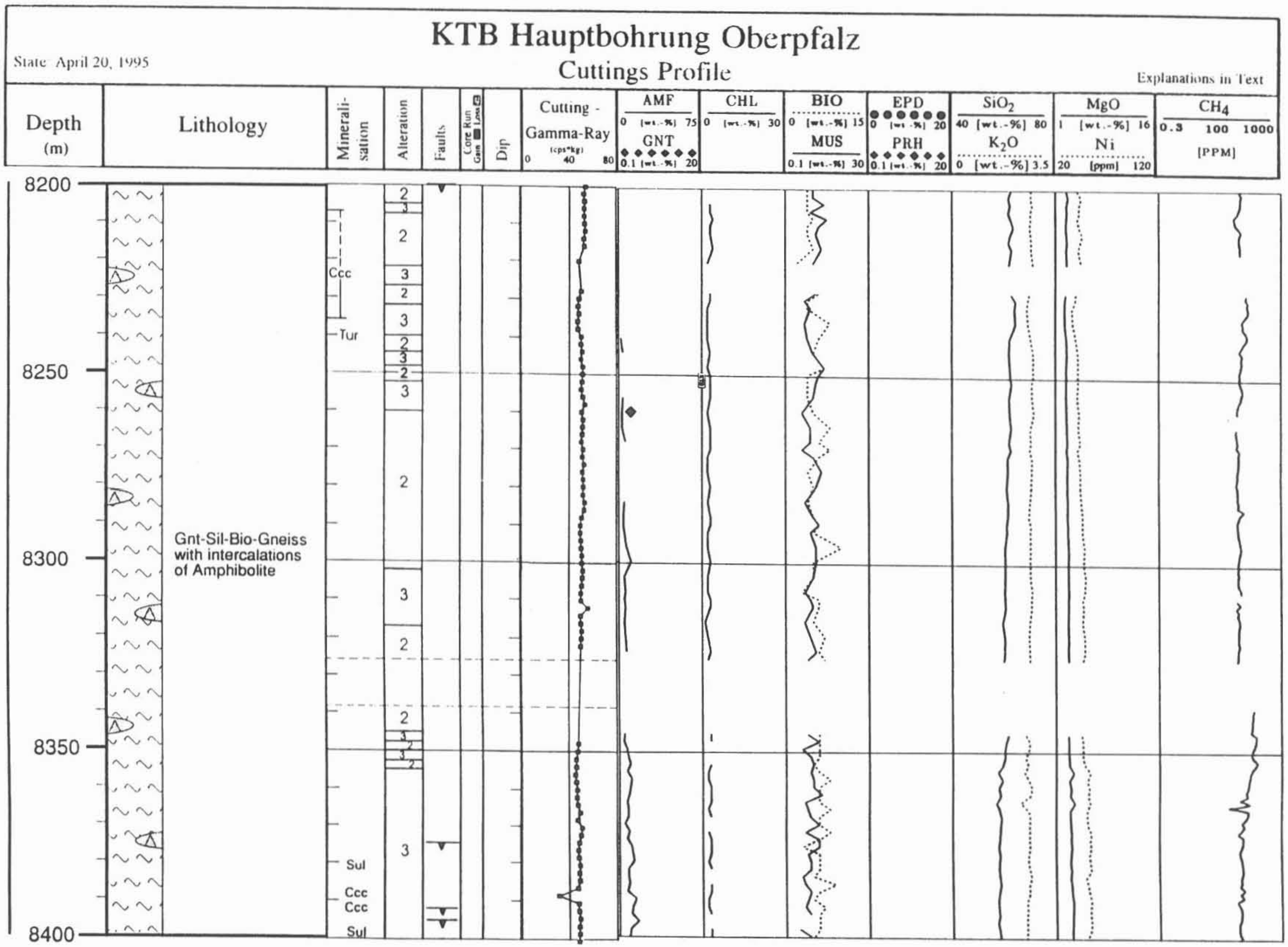

Fig. B.9.5: Continuation

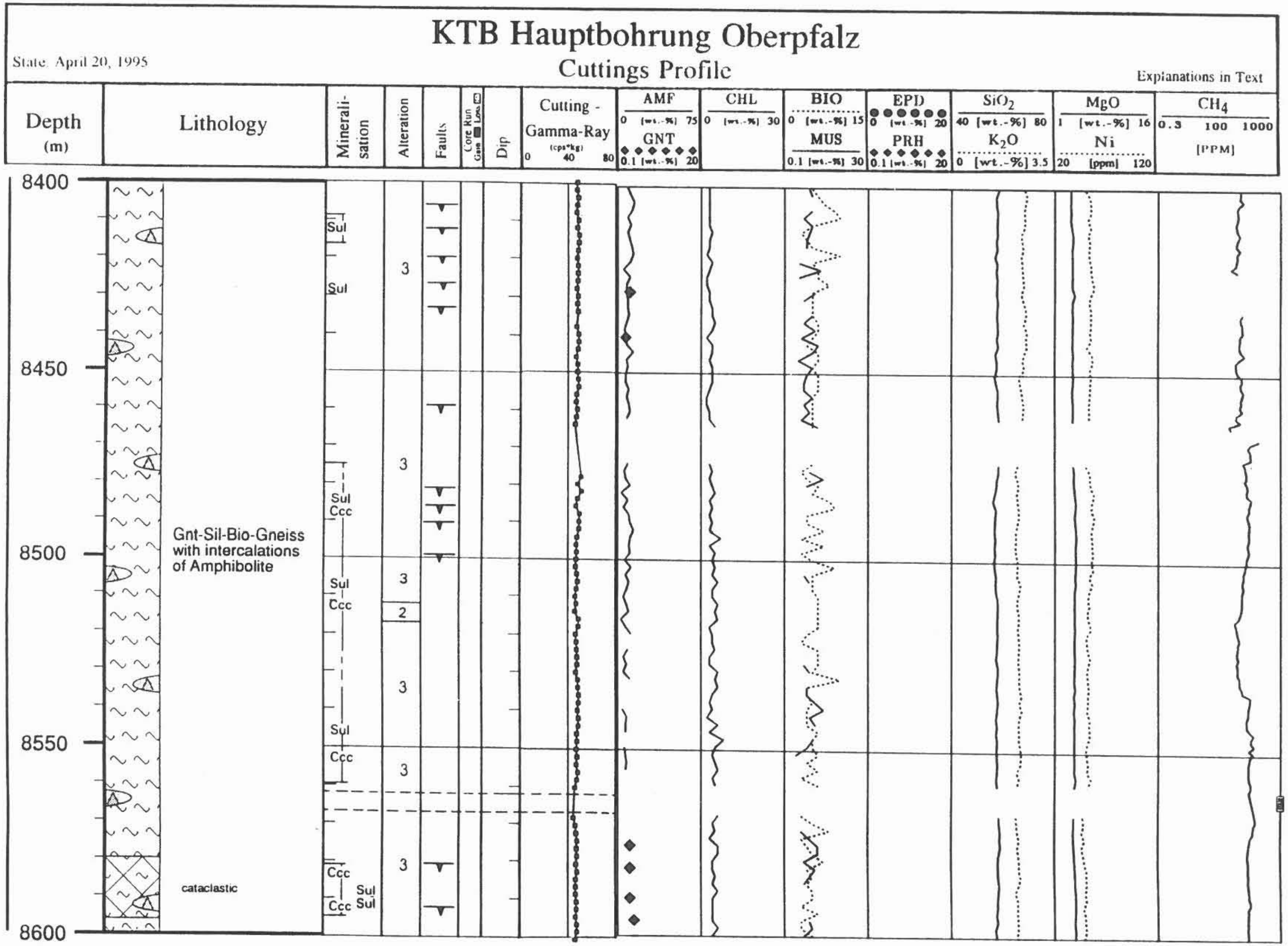

Fig. B.9.5: Continuation

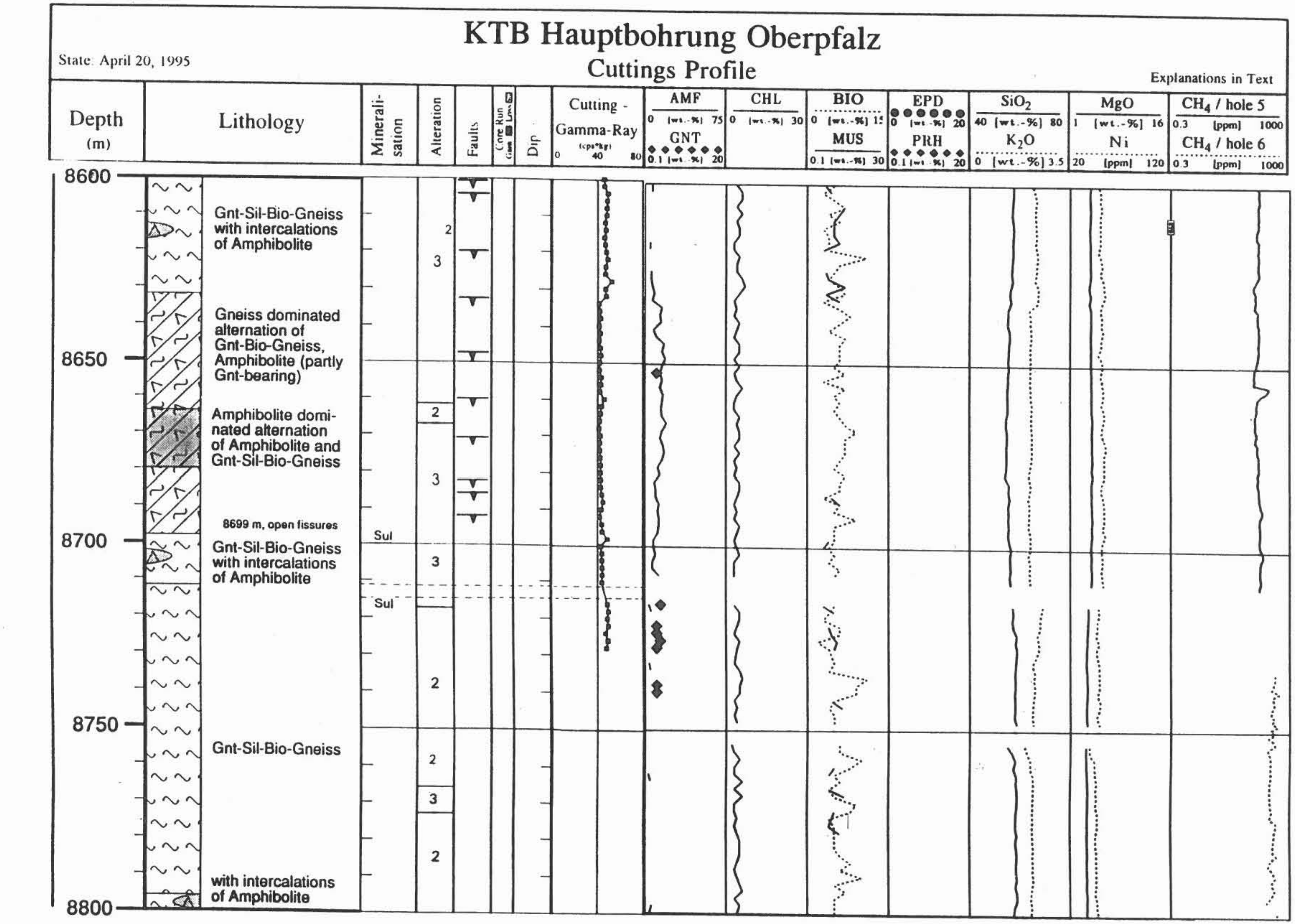

Fig. B.9.5: Continuation

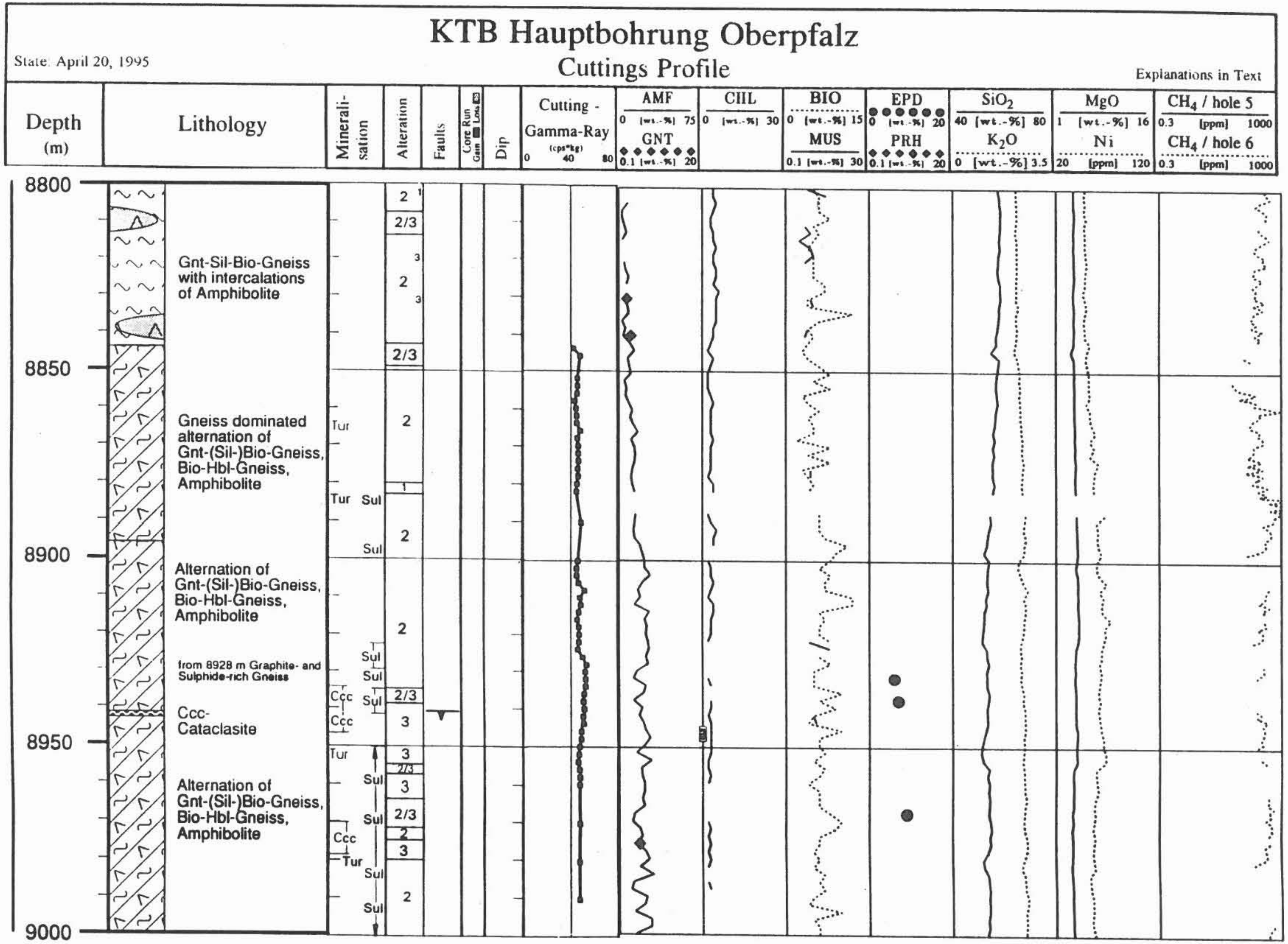

Fig. B.9.5: Continuation

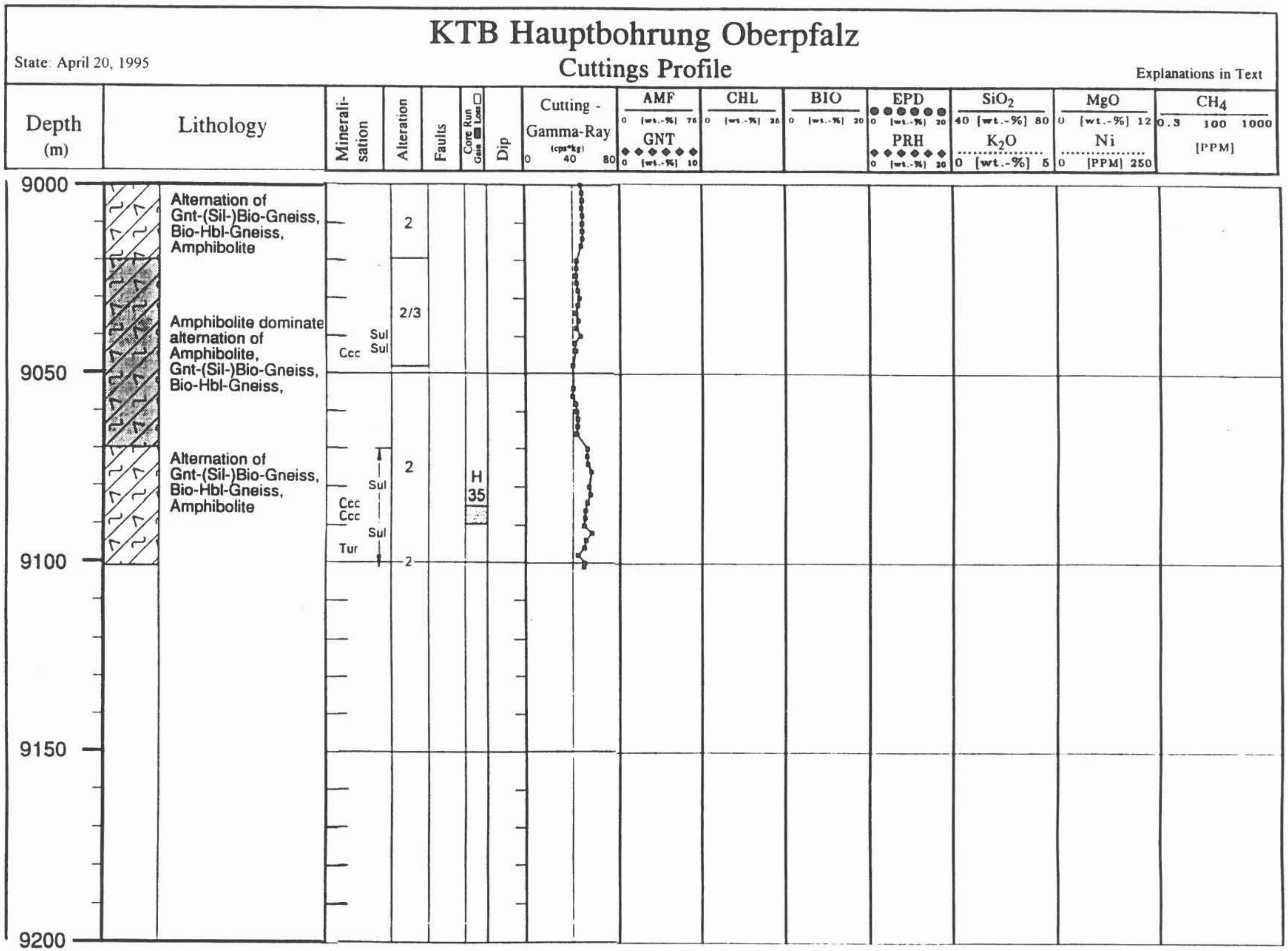

Fig. B.9.5: Continuation